UILU-ENG-80-2013

CIVIL ENGINEERING STUDIES
Structural Research Series No. 480

VIBRATION OF BUILDINGS UNDER RANDOM WIND LOADS

by
ERDAL SAFAK
and
DOUGLAS A. FOUTCH

Technical Report of Research
Supported by the
National Science Foundation
under
Grant ENV 77-07190
and
Grant PFR 80-02582

DEPARTMENT OF CIVIL ENGINEERING
UNIVERSITY OF ILLINOIS
AT URBANA-CHAMPAIGN
URBANA, ILLINOIS
MAY 1980

Page Intentionally Left Blank

ACKNOWLEDGMENT

This report is based on the doctoral dissertation by Erdal Safak submitted to the Graduate College of the University of Illinois at Urbana-Champaign in partial fulfillment of the requiremdnts for the Ph.D. degree. The study was directed by Douglas A. Foutch, Assistant Professor of Civil Engineering. Support was provided by the National Science Foundation under Grants ENV 77-07190 and PFR 80-02582. Computer support was also provided in part by the Research Board of the Graduate College of the University of Illinois at Urbana-Champaign. The critical reviews and suggestions of Dr. D. A. Pecknold and Dr. Y. K. Wen given throughout the study are greatly appreciated.

The authors would like to thank the Cambridge University Press for permission to use a figure published in the Journal of Fluid Mechanics.

Any opinions, findings and conclusions or recommendations expressed in this report are those of the authors and do not necessarily reflect the views of the National Science Foundation.

TABLE OF CONTENTS

LIST OF TABLES

LIST OF FIGURES

Figure Page

CHAPTER 1

INTRODUCTION

Wind loads are one of the principal loads acting on above ground structures. Accurate and detailed analysis of the structures subjected to wind effects, therefore, is important for safety, human comfort and economy.

Until rather recently wind loads were considered as static loads. As design practices have resulted in more slender, taller and lighter buildings, the dynamic effect of the wind has become more important. In recognition of this fact, Davenport introduced the concept of the gust loadings factor through which the dynamic part of a building's response is calculated [3]. Using the principles of random vibration analysis, an expression for the ratio of the total response of a building to its static response was developed and was called the gust factor. The design equivalent static wind loads were then obtained by multiplying the static wind load by this gust factor. Significant research has been done concerning the gust factor method over the past twenty years [6], [34], [37], [27]. An extensive discussion of different approaches and the review of design codes can be found in reference [30].

The work on the gust factor methods and the majority of the research to develop other, more sophisticated, methods of analysis has been directed toward predicting the expected maximum along-wind translational response of structures due to buffeting by atmospheric turbulence. Many buildings designed and constructed, however, are not

perfectly symmetric. Thus, under the influence of dynamic wind loads they would vibrate in three directions, along-wind, cross-wind and torsional, and not just in the along-wind direction. Torsional vibration of a building would clearly develop in a structure whose center of mass and center of resistance do not coincide at every point along the height. They should also be expected in a symmetric structure whose axis of symmetry is not parallel to the direction of the flow. In this case nonsymmetric pressure distributions on the faces of the buildings would produce a torque. As will be shown in this study, even a perfectly symmetric structure under symmetric flow would experience torsional vibrations due to the spatial randomness of fluctuating wind pressures.

Full scale measurements and boundary layer laboratory tests have shown that the cross-wind and torsional vibrations of buildings can be very large. In an experimental study of the vibration of a cubic body in a steady flow, Huh found that for angles of attack of 15°-25° almost pure rotational oscillations resulted [14]. Koten reported that the measurements of wind excited movements of the top of seven different buildings in the Netherlands clearly showed that cross-wind displacements and torsion were an important factor [17]. In some cases, stresses due to torsion were as large as due to along-wind vibrations. The ambient wind induced vibrations of buildings, measured by G. T. Taoka, et. al. [32] and by G. C. Hart, et. al. [11] in two separate investigations, also showed torsional response as being of great importance. The measured cross-wind vibrations of the buildings presented in reference [17] were also quite large. The root-mean

square (rms) values of cross-wind vibrations were larger than those of along-wind vibrations in all of the cases, except one. The same kind of behavior was observed in the John Hancock Building in Chicago [8]. Measurements under 40 mph. wind showed that the r.m.s. value of cross-wind vibrations at the top was nine times larger than that of along-wind vibrations. Wind tunnel tests of aeroelastic prismatic building models led Saunders to conclude that the cross-wind motion for rectangular buildings is primarily due to vortex-shedding [25]. Vickery investigated vortex-shedding earlier and presented different spectra for along-wind and cross-wind forces using two dimensional models [35], [36]. More recently Kareem illustrated the independence of along-wind and cross-wind forces, and reached conclusions similar to those of Saunders [16].

All of those findings clearly show that there is a need for a better model of building behavior for wind analysis. Hart presented a procedure for the dynamic analysis of three-dimensional multi-story buildings subjected to multiple stochastic wind forces [10]. He assumed story floors to be rigid in their own plane and specified three generalized coordinates, two orthogonal translations and a rotation, at the center of mass of each floor. Due to the lack of measured data on full scale and model buildings pertaining to cross-spectral densities of wind forces his procedure was not applicable to practical problems. Patrickson and Friedmann studied the coupled lateral and torsional vibrations of buildings using both deterministic and probabilistic methods of analysis [24]. Their results showed that for realistic

values of offsets between the mass center and the elastic center and/or the aerodynamic center, the torsional effects are comparable to those due to the lateral response. They also found that the increase on velocities and accelerations due to torsional vibrations was higher than that for displacements. Their study based on the results of the experiments done by Vivekananda [40] on square section beams. They did not consider the horizontal variation of the wind pressures around the building systematically, instead they assumed a hypothetical point which the total pressure vector was applied. More recently Sidarous and Vanderbilt introduced an analytical methodology for dynamic building response to wind loading using a model similar to that of Hart [26].

In this study a methodology for analyzing the coupled along-wind, cross-wind and torsional vibrations of wind excited structures is presented. The method is based on random vibration concepts and yields the expected maximum translational responses and the torsional response. The main objective was to develop a model for analyzing coupled along-wind, cross-wind and torsional response of structures that paralleled those used for analyzing along-wind responses. Thus, the approach would have the advantage both of being able to more thoroughly utilize the existing body of knowledge regarding wind structure and its effects and of being familiar to many design engineers.

A description of the structure of the wind near the ground is given in Chapter 2. The turbulence parameters, wind velocity profiles and suggested spectrum curves of the horizontal gustiness of the wind are introduced.

In Chapter 3, a discussion of wind loads on buildings is presented. The force mechanisms of along-wind and across-wind vibrations, wake buffeting and galloping are explained.

The responses of several single-mass type structures are investigated in Chapter 4 in order to identify which wind and structural properties significantly influence the torsional response and to determine whether the predicted torsional response is large enough to warrant extending the method to building-type structures. The results clearly indicate that torsional vibration can contribute a significant amount to the total motion of a wind excited structure.

Finally, the vibration of building type structures subjected to wind is formulated in Chapter 5. The structures are modeled as either shear beams or flexural beams with varying cross-sectional properties along the height. The response values of this analytical model are compared with those of full scale measurements and are found to be very satisfactory. Then, the effects of various structural parameters on the expected maximum translational responses and the rotational response are investigated.

A summary of the results and conclusions of the investigation are presented in Chapter 6. Recommendations for further research are also given.

CHAPTER 2

STRUCTURE OF THE WIND NEAR THE GROUND

2.1 - Introduction:

In this chapter a description of the forces in nature that generate the wind is given. Several of the properties of the wind near the ground that are of interest to engineers are also discussed. Suggested formulas to describe the structure of the wind mathematically are presented. These discussions will summarize the more complete descriptions which can be found in references [21], [9], [13], [31], [7].

2.2 - Structure of the wind:

The wind derives its energy from solar radiation which is strongest at the equator and weakest at the poles. This, and the radiation away from the earth, produces temperature differences and consequently pressure differences. The air in the atmosphere accelerates under the influence of these pressure gradients. The rotation of the earth about its own axis gives an additional acceleration, which is called Coriolis acceleration. In the free atmosphere away from the ground, the pressure gradient is balanced by the inertial effects and the motion is not affected by the earth's surface. The direction of the wind is not perpendicular but parallel to the isobars because of the effect of the rotational and centrifugal forces.

The layer in which the movement of the air is influenced by the surface friction is called the planetary boundary layer. The thickness of this layer, so-called gradient height, varies depending on the roughness of the terrain and is higher for rougher terrains. The wind

velocity at the gradient height is not influenced by the surface roughness and is called the gradient velocity. In this layer the air movement is not steady but gusty and the direction of the flow is no longer parallel to the isobars. This sort of activity in an air stream is called turbulence, and can be described as a random motion superimposed on a steady flow.

2.3 - Intensity and scale of turbulence:

The structure of turbulence is defined by two parameters, the intensity of turbulence and the scale of turbulence. The intensity of turbulence is a measure of the amplitude of the velocity fluctuations and is defined as the ratio of the r.m.s. value of the fluctuating velocity components to the mean velocity component. The longitudinal scale of the turbulence is a measure of the average size of the turbulent eddies in the direction of the mean flow. If it is assumed that the velocity vector, $V(t)$ at time t is the sum of a mean component, V_o, and fluctuating component, $w(t)$, (i.e. $V(t) = V_o + w(t)$), the mathematical expressions for the intensity, I, and the scale factor, L_x, are [31]

$$I = \frac{\sqrt{\overline{w(t)^2}}}{V_o} \quad , \tag{2.1}$$

and

$$L_x = V_o \frac{\int_o^\infty R_w(\tau)\, d\tau}{\overline{w(t)^2}} \tag{2.2}$$

where bar denotes the time average. $R_w(\tau)$ is known as the auto-covariance function which is given by

$$R_w(\tau) = \lim_{T \to \infty} \frac{1}{T} \int_{-T/2}^{T/2} w(t) \cdot w(t + \tau)\, dt \qquad (2.3)$$

It provides a measure of the independence between the values of w at times t and $t + \tau$. A schematic representation of $V(t)$, V_o, $w(t)$ and $R_w(\tau)$ is given in Figure (2.1)

2.4 - Velocity Profiles:

As given in the previous section, the total velocity of the wind at a point may be written as the sum of two components. In cartesian coordinates, assuming that the mean wind flow is parallel to the x axis it may be written

$$V(y,z,t) = V_o(z) + w(y,z,t) \qquad (2.4)$$

where $V_o(z)$ is the mean wind velocity which varies only with height above the ground and $w(y,z,t)$ is the fluctuating wind velocity which varies randomly in space and time. For the purpose of estimating the response of structures to wind leading it is useful and convenient to assume that the boundary layer flow is horizontally homogeneous. This assumption implies that the terrain is considered to be horizontal and the roughness of the terrain is assumed to be uniform over a sufficiently large fetch. In earlier structural analysis methods the mean wind

profile in horizontally homogenous terrain was represented by a power law model [5] , which is given by

$$V_o(z) = V_G \left(\frac{z}{z_G} \right)^{\alpha} \tag{2.5}$$

where V_G = gradient wind velocity

z_G = gradient height

α = the exponent.

z_G and α are dependent on the roughness of the terrain and their approximate values are z_G = 900, 1300, 1700 feet and α = 0.16, 0.28, 0.40 for open country, suburban terrain and for the center of large cities respectively. The relationship between the velocities over two adjacent terrain can be found by eliminating the constant gradient wind velocity, V_G. Thus

$$\frac{V_{o_1}(z)}{V_{o_2}(z)} = \frac{\left(\frac{z}{z_{G_1}} \right)^{\alpha_1}}{\left(\frac{z}{z_{G_2}} \right)^{\alpha_2}} \tag{2.6}$$

A more recent model for the profile of the mean wind velocity was suggested by Simiu [28] for use in structural design. It assumes a logarithmic profile which is given by:

$$V_o(z) = 2.5\, u_* \ell n \frac{z - z_d}{z_o} \tag{2.7}$$

where z_d = zero plane displacement

z_o = roughness length

u_* = friction velocity

The expression for friction velocity is

$$u_* = \frac{V_o(z_R)}{2.5 \ell n \frac{z_R - z_d}{z_o}} \tag{2.8}$$

in which z_R is any given reference height. The flow parameters z_o and z_d are determined empirically and are the functions of the nature, height and distribution of the roughness elements. As noted in reference [28], z_d may in all cases be assumed to be zero, except that in centers of large cities the smaller of the values z_d = 65.5 feet and $z_d = 0.75\bar{h}$ where $\bar{h}$ is the average height of the buildings in the surrounding area may be used. The values of roughness length z_o vary from 0.016 feet for coastal areas to 2.620 feet for the centers of large cities. The standard reference height is z_R = 33 feet. The relationship between wind velocities over two adjacent terrains can be found through the relationship between the friction velocities, which is approximately given by

$$\frac{u_{*1}}{u_{*2}} = \left(\frac{z_{01}}{z_{02}} \right)^{0.0706} \tag{2.9}$$

2.5 - Spectrum of turbulence:

Random vibration techniques have been found to provide the most powerful techniques to deal with structure-flow interaction problems. One of the classical methods is the spectral analysis technique. In order to use this method first the power spectrum of the input, which is the wind velocity in this case, needs to be determined.

The power spectrum is a representation of the distribution of the energy of the fluctuations in the wind with frequency. The spectrum of horizontal wind speed near the ground over an extended frequency range was calculated by Van der Hoven at Brookhaven, New York (Figure 2.2). A distinctive feature of this spectrum curve is that energy appears to be distributed into two frequency region separated by a large gap. The lower-frequency side of the gap corresponds to movements of air masses on a large-scale (weather map fluctuations) and the high frequency side of the gap corresponds to gustiness of the wind which is a consequence of the mechanical stirrings of the lower layers of the atmosphere by the roughness of the terrain. Thus, from these observations, it would seem that the components of a high-wind of most significance to the dynamics of structures are contained in the high frequency part of the wind spectrum. In this part the period of the contributions is less than an hour.

After analyzing numerous measurements at various sites, Davenport suggested the following empirical formula for this part of the spectrum curve, the so-called spectrum of horizontal gustiness [2]

$$S_w(n) = \frac{4KV_o^2\,(33)}{n} \cdot \frac{X^2}{(1 + X^2)^{4/3}} \qquad (2.10)$$

where $X = 4000\,\dfrac{n}{V_o(33)}$ in feet, n is the frequency in cps.,

and $V_o(33)$ is the mean wind velocity at the reference height of 33 feet. K is the surface drag coefficient which varies from 0.005 for open country to 0.050 for city centers. Davenport's spectrum is a single curve in nondimensional form as shown in Figure (2.3). In order to maintain the consistency that the energy in any frequency interval is represented by the area under the spectrum curve, at the logarithmic scale the vertical axis was taken $n.S_w(n)$ rather than $S_w(n)$ (i.e. $\int S_w(n)dn = \int n.S_w(n).\ d(Logn)$). The spectrum curve is independent of height and it has a peak at a wave length 2000 feet (i.e. $V_o(33)/n = 2000$). The area under the curve is equal to $6.0\ KV_o^2(33)$ and has the dimensions of energy as it should. Davenport's expression is currently used in building codes in many countries [1], [22].

Simiu proposed another equation for the spectrum of horizontal gustiness that is believed to be better founded in theory and reflects the dependence of the spectrum on the height [29]. Simiu's spectrum is given by the following expression

$$S_w(n) = \frac{u_*^2}{n} \cdot \frac{200f}{(1 + 50f)^{5/3}} \qquad (2.11)$$

in which $$f = \frac{n.z}{V_0(z)} \qquad (2.12)$$

and u_* is the friction velocity given by equation (2.8). This curve is slightly conservative for high frequencies. A more accurate and complicated form of it is given in reference [29].

CHAPTER 3

WIND FORCES ON BUILDINGS

3.1 - Introduction:

In this chapter a discussion of wind loads on buildings is presented. The force mechanisms of along-wind and cross-wind vibrations, wake buffeting and galloping are explained. Mathematical expressions for the forces used in the analysis are discussed.

Wind excited vibrations of buildings are due to individual or combined effects of the following dynamic force mechanisms in the wind: buffeting in the along-wind direction due to turbulence, buffeting in the across-wind direction due to vortex shedding, wake buffeting, and galloping. Each of these will be discussed in the following sections.

3.2 - Buffeting in the along wind direction due to turbulence:

As noted earlier, the wind velocity vector in the planetary boundary layer is composed of a steady mean part and the superimposed random fluctuating part (gust). The mean velocity is assumed to be constant over a long period when compared to the periods of vibration of the structure. This produces a static wind force and the random fluctuating part produces the dynamic wind force.

The pressure acting at a point of a fixed body in a turbulent flow is given by [31]

$$P(t) = \frac{1}{2} C_p . V^2(t) + \rho . C_m . W . \frac{dV(t)}{dt} \qquad (3.1)$$

where ρ = density of the air (0.0024 slugs/ft^3 or 1.25 kg/m^3)

C_p = pressure coefficient

$V(t)$ = total wind velocity

C_m = added mass coefficient

W = width of the body

This somewhat simplified representation of wind loads is called the quasi-static representation. Implicit in this expression are the assumptions that the aerodynamic force develops instantaneously and the disturbance in the oncoming flow by the object can be neglected. In the absence of a more complete theory this quasi-steady representation has been used throughout this study. The pressure coefficient C_p, and the added mass coefficient C_m are determined experimentally and depend upon the geometry of the object, the Reynolds number and the frequency of the velocity fluctuations. The velocity $V(t)$ in equation (3.1) is the relative velocity of the flow with respect to the object; therefore, the vibration velocity of the object should be included in the calculations. For building type structures this velocity is very small in comparison to the velocity of the wind and may be neglected. The second term in equation (3.1) is called the added mass term and can be significant if sudden changes in the velocity vector are likely to occur, such as in a tornado [41]. For strong wind flow conditions, Vickery and Kao examined the relative importance of the added mass term and concluded that it may be neglected for the purpose of determining pressures on bluff bodies [39]. With this and dividing the velocity into its mean and fluctuating components equation (3.1) can be written

$$P(t) = \frac{1}{2} \rho C_p [V_o + w(t)]^2 \tag{3.2}$$

or

$$P(t) = \frac{1}{2} \rho C_p . V_o^2 + \rho C_p . V_o . w(t) + \frac{1}{2} \rho C_p w^2(t) \tag{3.3}$$

The first term is the static mean wind pressure and the second and the third terms represent the dynamic wind pressure. For tall buildings, the intensity of turbulence which is the ratio of the r.m.s. value of the fluctuating wind velocities to the mean wind velocity, may vary from 0.05 to 0.30 depending upon building height and roughness of terrain. Therefore, the last term which is proportional to $w^2(t)$ is much smaller than the other terms. The contribution of this term to the total along-wind response of a tall structure was calculated using numerical simulation techniques by Vaicaitis and et.al. and found to be in the order of 3% [33]. Wind tunnel measurements have also showed that the contribution from non-linear terms to measured pressures were negligibly small [39]. Thus, it would be permissible and also convenient to linearize equation (3.3) as shown below.

$$P(t) = P_o + p(t) \tag{3.4}$$

with

$$P_o = \frac{1}{2} \rho C_p V_o^2 \tag{3.5}$$

and $$p(t) = \rho\, C_p . V_o . w(t) \qquad (3.6)$$

where P_o is the static mean wind pressure and p(t) is the randomly fluctuating wind pressure. Since P_o is not time dependent, the structure's response to it can be found through the static analysis. The response for p(t) will be determined using spectral analysis techniques. The convenience of having linear relationship between w(t) and p(t) is clear when it is remembered that w(t) is customarily assumed to be a stationary Gaussian random variable with zero mean. Thus, the fluctuating pressure, p(t), and the resultant response of a linear structure would also be Gaussian random variables with zero means. Thus, their spectral density functions and average values could easily be calculated in terms of those of w(t).

3.3 - Buffeting in the across-wind direction due to vortex shedding:

Recent laboratory tests on dynamic models have confirmed that vortex sheddings are the main reason for across-wind direction vibrations [25]. The mechanism of vortex shedding is shown in Figure (3.1). When a bluff body is exposed to wind, eddies form at the points of separation and a regular pattern of vortices moving clockwise and counterclock wise (so-called Karman Vortex Street) develops. The formation of vortices cause velocity differences, and consequently pressure differences, between the upper and lower sections of the wake. Consequently, a fluctuating lift force acts perpendicular to the mean flow and changes its direction at the shedding frequency. For a fixed mean stream velocity, the frequency of vortex shedding is rather regular

(nearly constant in many cases) and depend upon the shape and size of the body and the Reynolds number. If the cross-section of the body is noncircular, it also depends on the wind direction. This regular pattern of the vortex shedding is characterized with a dimensionless constant, the so called Strouhal number, which is given by

$$S = \frac{n_s . W}{V_o} \tag{3.7}$$

where n_s is the dominant frequency of the vortex shedding. For a body having a rectangular or square cross section the Strouhal number is almost independent of the Reynolds number. For square cross-sections with wind blowing perpendicular to a face it can be taken $S = 0.11$ [9]. The lift force per unit length at height z of a building for normally incident wind can be written as

$$F_L(z,t) = \frac{1}{2} \rho W . V_o^2 (z) . C_L(t) \tag{3.8}$$

where $C_L(t)$ is the randomly fluctuating lift coefficient. The spectra of $C_L(t)$ is concentrated around the vortex shedding frequency and has a very small bandwidth (Figure 3.2) [35]. This spectrum curve can be approximated by the following Gaussian type curve which has a sharp peak at $n = n_s$

$$S_{C_L}(n) = \sigma_{C_L}^2 . \frac{1}{\sqrt{\pi}\, B n_s} \exp \left[- \left(\frac{1 - n/ns}{B} \right)^2 \right] \tag{3.9}$$

where $\sigma_{C_L} = \sqrt{\overline{C_L^2(t)}}$, the standard deviation of $C_L(t)$ and B is the bandwidth. When it is normalized by $\sigma_{C_L}^2$ the area under the spectrum curve is constant, such that

$$\int_0^\infty \frac{1}{\sqrt{\pi}\, Bn_s} \exp\left[-\left(\frac{1 - n/ns}{B} \right)^2 \right] dn = 1.00 \qquad (3.10)$$

The value of σ_{C_L} is given $\sigma_{C_L} = 0.60$ for buildings with square cross-section and normally incident wind [9]. This value which is given for the centerline of the side face represents the total lift force at that height. Thus, the sidewise correlation (also called chordwise correlation) of the lift force is automatically included in the value.

3.4 - Wake Buffeting

Wake buffeting occurs if one structure is located in the wake of another structure. Vortices shed from the upstream structure may cause oscillation of the downstream structure. These oscillations may be very significant for the downstream structure if the two structures are similar in shape and size and less than ten diameters apart [9]. Since wake buffeting is a rather special and complex phenomenon wind tunnel tests are required for this type of analysis.

3.5 - Galloping:

Galloping is an oscillation induced by the forces which are generated by the motion itself. These forces, in general, oppose the motion and produce positive aerodynamic damping (stabilizing effect).

Sometimes, in structures like transmission lines or long slender towers with sharp edged cross sections these forces with the continuous change in the angle of the approach of the wind result in negative damping which may be larger than the positive structural damping. The reason for this is the peculiarity of the relationship between lift and drag coefficients of the cross-section for different values of the angle of approach.

To understand the mechanism of galloping consider a body, as shown in Figure (3.3), in a flow with velocity V. As the body moves with a velocity $\dot{y}$ perpendicular to the direction of the flow, the angle of attack, α, of the relative wind velocity, V_{rel}, can be written

$$\alpha = \text{artan} \frac{\dot{y}}{V} \tag{3.11}$$

The drag and lift forces produced by the relative velocity are given by

$$D = C_D \cdot \frac{1}{2} \rho . A . V_{rel}^2 \tag{3.12}$$

$$L = C_L \cdot \frac{1}{2} \cdot \rho . A . V_{rel}^2 \tag{3.13}$$

where C_D and C_L are the drag and lift coefficients at angle of attack α, respectively, and A is the frontal area of the body. The sum of the components of these forces in the direction of y is

$$F_y = -(C_D.\sin\alpha + C_L.\cos\alpha)\,\frac{1}{2}\rho A V^2.\sec^2\alpha \qquad (3.14)$$

or $$F_y = C_{F_y}\,\frac{1}{2}\rho A V^2 \qquad (3.15)$$

where $$C_{F_y} = -(C_L + C_D \tan\alpha)\sec\alpha \qquad (3.16)$$

As can be seen from Eq. (3.11) α increases with increasing $\dot{y}$. In order to have a stable system, therefore, F_y should decrease as α increases. This can be satisfied if

$$\frac{d\,C_{Fy}}{d\alpha}\Bigg|_{\alpha = 0} < 0 \qquad (3.17)$$

or

$$\frac{d\,C_L}{d\alpha} + C_D > 0 \qquad (3.18)$$

Thus instability will occur only if

$$\frac{d\,C_L}{d\alpha} + C_D < 0 \qquad (3.19)$$

This condition is known as "Den Hartog's Criterion" and a necessary condition for aerodynamic instability [31]. It is also sufficient when the left hand side of the Eq. (3.19) becomes small enough to offset structural damping forces.

Tall buildings with the values of damping, height and cross-section that they may have in current design practice are not susceptible to galloping. Davenport and Novak indicated that hurricane size wind velocities for a smooth flow (possibly much higher velocities for turbulent flow) would require to start galloping oscillations in a tall building [26].

CHAPTER 4

VIBRATION OF SINGLE-MASS STRUCTURES

4.1 - Introduction:

In this chapter the vibration of a single-mass structure under wind loads is formulated. The method is based on random vibration concepts and yields the expected maximum translational and torsional responses. The objective of this chapter is to identify which wind and structural properties significantly influence the torsional response and to determine whether the predicted torsional responses were large enough to warrant extending the method to building-type sturctures for use in design.

4.2 - Equations of vibration:

Consider the schematic of an idealized single-mass structure with approaching wind shown in Figure (4.1). The center of the coordinate system is located at the mass center; W is the frontal width and D is the vertical depth of the structure. W_1 and W_2 denote the distances from the edges of the structure to the center of the coordinate system ($W_1 + W_2 = W$) and W_e is the distance between the elastic center and the mass center. It was assumed that the structure is symmetric in cross-wind direction and the along-wind dimension of the structure, L, is small in comparison to W. Therefore the effect of the cross-wind forces on torsional vibrations was neglected. With the coordinate system and notation shown in Figure (4.2), the equations of motion of the system may be written

$$m\ddot{x} + c_x\dot{x} + k_x x + k_x . W_e . \theta = F(t) \tag{4.1}$$

$$I_m\ddot{\theta} + c_\theta\dot{\theta} + k_x W_e x + (k_\theta + k_x W_e^2)\theta = T(t) \tag{4.2}$$

where m : total mass of the structure

I_m : mass moment of inertia

k_x, k_θ : translational and rotational stiffnesses

c_x, c_θ : translational and rotational dampings

$F(t)$, $T(t)$: fluctuating force and torque

Since $F(t)$ and $T(t)$ are random variables in space and time, the dynamic responses $x(t)$ and $\theta(t)$, will also be random variables. Therefore the solution procedure requires the application of the random vibration theory. Using classical spectral analysis technique the relationship between forces and responses in the frequency domain may be written [20]

$$[S_r(n)] = [H(n)]\,[S_f(n)]\,[H^*(n)]^T \tag{4.3}$$

where

n : frequency in cycles per second

$[S_r(n)]$: spectral density matrix of the response vector $\{r\}$

$[S_f(n)]$: spectral density matrix of the force vector $\{f\}$

$[H(n)]$: system frequency response matrix and (*) denotes the complex conjugate.

The response and force vectors, from Eqs. (4.1) and (4.2), may be written

$$\{r\} = \begin{Bmatrix} x(t) \\ \theta(t) \end{Bmatrix} \tag{4.4}$$

and

$$\{f\} = \begin{Bmatrix} F(t) \\ T(t) \end{Bmatrix} \tag{4.5}$$

Therefore, the explicit forms of $[S_r(n)]$ and $[S_f(n)]$, from App.(A), are

$$[S_f(n)] = \begin{bmatrix} S_{xx}(n) & S_{x\theta}(n) \\ S_{\theta x}(n) & S_{\theta\theta}(n) \end{bmatrix} \tag{4.6}$$

$$[S_f(n)] = \begin{bmatrix} S_{FF}(n) & S_{FT}(n) \\ S_{TF}(n) & S_{TT}(n) \end{bmatrix} \tag{4.7}$$

A typical term $S_{ij}(n)$ of the matrices given above is the cross spectral density function of the random variables (i) and (j). Definition of the cross spectral density function is given in Appendix (A). The derivation of the system tranfer matrix is well known and may be written [20]

$$[H(n)] = \{ -\omega^2 [M] + i\omega [C] + [K]\}^{-1} \tag{4.8}$$

where [M], [C] and [K] are respectively the system mass, damping and stiffness matrices and ω is the frequency in radians per second ($\omega = 2\pi n$).

The explicit forms of [M], [C] and [K], from Eqs. (4.1) and (4.2), are

$$[M] = \begin{bmatrix} m & o \\ o & I_m \end{bmatrix} \tag{4.9}$$

$$[C] = \begin{bmatrix} c_x & o \\ o & c_\theta \end{bmatrix} \tag{4.10}$$

$$[K] = \begin{bmatrix} k_x & k_x W_e \\ k_x W_e & k_\theta + k_x W_e^2 \end{bmatrix} \tag{4.11}$$

Thus, [H(n)] is a 2x2 matrix and may be written

$$[H(n)] = \begin{bmatrix} H_{xx}(n) & H_{x\theta}(n) \\ H_{\theta x}(n) & H_{\theta\theta}(n) \end{bmatrix} \tag{4.12}$$

The physical meaning of a typical element, for instance $H_{\theta x}(n)$, of the frequency response matrix is that it is the ratio of the steady state response $\theta(t)$ to the harmonic excitation $f_x(t) = e^{i\omega t}$. Since all of the elements of [H(n)] are readily determined from the properties of the structure, one needs only to derive the elements of the input spectral density matrix to be able to determine the spectral density matrix of the response.

The along-wind fluctuating pressure at a point on the structure's face, as explained in Chapter 3 and given by Eq. (3.6), may be written

$$p(y,z,t) = \rho\, C_p(y,z)\, V_o(z)\, w(y,z,t) \tag{4.13}$$

where $V_o(z)$ and $w(y,z,t)$ are respectively the mean and fluctuating wind velocities and $C_p(y,z)$ is the pressure coefficient at that point with ρ being the mass density of the air. These fluctuating pressures produce the randomly varying force and torque which can be approximated

$$F(t) \tilde{=} \rho C_D \iint_A V_o(z)\, w(y,z,t)\, dydz \tag{4.14}$$

$$T(t) \tilde{=} \rho C_D \iint_A y\, V_o(z)\, w(y,z,t)\, dydz \tag{4.15}$$

where A is the area of the frontal face and C_D is the sum of the averaged pressure coefficients of the windward and leeward faces. The use of of C_D in this manner implies that it can be assumed constant for every point and the pressure fluctuations on the windward and leeward faces are perfectly correlated. Even though experiments have suggested that the latter assumption is not usually true [18], it results in conservative estimates of displacements [29], it greatly simplifies the following derivations, and this simplification is probably not unwarranted in light of all the other assumptions that are made. The entries in the 2x2 spectral density matrix of the forces are given in Eq. (4.7) and

they are the Fourier transforms of the correlation functions of the force and torque and of their cross-correlation function as explained in detail in Appendix (A). They may, from Eqs. (4.14), (4.15) and App.(A), be written in terms of the cross-spectra of the fluctuating velocity

$$S_{FF}(n) = (\rho C_D)^2 \int_A \int_A V_o(z_1) V_o(z_2)\, S_w(y_1,z_1,y_2,z_2,n)\, dy_1 dy_2 dz_1 dz_2 \qquad (4.16)$$

$$S_{TT}(n) = (\rho C_D)^2 \int\int\int\int y_1 y_2\, V_o(z_1) V_o(z_2)\, S_w(y_1,z_1,y_2,z_2,n) dy_1 dy_2 dz_1 dz_2 \qquad (4.17)$$

$$S_{FT}(n) = (\rho C_D)^2 \int_A \int_A y_2\, V_o(z_1) V_o(z_2) S_w(y_1,z_1,y_2,z_2,n)\, dy_1 dy_2 dz_1 dz_2 \qquad (4.18)$$

Based on experimental evidence, the cross-spectra of the wind velocity may be written as the product of the spectrum of the wind velocity and the coherence function [37]

$$S_w(y_1,z_1,y_2,z_2,n) = S_w^{1/2}(z_1,n) S_w^{1/2}(z_2,n)\, Coh(y_1,z_1,y_2,z_2,n) \qquad (4.19)$$

The suggested expressions for $S_w(z,n)$ are given in Chapter 2 by the equations (2.10) and (2.11). Note that Davenport's model, Eq. (2.10), is independent of z. The coherence function may be represented by the following expression [37]

$$\mathrm{Coh}(y_1,z_1,y_2,z_2,n)= \exp\left[- \frac{2n[C_y^2(y_1-y_2)^2 + C_z^2(z_1-z_2)^2]^{1/2}}{V_o(z_1) + V_o(z_2)} \right] \qquad (4.20)$$

where C_y and C_z are called the exponential decay coefficients for the y and z directions respectively. The approximate values of the exponential decay coefficients used in wind analysis are C_y=16, and C_z=10. However experiments show that those values may differ depending upon terrain roughness, height above ground, and wind speed, and therefore represent a source of uncertainty [31]. As seen from Eq.(4.20) the coherence function is dependent upon the relative distances between the points rather than the location of the points.

Thus far, the development of the random along-wind forces on a structure has been general and would apply to any structure that is rectangular in plan. The computations may be greatly simplified for the simple two-degree-of-freedom structure of Figure (4.1). Since the mean wind velocity varies slowly with height

$$V_o(z_1) \approx V_o(z_2) \approx V_o(H) = V_o \qquad (4.21)$$

where H is the height to the center of the structure. The coherence function given in Eq.(4.20) can be separated into its y and z components by using the approximation suggested in reference [7]. Also using the approximation given above for the mean velocity and introducing the nondimensional variables

$$\varepsilon = \frac{y}{W} \qquad \text{and} \qquad \eta = \frac{z}{D} \tag{4.22}$$

Eq.(4.20) becomes

$$\text{Coh}(\varepsilon_1,\varepsilon_2,\eta_1,\eta_2,n) = \exp\left[-\frac{n\phi}{V_o}\left[C_y W \mid \varepsilon_1-\varepsilon_2\mid + C_z D \mid \eta_1-\eta_2\mid\right]\right] \tag{4.23}$$

$$\text{where} \qquad \phi = \frac{\sqrt{1+r^2}}{1+r} \qquad \text{with} \qquad r = \frac{C_y W}{C_z D} \tag{4.24}$$

Using Eqs.(4.19) and (4.21) and changing the variables of the integrals as given by Eq.(4.22), Eqs.(4.16) - (4.18) may be put in more compact form

$$S_{FF}(n) = \frac{4F_o^2}{V_o^2} S_w(n)\, J_{xx}(n) \tag{4.25}$$

$$S_{TT}(n) = \frac{4F_o^2\, W^2}{V_o^2} S_w(n)\, J_{\theta\theta}(n) \tag{4.26}$$

$$S_{FT}(n) = \frac{4F_o^2\, W}{V_o^2} S_w(n)\, J_{x\theta}(n) \tag{4.27}$$

where F_o is the mean static wind force on the structure given by the following equation

$$F_o = \frac{1}{2} \rho C_D V_o^2 WD \tag{4.28}$$

and $J_{xx}(n)$, $J_{\theta\theta}(n)$ and $J_{x\theta}(n)$ are the nondimensional aerodynamic admittance functions which are defined as shown below

$$J_{xx}(n) = \int_0^1 \int_{-W_{2/W}}^{W_{1/W}} \text{Coh}(\varepsilon_1,\varepsilon_2,\eta_1,\eta_2,n)\, d\varepsilon_1 d\varepsilon_2 d\eta_1 d\eta_2 \tag{4.29}$$

$$J_{\theta\theta}(n) = \int_0^1 \int_{-W_{2/W}}^{W_{1/W}} \varepsilon_1\varepsilon_2\, \text{Coh}(\varepsilon_1,\varepsilon_2,\eta_1,\eta_2,n)\, d\varepsilon_1 d\varepsilon_2 d\eta_1 d\eta_2 \tag{4.30}$$

$$J_{x}(n) = \int_0^1 \int_{-W_{2/W}}^{W_{1/W}} \varepsilon_2\, \text{Coh}(\varepsilon_1,\varepsilon_2,\eta_1,\eta_2,n)\, d\varepsilon_1 d\varepsilon_2 d\eta_1 d\eta_2 \tag{4.31}$$

Since coherence function is symmetric with respect to $\varepsilon_1=\varepsilon_2$, $J_{x\theta}(n) = J_{\theta x}(n)$ and consequently $S_{FT}(n) = S_{TF}(n)$. Using Eq.(4.23) the admittance functions can be evaluated analytically. Their final forms are given by the following expressions and their variations with frequency for different values of W_1 and W_2 are given in Figure (4.4).

$$J_{xx}(n) = \left[\frac{2}{D_y^2}\left(e^{-D_y} + D_y - 1\right)\right]\cdot\left[\frac{2}{D_z^2}\left(e^{-D_z} + D_z - 1\right)\right] \tag{4.32}$$

$$W^2 J_{\theta\theta}(n) = \left[\frac{2}{3D_y} (W^2 - 3W_1W_2) - \frac{1}{D_y^2} (W_1^2 + W_2^2) + \frac{2W^2}{D_y^4} - \right.$$

$$\left. - \frac{2}{D_y^4} (W^2 + D_y W^2 + D_y^2 W_1 W_2) e^{-D_y} \right] \cdot \left[\frac{2}{D_z^2} (e^{-D_z} + D_z - 1) \right] \qquad (4.33)$$

$$WJ_{x\theta}(n) = \frac{(W_1 - W_2)}{2} J_{xx}(n) \qquad (4.34)$$

where $$D_y = \frac{nC_y W}{V_o} \quad \text{and} \quad D_z = \frac{nC_z W}{V_o} \qquad (4.35)$$

As seen from Figure (4.4) $J_{yy}(n)$ is invariant with respect to coordinate center and $J_{\theta\theta}$, $J_{y\theta}$ increase as the geometric offset increases. The spectral density matrix of the excitation is now defined and the input-output relationship given by Eq.(4.3) can be written more explicitly as shown below

$$\begin{bmatrix} S_{xx} & S_{x\theta} \\ S_{\theta x} & S_{\theta\theta} \end{bmatrix} = \begin{bmatrix} H_{xx} & H_{x\theta} \\ H_{\theta x} & H_{\theta\theta} \end{bmatrix} \cdot \frac{4F_o^2 S_w(n)}{V_o^2} \cdot \begin{bmatrix} J_{xx} & WJ_{x\theta} \\ WJ_{\theta x} & W^2 J_{\theta\theta} \end{bmatrix} \begin{bmatrix} H^*_{xx} & H^*_{x\theta} \\ H^*_{\theta x} & H^*_{\theta\theta} \end{bmatrix}^T$$

(4.36)

where all of the S, H and J terms are functions of frequency n. Note that for $W_e = 0$ (mass center and elastic center coincide) $H_{\theta x} = H_{x\theta} = 0$. Thus, the equations of motion for free vibration are uncoupled. However, as long as $W_1 \neq W_2$ (mass center is not at the geometric center), they are statistically coupled (correlated) due to the fact that $J_{x\theta} = J_{\theta x} \neq 0$ in equation (4.36). If both $W_e = 0$ and $W_1 = W_2$ all the off diagonal terms of the matrices in Eq.(4.36) are zero. In other words the equations are uncoupled and the excitations F(t) and T(t) are uncorrelated; therefore, the responses x(t) and θ(t) are also uncoupled and uncorrelated.

4.3 - Maximum values of the response

Once the functions of the spectral density matrix of the response have been formulated, the mean square translational and rotational motions as well as their correlation coefficient may be computed

$$\sigma_x^2 = \int_0^\infty S_{xx}(n)\, dn \tag{4.37}$$

$$\sigma_\theta^2 = \int_0^\infty S_{\theta\theta}(n)\, dn \tag{4.38}$$

and

$$\rho_{y\theta} = \frac{1}{\sigma_y \sigma_\theta} \int_0^\infty S_{y\theta}(n)\, dn \tag{4.39}$$

Since the fluctuating wind velocity, and consequently F(t) and T(t), have been defined as zero-mean Gaussian random variables, the responses

$x(t)$ and $\theta(t)$ of this linear system are also zero-mean Gaussian random variables. Thus, the standard deviations and the correlation coefficient given by Eqs.(4.37)-(4.39) are sufficient to describe the response statistics.

If it is assumed that the total displacement of a point on the structure, $x(y,z,t)$, is independent of height, z, the translation of any point may be written

$$x(y,z,t) \approx x(y,t) = x_o + x(t) + y\,[\theta_o + \theta(t)] \tag{4.40}$$

where x_o and θ_o are respectively the static displacement and the rotation of the center of the structure due to the static mean wind force. The spectral density function of $x(y,t)$ may, from Eq.(4.40) and App(A), be written

$$S_x(y,n) = S_{xx}(n) + y^2 S_{\theta\theta}(n) + 2y.\text{Real}[S_{y\theta}(n)] \tag{4.41}$$

The mean square value of $x(y,t)$ is

$$\sigma_x^2(y) = \int_o^\infty S_x(y,n)\,dn \tag{4.42}$$

The expected maximum value of $x(y,t)$ in a time interval T can be written as the sum of its mean value plus a factor of its standard deviation. That is

$$E\,[x_{max}(y,t)] = x_o + y.\theta_o + g.\sigma_x(y) \tag{4.43}$$

The factor g is called the peak factor and for a Gaussian random variable it is approximated by the following expression which was developed by Davenport [4]

$$g = \sqrt{2\ell n(\nu T)} + \frac{0.577}{\sqrt{2\ell n(\nu T)}} \tag{4.44}$$

where

$$\nu = \frac{\int_0^\infty n^2 S_x(y,n)\, dn}{\int_0^\infty S_x(y\ n)\, dn} \tag{4.45}$$

The expected maximum value can be taken as the most probably value due to the fact that the bandwidth of the maximum probability distribution function is very narrow. The time interval, T, is taken T=3600 seconds in wind analysis. Thus, an estimate of the most probable maximum displacement including torsion of any point on the structure can be made.

4.4 - Numerical Examples:

The equations derived above were used to analyze the responses of several variations of the structure in Figure 4.1. The basic structure has a width, W, equal to 20 feet and a depth, D, equal to 20 feet for an exposure area of 400 sq. ft. The reference wind velocity of 80 miles per hour and the translational natural frequency, n_y, of 1.0 Hz were held constant for all examples. The effects of magnitude of the torsional

natural frequency, the structure's width, and the location of the centers of mass and rigidity on the maximum probable response values were examined. For each example where the structure is nonsymmetric, the expected maximum edge displacement, max Y_A, computed using equation (4.43) is normalized by the expected maximum displacement that would be computed if the dynamic torsional motion were ignored. The latter quantity is simply the expected maximum along-wind displacement for the center of a symmetric structure plus the displacement due to the static rotation, $x\theta_o$. The normalization was done this way because designers would normally compute the mean rotation in their calculations. Thus, the results reflect the consequence of ignoring only the dynamic torsional response in design.

The examples may be divided into three classes according to the form of equation (4.36). For a perfectly symmetric structure the centers of mass and resistance both lie on the vertical centerline of the structure's face. For this case all of the off-diagonal terms in equation (4.36) are identically equal to zero. Thus, the equations of motion are uncoupled. This means that the translational and rotational motions are statistically independent and may be evaluated independently. Note that torsional vibrations will still be excited, however, due to the spatial randomness of the wind.

The effects of varying the structure's torsional natural frequency on the expected maximum displacement of point A are shown in Figure (4.3) As n_θ decreases with respect to n_y, the motions at the edge of the structure due to torsional vibrations become large and may actually be

substantially larger than those due to translation. Most of the effect associated with lowering the torsional frequency results from the shape of the wind spectrum which increases with decreasing frequency in this region of the spectrum. This is also demonstrated in Figure (4.3) where results are shown for the 20' x 20' structure which was assumed to be excited by an artificial wind with a "white noise" spectrum, but with the same spatial correlation as the natural wind.

It should also be expected that increasing the width of the structure would increase the rotational response. This should result because pressures at the extreme edges of the structure would be less correlated and would lie further from the elastic center. Both of these effects would produce greater dynamic torque. This is demonstrated in Figure (4.3) for a structure with a width and depth equal to 30.0 and 13.33 ft. respectively. These values were chosen so that the total exposure area would remain constant.

The second class of structures has only one type of asymmetry, either geometric or structural. Geometric asymmetry occurs if a structure has its centers of mass and rigidity on the same line, but not on the centerline of the exposed face. The equations of motion for this case are still uncoupled (e.g. $H_{y\theta} = H_{\theta y} = 0$). However, the cross aerodynamic admittance functions, $J_{y\theta}$ and $J_{\theta y}$, are no longer zero. Therefore, the correlation coefficient for the responses is also non-zero and coupling of the responses results. The aerodynamic admittance functions for 20' x 20' structures with their center of the coordinate system located 10, 12, 14 and 16 feet from point A are shown in

Figure (4.4). Note that J_{yy} is invariant with respect to the coordinate center and that $J_{\theta\theta}$ and $J_{y\theta}$ increase as the geometric offset increases. Thus, the correlation coefficient is coordinate-system dependent. Also, as was mentioned above, $J_{y\theta}(n)$ is identically equal to zero for W_1 = 10 feet which corresponds to the coordinate system located at the geometric center of the structure. The correlation coefficients for these same structures with varying torsional frequency are shown in Figure (4.5). The highest correlation in the responses occurs when $n_\theta = n_y$ as should be expected. This value approaches 1.0 as the geometric offset increases. In general, the response correlation increases as n_θ approaches n_y and as W_1/W increases.

The effects of varying the rotational natural frequency and W_1/W on the maximum displacement at point A are shown in Figure (4.6). The results show the same trend as for the perfectly symmetric structures. The torsional natural frequency has the largest effect on the rotational response. In addition, the rotational response increases as W_1/W increases. Note that for a structure with its centers of mass and resistance offset only 10% of its width from the geometric center ($W_1/W = 0.6$), if the dynamic part of the torsional displacement of the edge of the structure is not computed the maximum displacement will be underestimated by about 25% for $n_\theta = n_y$ and by about 80% for $n_\theta = 0.5\ n_y$.

If the mass center is located at the structure's geometric center but the elastic center is not, structural nonsymmetry results and $H_{y\theta}(n)$ is no longer zero. The cross-aerodynamic admittance functions will again be zero, however, since the reference system is located at

the geometric center of the structure. Results for structures with different torsional frequencies and eccentricities are shown in Figure (4.7). These results are very similar to those for structures with only geometric nonsymmetry shown in Figure (4.6) Neglecting the dynamic part of the torsional displacement for a structure with an eccentricity of 10% of its width will once more lead to underestimates of the maximum total displacement of 25% for $n_\theta = n_y$ and 80% for $n_\theta = 0.5n_y$.

The most general case occurs when the centers of mass, resistance and geometry lie on different lines. This results in all of the matrices of equation (4.36) being full. Shown in Figure (4.8) are the results for structures with their mass center offset 10% of the structure's width (W_1 = 12 feet) from its geometric center. As expected, these motions increase with decreasing torsional natural frequency. Figure (4.8) is somewhat misleading since it shows decreasing torsional response with increasing eccentricity for W_e/W less that 0.1. In this region, the elastic center moves from the mass center for $W_e/W = 0$ to the geometric center for $W_e/W = 0.1$. The fact that the torsional motion decreases in this region indicates the distance between the elastic center and the geometric center where the average pressure center lies is more influential than the distance between the elastic and mass centers. For a structure with W_e = 2 feet the elastic center is at the geometric center. By ignoring the dynamic torsional response for this case, the maximum displacement of the edge of the structure would be underestimated by about 25% for $n_\theta = n_y$ and 50% for $n_\theta = 0.5\ n_y$.

4.5 - Discussion and Conclusions:

A method for estimating the expected maximum dynamic torsional response of a wind-excited two degree-of-freedom structure was presented. Aerodynamic admittance functions were derived which were used to estimate the spectral density function of the random torque and cross-spectral density function of the force and torque acting on the structure. These are required for estimating the structure's translational and torsional mean square responses. Results for several examples indicated that, in general, the dynamic torsional response increases as the width of the structure's exposed face increases, as the structural or geometric eccentricity increases and as the torsional natural frequency decreases. It was shown that for an eccentricity of only 10% of the structure's width, the total response of a structure can be significantly underestimated if the dynamic torsional response is not included in the analysis.

CHAPTER 5

VIBRATION OF BUILDINGS

5.1 - Introduction:

Structurally, the buildings of the current design practice can be categorized as frame systems, frame-shear wall systems or for very tall buildings, tubular systems. Vibration tests indicate that fundamental mode shapes of buildings under dynamic loading are about midway between the fundamental mode shape of a shear beam and of a flexural beam. For buildings with moderate heights and frame type structure it can be assumed that the change of the length of the columns due to the axial load is negligibly small and the story floors remain approximately horizontal during the displacements. Therefore, the lateral load is carried by the shear resistance of the frames and the behavior is similar to that of a shear beam. As the height of the building increases the axial displacements of the columns become more significant and the floor planes are no longer horizontal during the vibration of the buildings. Also, some buildings are designed to carry lateral loads only by shear walls. In these cases the behavior of the buildings can be predicted better by assuming a flexural beam mode shape. In this chapter equations for the coupled vibrations of a building are derived for a shear beam model while the final forms of the equations for flexural beam model are given in Appendix(B).

5.2 - Equations of Motion:

Consider the schematic of a building in Figure (5.1) with the wind blowing parallel to the x axis in a cartesian coordinate system.

The lateral displacements of the center line of the structure are denoted by $u(z,t)$ and $v(z,t)$ in the directions of x and y respectively; and the rotation by $\theta(z,t)$, positive in the counterclock wise direction. For simplicity the parameters z and t of the displacements and of the rotation were not written in most of the equations and they were simply denoted as u, v, θ. The coordinate center was assumed to be at the center of geometry. Therefore the z axis is at the center of the rectangular cross-section at every level along the height. Consider a small particle of the structure at height z as shown in Figure (5.1). Let the coordinates of this particle in the undeformed structure be x, y, z and the mass density $\rho(x,y,z)$. As the structure displaces u, v, θ in the corresponding directions the new coordinates of the point become

$$x' = x + u - y\theta \tag{5.1}$$

$$y' = y + v + x\theta \tag{5.2}$$

$$z' = z \tag{5.3}$$

and the relative displacements are

$$\Delta x = u - y\theta \tag{5.4}$$

$$\Delta y = v + x\theta \tag{5.5}$$

$$\Delta z = 0 \tag{5.6}$$

The kinetic energy gained by the particle located at that point is

$$t_{KE} = \frac{1}{2}\rho(x,y,z)\left[\left(\frac{\partial(\Delta x)}{\partial t}\right)^2 + \left(\frac{\partial(\Delta y)}{\partial t}\right)^2\right] \tag{5.7}$$

or

$$t_{KE} = \frac{1}{2}\rho(x,y,z)\left[(\dot{u} - y\dot{\theta})^2 + (\dot{v} + x\dot{\theta})^2\right] \tag{5.8}$$

where $\rho(x,y,z)$ is the mass density of the particle and ($\dot{}$) denotes the partial derivative with respect to time. The total kinetic energy of the structure is obtained by integration

$$T_{KE} = \frac{1}{2}\int_0^H \iint_{A(z)} \rho(x,y,z)\left[(\dot{u} - y\dot{\theta})^2 + (\dot{v} + x\dot{\theta})^2\right] dxdydz \tag{5.9}$$

where H is the height of the building and A(z) is the cross-sectional area at height z. Noting that

$$\iint_{A(z)} \rho(x,y,z)\, dzdy = m(z) \tag{5.10}$$

$$\iint_{A(z)} (x^2 + y^2)\,\rho(x,y,z)\, dxdy = I(z) \tag{5.11}$$

where m(z) and I(z) are the mass and moment of inertia per unit length

at height z, respectively. Also, if $x_g(z)$ and $y_g(z)$ denote the coordinates of the center of the mass at height z

$$\iint_{A(z)} x.\rho(x,y,z)\, dxdy = x_g(z)m(z) \tag{5.12}$$

$$\iint_{A(z)} y.\rho(x,y,z)\, dxdy = y_g(z)m(z) \tag{5.13}$$

Thus, the total kinetic energy of the structure is

$$T_{KE} = \frac{1}{2} \int_0^H [m(z)\, \dot{u}^2 + m(z)\, \dot{v}^2 + I(z)\, \dot{\theta}^2 + \tag{5.14}$$

$$+ 2\, x_g(z)m(z)\dot{v}\dot{\theta} - 2\, y_g(z)m(z)\dot{u}\dot{\theta}]\, dz$$

The strain energy of the same particle due to the displacements Δx, Δy and $\Delta z = 0$ can be written [32]

$$u_{SE} = \frac{1}{2}\left[G_{xz}(x,y,z)\left(\frac{\partial(\Delta x)}{\partial z}\right)^2 + G_{yz}(x,y,z)\left(\frac{\partial(\Delta y)}{\partial z}\right)^2\right] \tag{5.15}$$

or

$$u_{SE} = \frac{1}{2}\left[G_{xz}(x,y,z)\, (u' - y\theta')^2 + G_{yz}(x,y,z)\, (v' + x\theta')^2\right] \tag{5.16}$$

where $G_{xa}(x,y,z)$ and $G_{yz}(x,y,z)$ are the modulus of rigidity in x-z and

y-z planes at height z, respectively, and ( )' denotes the partial derivative with respect to z. The total strain energy of the structure may then be expressed as

$$U_{SE} = \frac{1}{2} \int_0^H \iint_{A(z)} [G_{xz}(x,y,z)\ (u'-y\theta')^2 + G_{yz}(x,y,z)(v'+ x\theta')^2] \ dxdydz \tag{5.17}$$

introducing the following notation

$$\iint_{A(z)} G_{xz}(x,y,z)\ dxdy = k_x(z) \tag{5.18}$$

$$\iint_{A(z)} G_{yz}(x,y,z)\ dxdy = k_y(z) \tag{5.19}$$

$$\iint_{A(z)} [x^2 G_{yz}(x,y,z) + y^2 G_{xz}(x,y,z)]\ dxdy = k_\theta(z) \tag{5.20}$$

$$\iint_{A(z)} x\ G_{yz}(x.y,z)\ dxdy = x_e(z)\ k_y(z) \tag{5.21}$$

$$\iint_{A(z)} y\ G_{xz}(x,y,z)\ dxdy = y_e(z)\ k_x(z) \tag{5.22}$$

where $k_x(z)$, $k_y(z)$ and $k_\theta(z)$ are the translational stiffnesses and the rotational stiffness at height z and $x_e(z)$ and $y_e(z)$ are the coordinates of the center of rigidity. The total strain energy of Eq.(5.17) becomes

$$U_{SE} = \frac{1}{2}\int_0^H [k_x(z)u'^2 + k_y(z)v'^2 + k_\theta(z)\theta'^2 + 2x_e(z)k_y(z)v'\theta' - 2y_e(z)k_x(z)u'\theta']\,dz \qquad (5.23)$$

The potential energy of the structure is equal to the sum of the strain energy and the potential energy of the conservative external forces. If $P_x(y,z,t)$ is the sum of the pressures at points y,z of the faces perpendicular to the x axis and $P_y(x,z,t)$ is the sum of the pressures at points x,z of the faces perpendicular to the y axis, the work done by these forces is

$$\Omega = \int_0^H\int_{-W/2}^{W/2} p_x(y,z,t)(u-y\theta)\,dxdydz - \int_0^H\int_{-D/2}^{D/2} p_y(x,z,t)(v + x\theta)dxdydz \qquad (5.24)$$

Introduce the following notations:

$$\int_{-W/w}^{W/2} p_x(y,z,t)dy = f_x(z,t) \qquad (5.25)$$

$$\int_{-D/2}^{D/2} p_y(x,z,t)\, d_x = f_y(z,t) \tag{5.26}$$

$$\int_{-D/2}^{D/2} x p_y(x,z,t)dx \; - \int_{-W/2}^{W/2} y p_x(y,z,t)dy = f_\theta(z,t) \tag{5.27}$$

where $f_x(z,t)$ and $f_y(z,t)$ are the forces per unit length at height z acting in the x and y directions, respectively and $f_\theta(z,t)$ is the torque, positive is counterclock wise, Eq. (5.24) now be written

$$\Omega = \int_0^H [f_x(z,t)u + f_y(z,t)v + f_\theta(z,t)\theta\,]\, dz \tag{5.28}$$

The potential energy of these forces is equal to - Ω. Therefore, the potential energy of the structure can be written

$$V_{PE} = U_{SE} - \Omega \tag{5.29}$$

If the structural damping is assumed to be of the viscous type and uncoupled, the nonconservative damping forces can be written

$$R_u = -c_x(z)\, \dot{u} \tag{5.30}$$

$$R_v = -c_y(z)\, \dot{v} \tag{5.31}$$

$$R_\theta = - c_\theta(z)\, \dot{\theta} \tag{5.32}$$

Lagrange's equations for a nonconservative system are

$$\frac{d}{dt}\frac{\partial L}{\partial \dot{u}} - \frac{\partial L}{\partial u} = R_u \tag{5.33}$$

$$\frac{d}{dt}\frac{\partial L}{\partial \dot{v}} - \frac{L}{\partial \dot{v}} = R_v \tag{5.34}$$

$$\frac{d}{dt}\frac{\partial L}{\partial \dot{\theta}} - \frac{\partial L}{\partial \theta} = R_\theta \tag{5.35}$$

in which L is called the Lagrangian function and is equal to

$$L = T_{KE} - V_{PE} \tag{5.36}$$

Application of these equations results in the following equations of vibration

$$m(z)\ddot{u} - y_g(z)m(z)\ddot{\theta} - [k_x(z)u' - y_e(z)k_x(z)\theta']' - f_x(z,t) = -c_x(z)\dot{u}$$

$$m(z)\ddot{v} + x_g(z)m(z)\ddot{\theta} - [k_y(z)v' + x_e(z)k_y(z)\theta']' - f_y(z,t) = -c_y(z)\dot{v}$$

$$-y_g(z)m(z)\ddot{u} + x_g(z)m(z)\ddot{v} + I(z)\ddot{\theta} - [-y_e(z)k_x(z)u' + x_e(z)k_y(z)v' + k_\theta(z)\theta']' -$$

$$-f_\theta(z,t) = -c_\theta(z)\dot{\theta} \tag{5.37}$$

Rearranging and putting them in matrix form gives

$$[m]\{d\} + [c]\{\dot{d}\} - ([k]\{d'\})' = \{f\} \tag{5.38}$$

where [m], [c], [k] are the mass, damping and stiffness matrices, respectively; {d} is the displacement vector and {f} is the force vector. Their explicit forms are given below

$$[m] = \begin{bmatrix} m(z) & 0 & -y_g(z)m(z) \\ 0 & m(z) & x_g(z)m(z) \\ -y_g(z)m(z) & x_g(z)m(z) & I(z) \end{bmatrix} \tag{5.39}$$

$$[c] = \begin{bmatrix} c_x(z) & 0 & 0 \\ 0 & c_y(z) & 0 \\ 0 & 0 & c_\theta(z) \end{bmatrix} \tag{5.40}$$

$$[k] = \begin{bmatrix} k_x(z) & 0 & -y_e(z)k_x(z) \\ 0 & k_y(z) & k_e(z)k_y(z) \\ -y_e(z)k_x(z) & x_e(z)k_y(z) & k_\theta(z) \end{bmatrix} \tag{5.41}$$

$$\{d\} = \begin{Bmatrix} u(z,t) \\ v(z,t) \\ \theta(z,t) \end{Bmatrix} \tag{5.42}$$

$$\{f\} = \begin{Bmatrix} f_x(z,t) \\ f_y(z,t) \\ f_\theta(z,t) \end{Bmatrix} \tag{5.43}$$

5.3 - Solution of the Equation System:

Eq. (5.37) is a set of coupled partial differential equations with variable coefficients. For deterministic forms of the excitation an analytical solution can be found only for special cases of the structure such as perfectly symmetric and constant mass, stiffness and damping. Also, for small values of nonsymmetry and separate natural frequencies approximate close form solutions can be obtained using perturbation theory. More information on that may be found in reference [12].

The excitation in this case is wind and can be best described as a stochastic process. Therefore Eq. (5.37) is a set of stochastic differential equations of the vibration and the solution requires application of the random vibration theory. Finding a solution to the above form of the equations is not possible so an approximate solution must be obtained. First, using the Galerkin method as given in reference [15] Eq. (5.37) will be transformed into a set of linear differential equations with constant coefficients; then the standard spectral analysis

techniques of the random vibration theory will be performed as it was done in Chapter 4.

Let's assume that the displacements and the rotation can be approximated as shown below

$$u(z,t) = \sum_{i=1}^{k} \phi_i(z)\, q_i(t) \tag{5.44}$$

$$v(z,t) = \sum_{i=1}^{\ell} \phi_i(z)\, q_{+1}\,(t) \tag{5.45}$$

$$\theta(z,t) = \sum_{i=1}^{m} \phi_i(z)\, q_{k+\ell+i}(t) \tag{5.46}$$

This approximation is valid if $\phi_i(z)$'s satisfy the forced boundary conditions which are u=0, v=0, and θ=0 at z=0 (no displacement and rotation) and u'=0, v'=0, θ'=0 at z=H (no shear and torque). An appropriate choice for $\phi_i(z)$ in this problem is the ith vibrational mode shape of the symmetric uniform shear beam. This mode shape is the same both for translational vibrations and the rotational vibration and is given by

$$\phi_i(z) = \sin \frac{(2i - 1)\,\pi}{2H} z \tag{5.47}$$

This is the reason for using the same index for $\phi(z)$ in Eqs. (5.44) - (5.46). The approximate values of the displacements given above become

closer to exact solutions as the indexes of the sums, k, ℓ, m in Eqs. (5.44) - (5.46) approach infinity.

Introducing the following:

$$[\phi] = \begin{bmatrix} \phi_1(z) \ldots \phi_k(z) & 0 \ldots 0 & 0 \ldots 0 \\ 0 \ldots 0 & \phi_1(z) \ldots \phi_\ell(z) & 0 \ldots 0 \\ 0 \ldots 0 & 0 \ldots 0 & \phi_1(z) \ldots \phi_m(z) \end{bmatrix} \tag{5.48}$$

and

$$q = \begin{Bmatrix} q_1(t) \\ \vdots \\ q_\ell(t) \\ \vdots \\ q_{\ell+k}(t) \\ \vdots \\ q_n(t) \end{Bmatrix} \tag{5.49}$$

with $k + \ell + m = n$ (5.50)

where $[\phi]$ is 3xn mode matrix and $\{q\}$ is n dimensional generalized displacement vector; Eqs. (5.44) - (5.46) can now be written

$$\{d\} = [\phi]\{q\} \tag{5.51}$$

Since this is an approximate solution, Eq. (5.38) becomes

$$[m][\phi]\{\ddot{q}\} + [c][\phi]\{\dot{q}\} - ([k][\phi'])'\{q\} = \{f\} + \{R\} \tag{5.52}$$

where $\{R\}$ is the 3 dimensional residual vector. The residual $\{R\}$ of this approximation can be thought of as the difference between the actual loading $\{f\}$ and the loading for which $\{d\} = [\phi]\{q\}$ is the exact solution. The goal is to make $[R]$ small in some sense. One approach is to make the generalized displacement vector $\{q\}$ satisfy the following condition

$$\int_0^H [W_g]\{R\}\, dz = 0 \tag{5.53}$$

where $[W_g]$ is the matrix of the "weighting functions". This method of minimizing the error is called "the weighted residual method". A widely used weighted residual method is the Galerkin method which uses the mode matrix as the weighting matrix. Therefore, Eq. (5.53) becomes

$$\int_0^H [\phi]^T\{R\}\, dz = 0 \tag{5.54}$$

or with Eq. (5.52)

$$\int_0^H [\phi]^T[m][\phi]\{\ddot{q}\}dz + \int_0^H [\phi]^T[c][\phi]\{\dot{q}\}dz - \int_0^H [\phi]^T\,[k][\phi']'\{q\}dz$$

$$- \int_0^H [\phi]^T\{f\}\, dz = 0 \tag{5.55}$$

The integral over the stiffness matrix can be simplified by partial integration as shown below

$$\int_0^H [\phi]^T([k][\phi'])' dz = [\phi]^T[k][\phi']\Big|_{z=0}^{z=H} - \int_0^H [\phi']^T[k][\phi'] dz \tag{5.56}$$

Since $[\phi] = 0$ at $z=0$ and $[\phi'] = 0$ at $z=H$ from the boundary conditions, the first term on the right-hand side of the equation is zero. Furthermore, with the new notations defined below

$$\int_0^H [\phi]^T[m][\phi] dz = [M] \tag{5.57}$$

$$\int_0^H [\phi]^T[c][\phi] dz = [C] \tag{5.58}$$

$$\int_0^H [\phi']^T[k][\phi'] dz = [K] \tag{5.59}$$

$$\int_0^H [\phi]^T\{f\} dz = \{F\} \tag{5.60}$$

Eq. (5.55) becomes

$$[M]\{\ddot{q}\} + [C]\{\dot{q}\} + [K]\{q\} = \{F\} \tag{5.61}$$

where [M], [C], [K] are the nxn generalized mass, damping and stiffness matrices, respectively and {F} is the generalized force vector. With this expression the equations of vibration are now reduced to n linear differential equations with constant coefficients.

If it were possible to express {F} analytically, {q} would have been obtained using the conventional methods of deterministic analysis. Since {F} is not deterministic but probabilistic with known statistical properties the solution procedure requires the application of the random vibration theory. One of the classical approaches is the spectral analysis technique. The relationship between the input and output spectral density matrices of the above set of equations can be written

$$[S_q(n)] = [H(n)][S_F(n)][H^*(n)]^T \tag{5.62}$$

where $[S_q(n)]$ is nxn spectral density matrix of output vector {q} , $[S_F(n)]$ is nxn spectral density matrix of input vector {F} , and [H(n)] is the frequency response function of the system with $(\ )^*$ denoting the complex conjugate. The definition of [H(n)] is such that if the excitation is

$$\{F(t)\} = \{F_o\}\, e^{i\omega t} \tag{5.63}$$

in which $\{F_o\}$ is a vector of constants, the response is

$$\{q(t)\} = [H(n)]\, F(t) \tag{5.64}$$

With this definition, from Eq. (5.61), it can be written

$$[H(n)] = \left(-\omega^2[M] + i\omega\,[C] + [K] \right)^{-1} \tag{5.65}$$

where ω is the radial frequency (i.e. $\omega=2\pi n$). The remaining of the formulation follows the same steps as given in Chapter 4.

The spectral density matrix of the displacement vector {d}, from Eq. (5.51) and App.(A), is

$$[S_d(z_1,z_2,n)] = [\phi(z_1)]\,[S_q(n)]\,[\phi(z_2)]^T \tag{5.66}$$

or with Eq. (5.62)

$$[S_d(z_1,z_2,n)] = [\phi(z_1)]\,[H(n)]\,[S_F(n)]\,[H^*(n)]^T\,[\phi(z_2)] \tag{5.67}$$

$[S_d(z_1,z_2n)]$ can be written more explicitly as

$$[S_d(z_1,z_2n)] = \begin{bmatrix} S_{uu}(z_1,z_2,n) & S_{uv}(z_1,z_2,n) & S_{u\theta}(z_1,z_2,n) \\ S_{vu}(z_1,z_2,n) & S_{vv}(z_1,z_2,n) & S_{v\theta}(z_1,z_2,n) \\ S_{\theta u}(z_1,z_2,n) & S_{\theta v}(z_1,z_2,n) & S_{\theta\theta}(z_1,z_2,n) \end{bmatrix} \tag{5.68}$$

A typical term, $S_{u\theta}(z_1,z_2,n)$ for example, is the cross spectral density function of the random variables u at height z_1 and θ at height z_2. The covariance matrix of the response is the integral of the spectral density matrix $[S_d(z_1,z_2,n)]$ over the frequency. That is

$$[\sigma_d^2\ (z_1,z_2)] = \int_o^\infty [S_d(z_1,z_2,n)]\ dn \tag{5.69}$$

For $z_1=z_2$ the diagonal terms of the covariance matrix are the mean square values of the response at that height and the correlations coefficients may be obtained from the off-diagonal terms. At the top of the building, for instance, those values become

$$\sigma_{uu}^2\ (H) = \int_o^\infty S_{uu}(H,n)\ dn \tag{5.70}$$

$$\sigma_{vv}^2\ (H) = \int_o^\infty S_{vv}(H,n)\ dn \tag{5.71}$$

$$\sigma_{\theta\theta}^2\ (H) = \int_o^\infty S_{\theta\theta}(H,n)\ dn \tag{5.72}$$

and

$$\rho_{uv}(H) = \frac{\int_o^\infty S_{uv}(H,n)\,dn}{\sigma_{uu}(H)\sigma_{vv}(H)} \tag{5.73}$$

$$\rho_{u\theta}(H) = \frac{\int_0^\infty S_{u\theta}(H,n)\,dn}{\sigma_{uu}(H)\sigma_{\theta\theta}(H)} \tag{5.74}$$

$$\rho_{v\theta}(H) = \frac{\int_0^\infty S_{v\theta}(H,n)\,dn}{\sigma_{vv}(H)\sigma_{\theta\theta}(H)} \tag{5.75}$$

The spectral density matrix of accelerations can be obtained from the spectral density matrix of displacements by the following relationship:

$$\left[S_a\ (z_1,z_2,n)\right] = (2\pi n)^4 \left[S_d(z_1,z_2,n)\right] \tag{5.76}$$

The covariance matrix for accelerations, therefore, is

$$[\sigma_a^2\ (z_1,z_2)] = \int_0^\infty [S_a(z_1,z_2,n)]\,dn \tag{5.77}$$

Because it was assumed that the input forces were stationary Gaussian random variables with zero means, the response components of this linear structure are also Gaussian and have zero means. Therefore, the covariance matrix is sufficient to define all the response statistics.

5.4 - Maximum values of response:

Critical values of displacements occur at the corners. At the top of the building the along-wind and across-wind displacements of a corner,

$x = \frac{D}{2}$ and $y = \frac{W}{2}$ for example, can be found

$$u_c(t) = u(H,t) - \frac{W}{2}\ \theta(H,t) \tag{5.78}$$

$$v_c(t) = v(H,t) + \frac{D}{2}\ \theta(H,t) \tag{5.79}$$

The spectral densities of $u_c(t)$ and $v_c(t)$, from App. (A), are

$$S_{u_c}(n) = S_{uu}(H,n) + \frac{W^2}{4}\ S_{\theta\theta}(H,n) - 2\,\frac{W}{2}\,R_e\,[S_{u\theta}(H,n)] \tag{5.80}$$

$$S_{v_c}(n) = S_{vv}(H,n) + \frac{D^2}{4}\ S_{\theta\theta}(H,n) + 2\,\frac{D}{2}\,R_e\,[S_{v\theta}(H,n)] \tag{5.81}$$

and the mean sqaure values

$$\sigma^2_{u_c} = \int_0^\infty S_{u_c}(n)dn = \sigma^2_{uu} + \frac{W^2}{4}\cdot\sigma^2_{\theta\theta} - 2\,\frac{W}{2}\cdot\rho_{u\theta}\cdot\sigma_{uu}\,\sigma_{\theta\theta} \tag{5.82}$$

$$\sigma^2_{v_c} = \int_0^\infty S_{v_c}(n)dn = \sigma^2_{vv} + \frac{D^2}{4}\ \sigma^2_{\theta\theta} + 2\,\frac{D}{2}\cdot\rho_{v\theta}\cdot\sigma_{vv}\,\sigma_{\theta\theta} \tag{5.83}$$

The expected maximum values of these displacements can be calculated

$$\max u_c = \bar{u}_c + g_u \sigma_{u_c} \tag{5.84}$$

$$\max v_c = \bar{v}_c + g_v \sigma_{v_c} \tag{5.85}$$

where $\bar{u}_c$ and $\bar{v}_c$ are the mean displacements of the corner due to the static mean wind load. Their values are

$$\bar{u}_c = \bar{u}(H) - \frac{W}{2} \bar{\theta}(H) \tag{5.86}$$

$$\bar{v}_c = \bar{v}(H) + \frac{D}{2} \bar{\theta}(H) \tag{5.87}$$

with $\bar{u}(H)$, $\bar{v}(H)$ and $\bar{\theta}(H)$ being the mean displacements and rotation at the top of the building. The parameters g_u and g_v are called the peak factors discussed in Chapter (4). Applying the results to this problem it can be wirtten

$$g_u = \sqrt{2 \log \nu_u T} + \frac{0.577}{\sqrt{2 \log \nu_u T}} \tag{5.88}$$

$$g_v = \sqrt{2 \log \nu_v T} + \frac{0.577}{\sqrt{2 \log \nu_v T}} \tag{5.89}$$

where

$$\nu_u = \frac{\int_0^\infty n^2 S_{u_c}(n)dn}{\int_0^\infty S_{u_c}(n)dn} \tag{5.90}$$

$$\nu_v = \frac{\int_0^\infty n^2 S_{vc}(n)dn}{\int_0^\infty S_{vc}(n)dn} \tag{5.91}$$

and T is the averaging time interval in seconds (generally T=3600 seconds). The expected maximum values of the accelerations can be found similarly by replacing the displacements with accelerations in Eqs. (5.78) through (5.91). The mean values of accelerations are always zero.

5.5 - Spectral density matrix of the excitation:

To complete the formulation the evaluation of $[S_F(n)]$ will be given in this last part. From Eq.(5.60) and App.(A) it can be written

$$[S_F(n)] = \int_0^H\int [\phi(z_1)]^T [S_f(z_1,z_2,n)][\phi(z_2)]\, dz_1 dz_2 \tag{5.92}$$

where $[S_f(z_1,z_2,n)]$ is 3 x 3 spectral density matrix of the force vector $\{f\}$ and can be written explicitly

$$[S_f(z_1,z_2,n)] = \begin{bmatrix} S_{fxfx} & S_{fxfy} & S_{fxf\theta} \\ S_{fyfx} & S_{fyfy} & S_{fyf\theta} \\ S_{f\theta fx} & S_{f\theta fy} & S_{f\theta f\theta} \end{bmatrix} \tag{5.93}$$

in which a typical term $S_{fifj} = S_{fifj}(z_1,z_2,n)$ represents the cospectrum of the forces f_i at height z_1 and f_j at height z_2.

Since the recent investigations have indicated that the across-wind and along-wind forces are uncorrelated [16], it can be assumed that

$$S_{fxfy} = S_{fyfx} = 0 \tag{5.94}$$

The remaining terms of $[S_f(z_1,z_2,n)$ can be determined as shown below.

1. $S_{fxfx}(z_1,z_2,n)$:

From Eq.(5.25) and App.(A)

$$S_{fxfx}(z_1,z_2,n) = \int_{-w/2}^{w/2}\int S_{p_xp_x}(y_1,z_1,y_2,z_2,n)\, dy_1 dy_2 \tag{5.95}$$

Using the expression for $S_{p_xp_x}$ given in Eq.(4.16) with Eqs.(4.19,4.20) Eq.(5.95) can be written

$$S_{fxfx}(z_1,z_2,n) = (\rho C_D)^2 V_o(z_1)V_o(z_2) \cdot S_w^{1/2}(z_1,n) \cdot S_w^{1/2}(z_2,n) \qquad (5.96)$$

$$\cdot \int_{-W/2}^{W/2}\int \exp\left[-\frac{2n\phi}{V_o(z_1)+V_2(z_2)}\left(C_y|y_1-y_2| + C_z|z_1-z_2|\right)\right] dy_1 dy_2$$

After the integration

$$S_{fxfx}(z_1,z_2,n) =$$

$$= (\rho C_D)^2 \cdot V_o(z_1)V_o(z_2)\, S_w^{1/2}(z_1,n) S_w^{1/2}(z_2,n)\, J_{y_1}(z_1,z_2,n)\, J_{z1}(z_1,z_2,n) \qquad (5.97)$$

where

$$J_{y_1}(z_1,z_2,n) = \frac{2W^2}{(EC_y)^2}\left(e^{-E\,C_y} + EC_y - 1\right) \qquad (5.98)$$

$$J_{z_1}(z_1,z_2,n) = \exp\left(-\frac{E.C_z}{W}\cdot|z_1 - z_2|\right) \qquad (5.99)$$

with

$$E = \frac{2n\phi W}{V_o(z_1) + V_o(z_2)} \qquad (5.100)$$

2. $S_{fyfy}(z_1,z_2,n)$:

From Eq.(3.8) and App.(A) it can be written

$$S_{fyfy} = (\tfrac{1}{2}\rho W)^2 V_o^2(z_1) V_o^2(z_2) S_{C_L}(n) J_{x2}(z_1,z_2,n) J_{z2}(z_1,z_2,n) \tag{5.101}$$

where $S_{C_L}(n)$ is the spectral density of the lift coefficient C_L and is given in Eq.(3.9) As mentioned in Chapter 3, the given values of C_L and its spectrum includes the horizontal (chord-wise) correlation of the vortex pressures on the side faces; thus

$$J_{x2}(z_1,z_2,n) = 1.00 \tag{5.102}$$

For correlation along the height (spanwise correlation) there is no analytical expression currently available, but the labortary tests show that it can be approximated as

$$J_{z2}(z_1,z_2,n) \simeq \delta(z_1 - z_2).\ 2\ L_C \tag{5.103}$$

where L_C is the correlation length ($L_C = 3\ W$ for square sections)

3. $S_{f_\theta f_\theta}(z_1,z_2,n)$:

From Eq.(5.27), App.(A) and with the assumption that p_x and p_y are uncorrelated it can be written

$$S_{f_\theta f_\theta}(z_1,z_2,n) = \int_{-W/2}^{W/2}\int y_1 y_2\, S_{p_x p_x}(y_1,z_1,y_2,z_2,n)\, dy_1 dy_2 \; +$$

$$+ \int_{-D/2}^{D/2}\int x_1 x_2 S_{p_y p_y}(x_1,z_1,x_2,z_2,n) dx_1 dx_2 \qquad (5.104)$$

The first integral, I_1, can be determined using the similar procedure given in part (1). Thus,

$$I_1 = (\rho C_D)^2 V_o(z_1) V_o(z_2) S_w^{1/2}(z_1,n).S_w^{1/2}(z_2,n) \int_{-D/2}^{W/2}\int y_1 y_2$$

$$\exp\left[-E(C_y|y_1-y_2|+C_z|z_1-z_2|)\right] \cdot dy_1 \cdot dy_2 \cdot \qquad (5.105)$$

or after integrating

$$I_1 = (\rho C_D)^2 V_o(z_1) V_o(z_2) S_w(n)\, J_{y3}(z_1,z_2,n)\, J_{z3}(z_1,z_2,n) \qquad (5.106)$$

where

$$J_{y3}(z_1,z_2,n) + W^4\left[\frac{1}{6EC_y} - \frac{1}{2(EC_y)^2} + \frac{2}{(EC_y)^4}\left[1 - \left(1 + \frac{EC_y}{2} + \frac{EC_y^2}{2}\right)\cdot e^{-EC_y}\right]\right] \tag{5.107}$$

$$J_{z3}(z_1,z_2,n) = \exp\left[-\frac{E\,C_z}{W}\,|z_1-z_2|\right] \tag{5.108}$$

The second integral, I_2, shows the influence of the distribution of the vortex shedding pressures on torsional moment. Since it was assumed that the total vortex shedding force acts at the middle of the side face and the lift coefficients include the sidewise correlation it may be taken $I_2=0$. Implicit in this approximation is that the pressures on the side faces due to the vortex shedding are fully correlated in the horizontal direction. This is a nonconservative assumption for torsional motions.

4. $S_{fxf\theta}(z_1,z_2,n)$:

From Eqs.(5.25) and (5.27), App.(A) and the assumption of p_x and p_y being uncorrelated it can be written

$$S_{fxf\theta}(z_1,z_2,n) = -\int_{-W/2}^{W/2}\int y_2\, S_{p_xp_x}(y_1,z_1,y_2,z_2,n)\,dy_1dy_2 \tag{5.109}$$

$$S_{fxf\theta}(z_1,z_2,n) = (\rho C_D)^2 V_o(z_1)V_o(z_2)S_w(n) J_{y_4}(z_1,z_2,n)J_{z_4}(z_1,z_2,n)$$

(5.110)

where

$$J_{y_4}(z_1,z_2,n) = \int_{-W/2}^{W/2}\int y_2 \exp\left[-EC_y |y_1-y_2|\right]dy_1dy_2 \qquad (5.111)$$

and

$$J_{z_4}(z_1,z_2,n) - \exp\left[-\frac{EC_z}{W} |z_1-z_2|\right] \qquad (5.112)$$

It can be shown that for above boundaries of the integration

$J_{y_4}(z_1,z_2,n) = 0$

Therefore

$$S_{fxf\theta}(z_1,z_2,n) = 0 \qquad (5.113)$$

5. $S_{fyf\theta}(z_1,z_2,n)$:

From Eqs.(5.26) and (5.27), App.(A) and with the assumptions made earlier it can be written

$$S_{fyf\theta}(z_1,z_2,n) = \int_{-D/2}^{D/2}\int x_2 S_{p_yp_y}(x_1,z_1,x_2,z_2,n)\, dx_1dx_2 \qquad (5.114)$$

If it is assumed that the chordwise correlation of p_y is the function of $|x_1-x_2|$ for every z; it can be shown, then, that with the boundaries given above this integral is zero. Therefore

$$S_{fyf\theta}(z_1,z_2,n) = 0 \tag{5.115}$$

5.6 - Numerical Examples:

Using the formulation given above a computer program was developed to analyze buildings of rectangular cross-section under wind loads. The program allows a linear variation of the mass, stiffness and damping along the height as well as variations of the coordinates of the mass center and the elastic center.

Several aspects of the numerical solution of the above equations should be mentioned. The inversion of the complex matrix in Eq. (5.65) and the double integrations in Eq. (5.92) were performed by using the library subroutines of the Digital Computer Library at the University of Illinois, Urbana-Champaign. All single integrations were evaluated by using Simpson's method. Using only ten points to evaluate the integrals over the height was found to be satisfactory when the integrals involved along-wind and torsional force spectrums. To evaluate the integrals involving the across-wind force spectrum as many as thousand integration points were required for a reasonable accuracy. The reason for this is the fact that the across-wind force spectra has a very sharp peak at Strouhal frequency which varies with height while the spectra

and correlation functions of along-wind and torsional forces vary rather smoothly with height. It was also necessary to use a frequency interval that was very small in order to accurately define all the sharp peaks of the response spectra. After a few test runs a frequency increment of 0.005 cycles per second was found to provide an accuracy of the integration with an error less than one percent. For the uncoupled cases, the peaks of the response spectra are at the natural frequencies of the structure; therefore, a frequency sequence with very small increments around the natural frequencies and with larger increments in the other parts would be an appropriate choice. When the equations of motion are coupled the exact location of the peaks of the response spectra are unknown; therefore, the frequency sequence described above is not applicable. In this analysis the frequencies were started from zero and increased by 0.005 cycles per second up to the frequency which is two times that of the largest natural frequency of the structure; then, the the increment was increased to 0.05 cycles per second and was stopped when the frequency reached the five times that of the largest natural frequency.

The significance of the frequency spacing becomes evident when one considers that for each frequency the complex matrix of Eq. (5.65) must be inverted and the double integrations of Eq. (5.92) are evaluated; then, through Eq. (5.67) the spectrum curves of the responses are obtained. In a structure with the highest natural frequency of 0.4 cps, for example, the frequencies up to 2.0 cps are considered and the number of the frequency points is 250 in the first mode approximation. For the two mode approximation, however, the upper bound of the frequencies

considered was 6 cps, three times that of the first mode approximation and the number of the frequency points was 750. In addition to that, the size of the matrices that are dealt with becomes 6x6 for two mode approximation whereas it is 3x3 in first mode approximation. Thus, the second mode approximation involves inversion and double integration of 6x6 matrices 750 times while the first mode approximation involves inversion and double integration of 3x3 matrices 250 times. The cost of the two mode analysis was five times that of the first mode analysis for above structure. Only first modes were considered for each direction of the vibration in most of the buildings analyzed below.

One might reduce the cost by using a modal analysis technique whereby the first and second mode responses would be calculated separately and the results combined in an appropriate manner. This means a further reduction in accuracy, however. Computationally, this is equivalent to two first mode analyses. This approximation and the contribution of the second modes will be investigated in an example later. It should be noted, however, that theoretically, the response statistics of the building is not only the sum of those of the individual modal responses but also depends on the correlation between them. This can be shown mathematically if the statistics of one of the responses, u(z,t) for instance, is investigated. Using only two terms Eq. (5.44) is

$$u(z,t) = \phi_1(z)q_1(t) + \phi_2(z)q_2(t) \tag{5.116}$$

In terms of the spectral densities it can be written

$$S_u(z,n) = \phi^2(z)\, S_{q_1q_1}(n) + \phi_2^2(z)\, S_{q_2q_2}(n) +$$

$$+ \phi_1(z)\phi_2(z)\,[S_{q_1q_2}(n) + S_{q_2q_1}(n)] \qquad (5.117)$$

The first term on the right hand side is the first mode effect and the second term gives the second mode effect. The third term represents the correlation between two modes and in general will not be zero. Thus, it is quite clear that the results would not be as accurate if modal analysis were used. This will also be shown in an example.

In order to test the method of analysis given above, three structures were analyzed for which full scale measurements of responses were available. The first structure analyzed was the John Hancock building located in Chicago, Illinois. The dimensions, natural frequencies and damping values of the building and the direction and velocity of the wind during the measurements were taken from reference [8] and are given in Figure (5.2). The natural frequency and damping percentage for torsion were assumed to be 0.25 cps and 0.60 percent respectively. These values are higher relative to the translational ones than what would normally be expected in a rectangular building. The reason for using higher values was the tapered shape and tube nature of the building in which all the lateral stiffness is located at the exterior of the building. Since the building is very tall and slender it was modeled as a flexural beam with varying cross-section. Only first mode shapes for each direction of the vibration were used in the analysis.

The reference wind velocity measured at nearby Midway Airport during the test was 20 mph at a reference height of 40 feet. Simiu's models were used for the velocity profile and the gust spectra. The calculated mean wind velocity at the top of the building was 35 mph. The results of the analysis and full scale measurements are also given in Figure (5.2). The responses calculated using Davenport's velocity profile and gust spectrum models were about 30 to 40 percent smaller than those calculated above. The main reason for this was that Davenport's velocity profile model resulted in smaller velocities than those of Simiu's for the same reference wind velocity. In this example the tapered shape of the building represents a source of uncertainty due to the fact that the structure of the pressures over the faces of the building and their correlations are probably different than those given earlier for rectangular buildings. In addition to that, the given wind velocity is not the site velocity. It is a reference velocity taken far away from the site. The latter one makes this example a test not just of the modeling of the building behavior but also of the modeling of the turbulent flow structure. In light of all these, the results are remarkably good since the computed values of root-mean-square displacement are within 10% of the measured quantities.

The other two buildings analyzed were studied by Van Koten in the Netherlands [17]. The caracteristics of the buildings and the wind direction and velocities are given in Figures (5.3) and (5.4). The measurements of the along-wind and across-wind dynamic displacements were made for the corners of the top of the buildings. Therefore given

values of the standard deviations automatically include the effect of the torsional vibrations. The ratio of the standard deviation of the across-wind vibrations to that of the along-wind vibrations is also given in Figures (5.3) and (5.4) for each building. The reason for giving the ratios instead of the absolute values is that the measured values given in reference [17] are not the absolute values but relative ones. Again, the calculated responses agree quite well with the measured ones.

An interesting fact confirmed by the measurements and also found through the analysis is that the amplitude of the cross-wind vibrations is in many cases substantially larger than the along-wind vibration, and thus too large to neglect in the wind analysis of a building. The results also show that in spite of the gross simplifications made in defining the across-wind forces the suggested method of analysis gives a very good prediction of the building's behavior under wind loading. The current wind code does not give any provision for across-wind vibrations. Thus, there has been no available method for designers to use to estimate the across-wind vibrations of buildings.

The second part of the numerical work was directed towards investigating the effects of various structural parameters of a building on its response. In these examples two basic buildings were considered. The first building had the dimensions of W=80 ft, D=80 ft and H=400 ft with the translational natural frequencies of n_x=0.40 cps. and n_y=0.40 cps. The dimensions of the second building are the same as the first one in plan, but with H=200 ft. The translational natural frequencies for this case were n_x=0.80 cps., n_y=0.80 cps. The damping

percentages were taken as 2% for all directions in both buildings. It was assumed for both structures that the center of the mass was at the center of geometry at every level along the height. The mean wind flow was assumed parallel to the x axis and the reference wind velocity was taken as 80 mph. which is the design wind velocity for Illinois measured at 33 ft. height in an open field. Both buildings were assumed to be in the center of a large city. Simiu's models for both velocity profile and gust spectrum were used in the analysis. The most probable maximum values of the displacements and accelerations of the corners of the top of the buildings were calculated and then normalized by those which would have been obtained by not including the torsional and across-wind vibrations. The static rotation due to the static wind force was included in the latter quantities which were denoted by u_o and $\ddot{u}_o$ in the figures since it would normally be considered in the design. Therefore, those normalized values show only the effect of dynamic across-wind and torsional wind forces on the response. They were denoted by r_u and r_v for displacements and by $r_{\ddot{u}}$ and $r_{\ddot{v}}$ for accelerations. Three values of the torsional natural frequency were considered for each case: smaller than translational frequencies (n_θ=0.875 n_x), equal to them (n_θ=n_x) and larger than them (n_θ= 1.125 n_x).

The effect of nonsymmetry in the y direction ($x_e \neq 0$) was investigated for the first case. The center of rigidity was moved along the x axis. Then, the variation of the normalized responses of the corners on top of the building for the above values of n_θ were computed for each building. The results are shown in Figure (5.5) for the first building and in Figure (5.6) for the second building.

The results clearly indicate that the response ratios increase significantly as the nonsymmetry increases and the torsional natural frequency decreases. In the first building (H = 400 ft), for instance, for ten percent nonsymmetry (i.e. $x_e/D = 0.10$) and $n_\theta = n_x = n_y$ the expected maximum values of the corner displacements would be 1.26 and 2.01 times larger than those that would be predicted by neglecting torsional and across-wind forces for u and v directions, respectively. The values for accelerations are $r_{\ddot{u}} = 1.20$ and $r_{\ddot{v}} = 1.83$. The ratios are higher for smaller values of n_θ and smaller for higher values of n_θ. The increases in the displacements and accelerations with increasing nonsymmetry are almost equal in this building. Because the structure is nonsymmetric only in y direction, the effects of cross-wind and torsional vibrations are higher for the y direction than they are for the x direction.

For the second building, the variations of r_u and r_v with x_e are similar to those of the first building for the displacements. The curves for accelerations, however, are quite different in this building. While $r_{\ddot{v}}$ increases slowly with increasing x_e, $r_{\ddot{u}}$ decreases and becomes almost constant. Again, for ten percent nonsymmetry and $n_\theta = n_x = n_y$ the response ratios are $r_u = 1.17$, $r_v = 1.86$ and $r_{\ddot{u}} = 1.12$ $r_{\ddot{v}} = 0.96$. The difference between the shape of the response curves of two buildings can be attributed to the effects of the building height on the spectral density functions and on the correlation functions of the wind forces.

The second case deals with the effects of nonsymmetry in the x direction. In this case the center of rigidity was moved along the y axis and the response ratios of the corners of the top of the buildings

were calculated. The results are given in figure (5.7) for the first building and in figure (5.8) for the second building. Again, the increase of the response ratios with decreasing n_θ is clearly shown. The increase of the responses with increasing non-symmetry is rather regular for all the components of the responses and also similar for both buildings. Because the non-symmetry is in the x direction, the components of the response in that direction are influenced more from the rotational and cross-wind vibrations. The typical values, for ten percent nonsymmetry ($y_e/W = 0.10$) and $n_\theta = n_x = n_y$, are $r_u = 1.51$, $r_v = 1.45$ and $r_{\ddot{u}} = 1.71$ $r_{\ddot{v}} = 1.40$ for the building of H = 400 feet; and $r_u = 1.50$, $r_v = 1.49$ and $r_{\ddot{u}} = 1.80$, $r_{\ddot{v}} = 1.04$ for the building of H = 200 feet.

The third and more general case involves the variation of the center of rigidity along one of the diagonals. In that case, since both along-wind and cross-wind forces contribute to the torsion, the response ratios are much higher than those of the previous cases. The ratios, for ten percent nonsymmetry along the diagonal (i.e. $x_e/D = 0.10$ and $y_e/W = 0.10$) and for $n_\theta = n_x = n_y$, are $r_u = 1.82$, $r_v = 2.31$ and $r_{\ddot{u}} = 1.55$, $r_{\ddot{v}} = 2.25$ for the first building; and $r_u = 1.63$, $r_v = 2.07$ and $r_{\ddot{u}} = 1.38$, $r_{\ddot{v}} = 1.43$ for the second building. The increase of the response ratios with increasing non-symmetry is also much sharper. The plots of the results are given in figure (5.9) for the first building and in figure (5.10) for the second building. Similar to the first case, the accelerations of the second building are not influenced by the non-symmetry as much as the displacements are.

For the fourth case, the effect of the building's width on the along-wind response of the corners was studied. This was shown to be very important for the simple structure of Chapter 4. Three values of W were considered for both buildings in this case. They are W = 80 ft, W = 160 ft and W = 200 ft. In order to keep the cross-sectional area and the mass constant the values of D are reduced proportionally with the increased values of W. The translational natural frequencies and the damping were kept the same as they were before. Only two values of torsional natural frequency, $n_\theta = n_x$ and $n_\theta = 1.250\ n_x$, were considered. Since for the above values of W and D the along-wind forces are more dominant, the nonsymmetry was considered only in the x direction. Only the along-wind direction response ratios were plotted. The plots are given in figure (5.11) for the first building and in figure (5.12) for the second building. As it can be seen from these figures, the increase of the width results in higher displacements and accelerations at the corners of the buildings. This is due to the increase of the torsional component of the fluctuating along wind forces. For the symmetric case of the building of H = 400 feet the response ratios, for $n_\theta = 1.25\ n_x$, are $r_u = 1.01$, $r_{\ddot{u}} = 1.12$ for W = 80 feet; $r_u = 1.06$, $r_{\ddot{u}} = 1.48$ for W = 160 feet; and $r_u = 1.06$, $r_{\ddot{u}} = 1.54$ for W = 200 feet. For a ten percent offset in the y direction ($y_e/W = 0.10$) those values become $r_u = 1.30$, $r_{\ddot{u}} = 1.48$ for W = 80 feet; $r_u = 1.58$, $r_{\ddot{u}} = 2.04$ for W = 160 feet; and $r_u = 1.61$, $r_{\ddot{u}} = 2.11$ for W = 200 feet. The response ratios of the second building are practically equal to those of the first one. As can be seen from the figures the variation of the displacement ratios with nonsymmetry is linear. The variation of the

acceleration ratios is very close to linear for $n_\theta = 1.25\ n_x$ but not for $n_\theta = n_x$.

In order to investigate the accuracy of the first made approximation two symmetric cases, one with $n_\theta = n_x = n_y$ and the other one with $n_\theta = 1.125\ n_x$, of the building of H = 400 were analyzed using two modes for each direction of the vibration. The characteristics of each case and the summary of the results are given in tables (5.1) and (5.2). As can be seen from the tables the second mode contribution to displacements is about one percent and may be neglected. The higher mode contributions to accelerations are significant, however. The expected maximum top-floor corner accelerations would be underestimated by about 15 percent if the higher modes are not included. For the normalized values of which the plots are given the effect of the second mode becomes less obvious since the normalizing quantity, too, has the second mode contribution.

It was mentioned in the beginning of this section that the modal analysis would not be as accurate for computing the response statistics because the effect of the correlation between the modal responses would be ignored. This was investigated in an example and the results are given in table (5.3). A symmetric building with H = 400 ft and $n_\theta = n_x = n_y$ was analyzed by using the first mode only and the second mode only for each direction. The results are combined by taking the square root of the sum of the squares for standard deviations and by taking the algebraic sum for the mean. Thus, in light of Eq. (5.87), the expected maximum response, for x direction for instance, is

approximated as

$$\max u = \bar{u}_{1st\ Mode} + \bar{u}_{2nd\ Mode} + \sqrt{(g_u\sigma_u)^2_{1st\ Mode} + (g_u\sigma_u)^2_{2nd\ Mode}}$$

Then, those results were compared to those of the two mode approximation. As can be seen from the table, the maximum values obtained through modal analysis are different, as much as 22 percent for $\ddot{u}$ for instance, than those of the two mode approximation because of the fact that the modal analysis in this problem is equivalent to assuming zero correlation between the modal responses. It is expected that for non-symmetric buildings the effect of the correlation between the modal responses would be even higher. The predictions of the maximum displacements are quite close to the more accurate calculations because the displacements are dominated by the first mode response. The accelerations, $\ddot{u}$ and $\ddot{v}$, are overestimated using modal analysis by 22 percent and 6 percent, respectively. The engineer would need to decide if the savings in analysis cost was worth the additional error.

In the last part of the analysis the responses of the shear beam model and flexural beam model were compared. Two symmetric buildings, one with H = 400 feet and the other with H = 200 feet were analyzed using a shear beam and a flexural beam model. The results for various response characteristics are given in tables (5.4) and (5.5). As one would expect the top-of-building responses of the flexural beam models are higher, by about 30 percent, than those of the shear beam models. The rotational responses were the same since the rotational mode shape was assumed to be the same in both models. It would be expected that

responses near the bottom of the structure would be larger for the shear beam than for the flexural beam.

5.7 - Discussion and Conclusions:

A method for estimating the expected maximum dynamic response of wind excited buildings was presented. The buildings were modeled as either shear beam or flexural beam with varying cross-sectional properties. The along-wind, across-wind and torsional vibrations and their couplings in nonsymmetric buildings were considered. The wind flow was assumed to be perpendicular to one of the faces of the building and only buildings with rectangular or square cross-sections were investigated. Galerkin's method was used to solve the equations of motion.

The along-wind pressures and their correlations were represented by the well known expressions that are already available in the literature. In light of the results of recent experiments the across-wind forces were assumed to be mainly due to the vortex shedding [25], [16]. The spectrum of the across-wind force was represented by an expression similar to that suggested by Vickery for tapered stacks [38]; except different values of the Strouhal number, bandwith and correlation length were used. Since the across wind forces on buildings have not been as extensively studied as the along-wind forces they represent a greater source of uncertainty in the analysis. The vertical and horizontal variation of the cross-wind pressures, their correlations and the variation of the force spectrum with different values of the aspect ratio of the building need more research. Therefore, some approximations were required. The chordwise correlation was assumed to be

included in the lift coefficients; then, the total across-wind force for unit height was applied at the mid-point of the side face. This assumption underestimates the torsional moment acting on the building. The vertical correlation function of the side pressures was approximated by a delta function and it was assumed that the total correlation length remains equal to that of the test results. The along-wind and the across-wind forces were assumed to be uncorrelated [16].

The torsional moment acting on the building was taken as the sum of the torque due to the random pressures on the front face of the building plus the torque of the across wind force due to the nonsymmetry of the building. Therefore, for a symmetric building the across-wind force does not excite any torsional vibrations.

In spite of the assumptions that are given above the results of the suggested method of analysis were found to be very satisfactory when compared to those of the full scale measurements in three buildings. It was also found that using Simiu's models for velocity profiles and gust spectrum results in a better approximation of the actual building behavior than that which would have been found by using Davenport's models. The results of both full scale measurements and model analysis clearly show that the across-wind and torsional vibration of wind excited buildings can be important and should be considered in design.

In order to see the influence of the building characteristics on the response, a parametric analysis was made on several model buildings. The results of those examples indicated that, in general, the dynamic response of the corners of the building increases as the torsional natural frequency decreases and as the structural nonsymmetry increases.

Figures (5.5) through (5.10) show that neglecting the across-wind and torsional vibrations, especially in the buildings which are non-symmetric in the cross-wind direction, results in grossly underestimating the corner responses. It was also shown in figures (5.11) and (5.12) that the increase of the frontal width increases the magnitude of the torsional vibrations as one would expect.

The first mode approximation for each direction of the vibration was found to be satisfactory for calculating displacements but not for accelerations. The contribution of the second mode was found to be as high as 25 percent for the root mean square value of the rotational vibrations in one of the examples.

It was also shown mathematically and with an example that the combination of the individual modal responses using modal analysis techniques would not give as accurate of a prediction of the total response as the more general method because the correlation of the responses of the two modes would be ignored.

Finally, the comparison of the results of the shear beam model and the flexural beam model was made. The flexural beam model was shown to give larger top-story responses.

CHAPTER 6

SUMMARY AND CONCLUSIONS

A method for analyzing the three-dimensional dynamic response of wind-excited buildings was presented. The wind and building models used in the analysis are similar to those currently used for analyzing along-wind response. The coupled along-wind, across-wind and torsional vibrations are computed using random vibration techniques; and the expected maximum translational responses and the torsional response are obtained.

After discussing in Chapters 2 and 3 the structure of the wind near the ground and the forces on buildings due to the wind, an investigation of the response of several single-mass structures was presented in Chapter 4. The objectives of this study were to identify which wind and structural properties influence the torsional response and to determine whether the predicted torsional responses are large enough to warrant extending the method to building-type structures. The following conclusions may be made based on the results of this study.

1. Torsional response of a wind-excited structure can produce displacements of the same magnitude as the total along-wind response.
2. The dynamic torsional response increases as the width of the structure's exposed face increases, as the structural or geometric eccentricity increases and as the torsional natural frequency decreases.
3. The correlation between the torsional dynamic response and the translational dynamic response is the highest

when the torsional and the translational natural frequencies are equal.

The method developed in Chapter 4 for computing torsional vibrations of single-mass structures was extended to buildings in Chapter 5. In addition a simplified model of the across-wind forces was also included so that the three dimensional vibration of buildings could be computed.

The along-wind pressures and their correlations were represented by well-known expressions that are already available in the literature. Across-wind forces were assumed to be mainly due to vortex shedding. Since they have not been as extensively studied as the along-wind forces some approximations in the mathematical modeling of the across-wind forces were required. In the light of recent experiments, the along-wind forces and the across-wind forces were assumed to be uncorrelated. It was also assumed that the chordwise correlation of the across-wind pressures is included in the lift coefficients and the total pressure for unit height acts at the mid-point of the side face; the vertical correlation is quite local (i.e. correlation is zero between to different point); and the spectrum of the across-wind force can be approximated by a narrow banded Gaussian curve. The torsional moment acting on the building was taken as the sum of the torque due to random wind pressures on the front and back faces plus the torque of the across-wind forces due to the nonsymmetry, if there is any, of the building in across-wind direction. The simple two-degrees-of-freedom structures of Chapter 4 were chosen in such a way that the across-wind forces could be neglected.

Only buildings with rectangular cross-section and normally incident wind were considered. The buildings were modeled as either a shear beam or as a flexural beam. Galerkin's method was used to solve the coupled equations of motion.

Three buildings for which full-scale measurements were available were analyzed. The calculated displacements were within 10 % of the measured responses. This was believed to be very good agreement considering the nature of some of the simplifications required to complete the analysis.

The next phase of the study was conducted to determine the influence of various geometric and mechanical properties of a building on its response. Expected maximum responses of the corners of the top of the building were computed and normalized by those which would have been obtained if the across-wind and torsional vibrations were neglected. Thus, the importance of across-wind and torsional dynamic responses could be ascertained. The results obtained for several buildings led to the following conclusions:

1. The across-wind vibration of a wind-excited tall building can be as much as several times greater than the along-wind response and thus should be included in analysis for design.
2. The torsional vibration of a building should be computed for design if it is nonsymmetric or if it is symmetric and its lowest torsional natural frequency is less than or equal to either of the lowest translational natural frequencies.

3. The amplitude of the torsional vibrations increases as the frontal width of the building increases, as the structural nonsymmetry increases and as the torsional natural frequency decreases.
4. Even a perfectly symmetric structure with normally incident wind can experience significant torsional vibrations if its frontal width is large and its torsional natural frequency is low compared to the lowest translational natural frequencies.
5. The first mode approximation for each direction of the vibration is satisfactory for calculating displacements but results in errors of approximately 15 percent for accelerations.
6. Computing first and second mode responses independently and combining the responses does not give as accurate results as the more complete method does because the correlation between the modal responses is neglected. The error in the approximation is on the order of 5 percent for displacements and 20 percent for accelerations. This method is less expensive, however. Thus, an engineering decision is required whether the savings in analysis cost is worth the additional error.
7. The flexural beam model gives larger top-story responses than the shear beam model by about 30 percent.

Due to the rather crude approximations made when defining the wind forces on a structure, this should be considered as an interim procedure. Further experimental research or full-scale structures is required. The correlation between the pressures on the front face

and on the back face of the structure is not fully defined. The available information on this problem involves the correlation between the pressures on two points which have the same horizontal and vertical coordinates. In order to calculate the torsional response more accurately one needs to know the correlation between the pressures on any arbitrary two points or the front face and on the back face of the structure. The across-wind forces on buildings also need more research. The chordwise and vertical correlations of the across-wind pressures and the variation of the across-wind force spectra for different ratios of the building's dimensions are not very clear and represent the source of the greatest uncertainty in the above analysis. The effect of the wind approaching the building at an arbitrary angle also needs to be determined. It is believed that the worst case for both along-wind and across-wind responses is for normally incident wind. However, this is probably not the case for torsional vibration. When these problems have been investigated experimentally the results may easily be incorporated into the above analysis procedure.

REFERENCES

1. "American National Standard Building Code Requirements for Minimum Design Loads in Buildings and other structures," American National Standards Institute, New York, New York, 1972.

2. Davenport, A.G., "The Spectrum of Horizontal Gustiness Near the Ground in High Winds," Journal of Royal Meteorological Society, 87, 1961, pp. 194-211.

3. Davenport, A.G., "The Application of Statistical Concepts to the Wind Loading of Structures," Proceedings, Institute of Civil Engineering, London, Vol. 19, pp. 449-472, 1961.

4. Davenport, A.G., "The Distribution of Largest Value of a Random Function with Application to Gust Loading," Proc., Inst. of Civil Eng., London, Vol. 28, 1964, pp. 187-196.

5. Davenport, A.G., "The Relationship of Wind Structure to Wind Loading," Proc. of the Symp. on Wind Effects on Buildings and Structures, Vol. 1, National Physical Laboratory, Teddington, U.K., 1965, pp. 53-102.

6. Davenport, A.G., "Gust Loading Factors," Jour. of Struc. Div., ASCE, Vol. 93, No. ST3, proc. paper 5255, June 1967, pp. 11-34.

7. Davenport, A.G., "The Prediction of the Response of Structures to Gusty Wind," Proc., Safety of Structures under Dynamic Loading, Int. Sem., Norwegian Inst. of Tech., June 1977, Volume 1, pp. 257-284.

8. Davenport, A.G., Hogan, M. and Vickery, B.J., "An Analysis of Records of Wind Induced Buildings Movement and Column Strain Taken at the John Hancock Center (Chicago)," Research Report, Faculty of Engineering Science, the University of Western Ontario, London, Canada, September 1970.

9. Davenport, A.G. and Novak, M., "Vibration of Structures Induced by Wind," Shock and Vibration Handbook, Chapter 29, part II, McGraw Hill Publications, 19, pp. 29.21-29.43.

10. Hart, G.C., "Building Dynamics Due to Stochastic Wind Forces," Jour. of Struc. Div., ASCE, Vol. 96, No. ST3, proc. paper 7154, March 1970, pp. 535-550.

11. Hart, G.C., DiJulio, R.M.,Jr. and Lew, M., "Torsional Response of High-Rise Buildings," Jour. of Str. Div., ASCE, Vol. 101, No. ST2, proc. paper 11126, February 1975, pp. 397-416.

12. Hoerner, J.B., "Modal Coupling and Earthquake Response of Tall Buildings, Ph.D. Thesis, California Institute of Technology, Pasadena, California, 1971.

13. Houghton, E.L. and Carruthers, N.B., "Wind Forces on Buildings and Structures, an Introduction," John Wiley and Sons Inc., New York, 1976.

14. Huh, C.K., "The Behavior of Lift Fluctuations on the Square Cylinders in the Wind Tunnel Test," Proc. Third Int. Conf. on Wind Effects on Buildings and Structures, Tokyo, 1971, pp. 911-920.

15. Hurty, W.C. and Rubinstein, M.F., "Dynamics of Structures," Prentice-Hall, Inc., Englewood Cliffs, New Jersey, 1964.

16. Kareem, A., "Wind Excited Motion of Buildings," Ph.D. Thesis, Colorado State University, Civil Engineering Department, 1978.

17. van Koten, H., "The Comparison of Measured and Calculated Amplitudes of Some Buildings and Determination of the Damping Effects of the Buildings," Proc. Third Int. Conf. on Wind effects on Buildings and Structures, Tokyo, 1971, pp. 825-839.

18. Lam Put, R., "Dynamic Response of a Tall Building to Random Wind Loads," Proceedings, International Conference on Wind Effects on Buildings and Structures, Tokyo, Japan, 1971, pp. III-4.1-11.

19. Langhaar, H.L., "Energy Methods in Applied Mechanics," John Wiley and Sons Inc., New York,

20. Lin, Y.K., "Probabilistic Theory of Structural Dynamics," Robert E. Krieger Publishing Company, Huntington, New York, 1976.

21. Lumley, J.L. and Panofsky, H.A., "The Structure of Atmospheric Turbulence," John Wiley and Sons, Inc., 1964.

22. "National Building Code of Canada," National Research Council, Ottawa, 1970.

23. Novak, M. and Davenport, A.G., "Aeroelastic Instability of Prisms in Turbulent Flow," Jour. of the Eng. Mech. Div., ASCE, Vol. 96, No. EMI, pp. 17-39, February 1970.

24. Patrickson, C.P. and Friedmann, P., "A Study of the Coupled Lateral and Torsional Response of Tall Buildings to Wind Loadings," School of Engineering and Applied Science, University of California Los Angeles, UCLA-ENG-76126, December 1976.

25. Saunders, J.W., "Wind Excitation of Tall Buildings," Ph.D. Thesis, Department of Mechanical Engineering, Menash University, Victoria, Australia, October 1974.

26. Sidarous, J.F.Y. and Vanderbilt, M.D., "An Analytical Methodology for Dynamic Building Response to Wind Loading," Structural Research Report No. 24, Civil Engineering Department, Colorado State University, Fort Collins, Colorado, November 1979.

27. Simiu, E., "Gust Factors and Along-wind pressure Correlations," Jour. of Struc. Div., ASCE, Vo.. 99, No. ST4, Proc. paper 9687, April 1973, pp. 773-783.

28. Simiu, E., "Logarithmic Profiles and Design Wind Speeds," Jour. of Eng. Mech. Div., ASCE, Vol. 99, No. EM5, Proc. paper 10100, October, 1973, pp. 1073-1083.

29. Simiu, E., "Wind Spectra and Dynamic Along wind Response," Jour. of the Struc. Div., ASCE, Vol. 100, No. ST9, Proc. paper 10815, Sept. 1974, pp. 1877-1910.

30. Simiu, E. and Marshall, R.D., "Wind Loading and Modern Building Codes," Meeting Preprint 2268, ASCE National Structural Meeting, Cincinnati, Ohio, April 22-26, 1974.

31. Simiu, E. and Scanlan, R.H., "Wind Effects on Structures, an Introduction to Wind Engineering," John Wiley and Sons, New York, 1978.

32. Taoka, G.T., Hogan, M., Khan, F. and Scanlan, R.H., "Ambient Response Analysis of Some Tall Structures," Jour. of Struc. Div., ASCE, Vol. 101, No. ST1, Proc. paper 11051, January 1975, pp. 49-65.

33. Vaicaitis, R., Shinozuka, M. and Takeno, M., "Response Analysis of Tall Building to Wind Loading," Jour. of the Struc. Div., ASCE, Vol. 99, No. ST3, Proc. paper 11194, March 1975, pp. 585-600.

34. Vellozzi, J. and Cohen, E., "Gust Response Factors," Jour. of Struc. Div., ASCE, Vol. 94, No. ST6, Proc. paper 5980, June 1968, pp. 1295-1313.

35. Vickery, B.J., "Fluctuating Lift and Drag on a Long Cylinder of Square Cross Section in a Smooth and in a Turbulent Stream," Journal of Fluid Mechanics, Vol. 25, part 3, 1966, pp. 481-494.

36. Vickery, B.J., "Load Fluctuations in Turbulent Flow," Jour. of Eng. Mech. Div., ASCE, Vol. 94, No. EM1, Proc. paper 5782, February 1968, pp. 31-46.

37. Vickery, B.J., "On the Reliability of Gust Loading Factors," Civil Engineering Transactions, April 1971, pp. 1-9.

38. Vickery, B.J. and Clark, A.W., "Lift or Across-wind Response of Tapered Stacks," Jour. of the Struc. Div., ASCE, Vol. 98, No. ST1, Proc. paper 8634, January 1972, pp. 1-20.

39. Vickery, B.J. and Kao, K.H., "Drag of Along-wind Response of Slender Structures," Jour. of the Struc. Div., ASCE, Vol. 98, No. ST1, Proc. paper 8635, January 1972, pp. 21-36.

40. Vivekananda, M., "Wind Excited Vibration of Square Beam and Suspended Cable," Doctor of Science Thesis, Department of Aeronautics and Astronautics, MIT, Cambridge, 1972.

41. Wen, Y.K., "Course Notes," Department of Civil Engineering, University of Illionis at Urbana-Champaign.

Table 5.1 - Comparison of top-story responses of one-mode and two-mode analysis ($n_\theta = n_x = n_y$)

Displacements (ft)			Accelerations (ft/sec^2)		
	One-mode Approx.	Two-mode Approx.		One-mode Approx.	Two-mode Approx.
σ_u	0.0862	0.0866	$\sigma_{\ddot{u}}$	0.2960	0.3404
σ_v	0.1850	0.1890	$\sigma_{\ddot{v}}$	0.3110	0.3224
σ_θ	0.000756	0.000756	$\sigma_{\ddot{\theta}}$	0.004274	0.005349
max u_c	0.5818	0.5819	max $\ddot{u}_c$	1.3579	1.6532
max v_c	0.7104	0.7287	max $\ddot{v}_c$	1.3742	1.5514
r_u	1.04	1.04	$r_{\ddot{u}}$	1.15	1.18
r_v	1.02	1.02	$r_{\ddot{v}}$	1.16	1.26

Building - I

H = 400 ft

W = D = 80 ft

$n_x = n_y = n_\theta = 0.40$ cps

Table 5.2 - Comparison of top-story responses of one-mode and two-mode analysis ($n_\theta = 1.125\ n_x = 1.125\ n_y$)

Displacements (ft)			Accelerations (ft/sec^2)		
	One-mode Approx.	Two-mode Approx.		One-mode Approx.	Two-mode Approx.
σ_u	0.0862	0.0866	$\sigma_{\ddot{u}}$	0.2960	0.3404
σ_v	0.1850	0.1890	$\sigma_{\ddot{v}}$	0.3110	0.3224
σ_θ	0.000564	0.000564	$\sigma_{\ddot{\theta}}$	0.003968	0.004943
max u_c	0.5728	0.5749	max $\ddot{u}_c$	1.3367	1.6217
max v_c	0.7059	0.7244	max $\ddot{v}_c$	1.3553	1.5210
r_u	1.02	1.02	$r_{\ddot{u}}$	1.14	1.16
r_v	1.01	1.01	$r_{\ddot{v}}$	1.14	1.24

Building - I

H = 400 ft

W = D = 80 ft

$n_x = n_y = 0.40$ cps

$n_\theta = 0.45$ cps

Table 5.3 - Comparison of top-story responses calculated by approximate modal analysis technique and by two-mode analysis

Response (ft, sec)	1st mode Contribution	2nd mode Contribution	Sum of Individual 1st and 2nd mode Contributions	2 mode Analysis
u_{mean}	0.2313	-0.0028	0.2285	0.2285
σ_u	0.0862	0.0058	0.0864	0.0866
σ_v	0.1847	0.0158	0.1853	0.1895
σ_θ	0.000756	0.000097	0.000760	0.000756
$\sigma_{\ddot{u}}$	0.2961	0.2801	0.4076	0.3404
$\sigma_{\ddot{v}}$	0.3110	0.0251	0.3120	0.3224
$\sigma_{\ddot{\theta}}$	0.004274	0.005360	0.006860	0.005350
max u_c	0.5818	0.0265	0.5802	0.5819
max v_c	0.7104	0.0638	0.7133	0.7287
max $\ddot{u}_c$	1.3579	1.4929	2.0181	1.6532
max $\ddot{v}_c$	1.3742	0.9134	1.6501	1.5514

Building - I

H = 400 ft

W = D = 80 ft

$n_x = n_y = n_\theta = 0.40$ cps

Table 5.4 - Comparison of top-story responses of shear-beam model and flexural-beam model (H = 400 ft)

Displacements (ft)			Accelerations (ft/sec^2)		
	Shear Beam Model	Flexural Beam Model		Shear Beam Model	Flexural Beam Model
u_{mean}	0.2313	0.3051		-	-
σ_u	0.0862	0.1146	$\sigma_{\ddot{u}}$	0.2961	0.4117
σ_v	0.1847	0.2478	$\sigma_{\ddot{v}}$	0.3110	0.4171
σ_θ	0.000564	0.000564	$\sigma_{\ddot{\theta}}$	0.003968	0.003968
max u_c	0.5278	0.7529	max $\ddot{u}_c$	1.3367	1.7546
max v_c	0.7059	0.9436	max $\ddot{v}_c$	1.3553	1.7219
r_u	1.02	1.01	$r_{\ddot{u}}$	1.14	1.07
r_v	1.01	1.01	$r_{\ddot{v}}$	1.14	1.08

Building - I

H = 400 ft

W = D = 80 ft

$n_x = n_y = 0.40$ cps

$n_\theta = 0.45$ cps

Table 5.5 - Comparison of top-story responses of shear-beam model and flexural-beam model (H = 200 ft)

Displacements (ft)			Accelerations (ft/sec^2)		
	Shear Beam Model	Flexural Beam Model		Shear Beam Model	Flexural Beam Model
u_{mean}	0.0427	0.0569		-	-
σ_u	0.0173	0.0230	$\sigma_{\ddot{u}}$	0.1829	0.2577
σ_v	0.0382	0.0514	$\sigma_{\ddot{v}}$	0.0460	0.0619
σ_θ	0.000116	0.000116	$\sigma_{\ddot{\theta}}$	0.002928	0.002928
max u_c	0.1135	0.1498	max $\ddot{u}_c$	0.9005	1.1730
max v_c	0.1453	0.1943	max $\ddot{v}_c$	0.5221	0.5481
r_u	1.03	1.01	$r_{\ddot{u}}$	1.19	1.10
r_v	1.01	1.01	$r_{\ddot{v}}$	3.01	2.35

Building - II

H = 200 ft

W = D = 80 ft

$n_x = n_y = 0.80$ cps

$n_\theta = 0.90$ cps

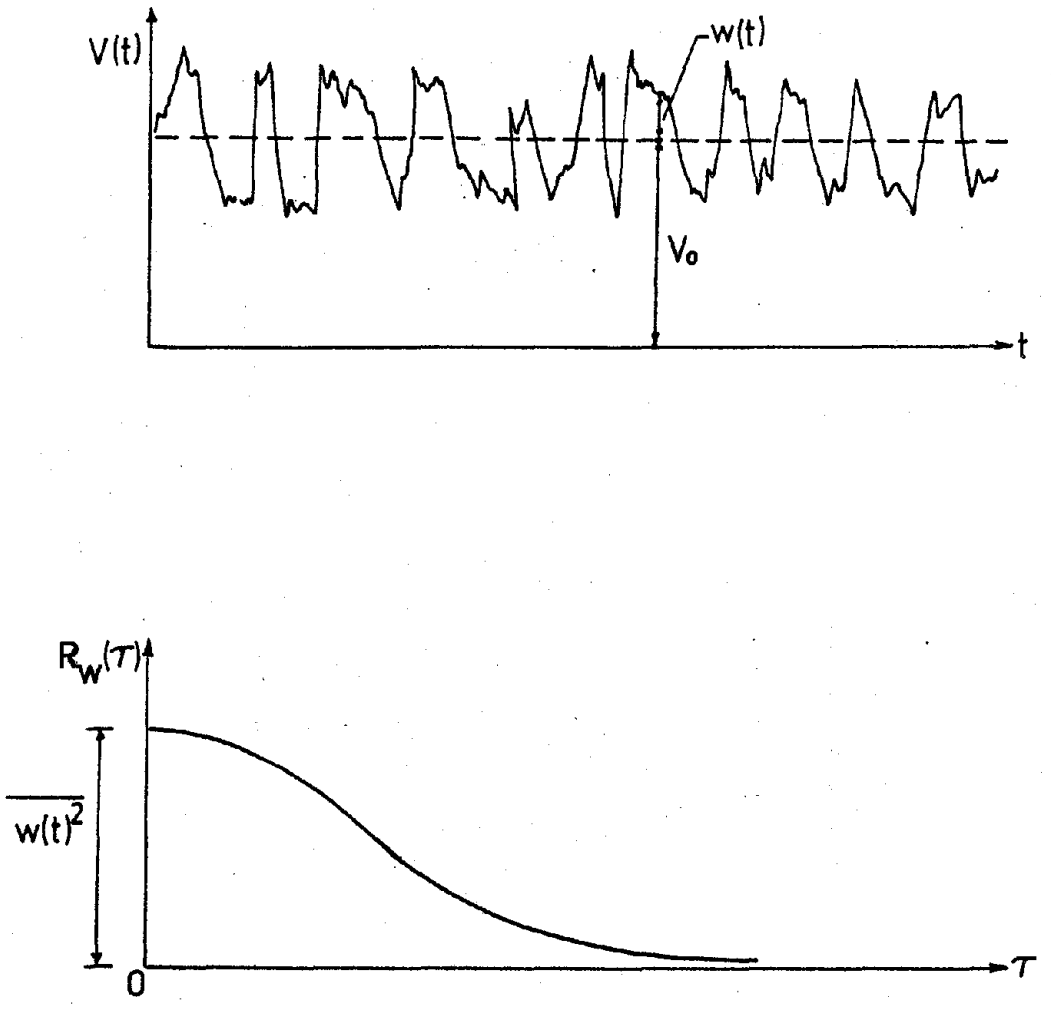

Figure 2.1 Mean and fluctuating wind velocities and autocovariance function

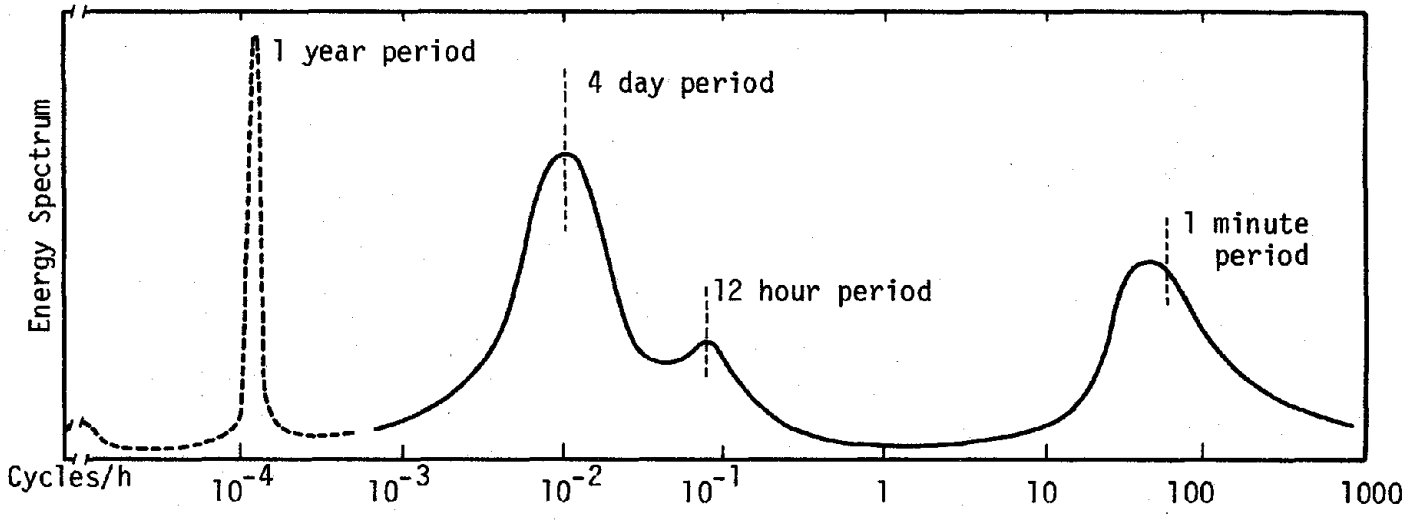

Figure 2.2 Spectrum of horizontal wind speed near the ground for an extensive frequency range (from measurements at 100 m. height by Van der Hoven at Brooklyn, N.Y., [13])

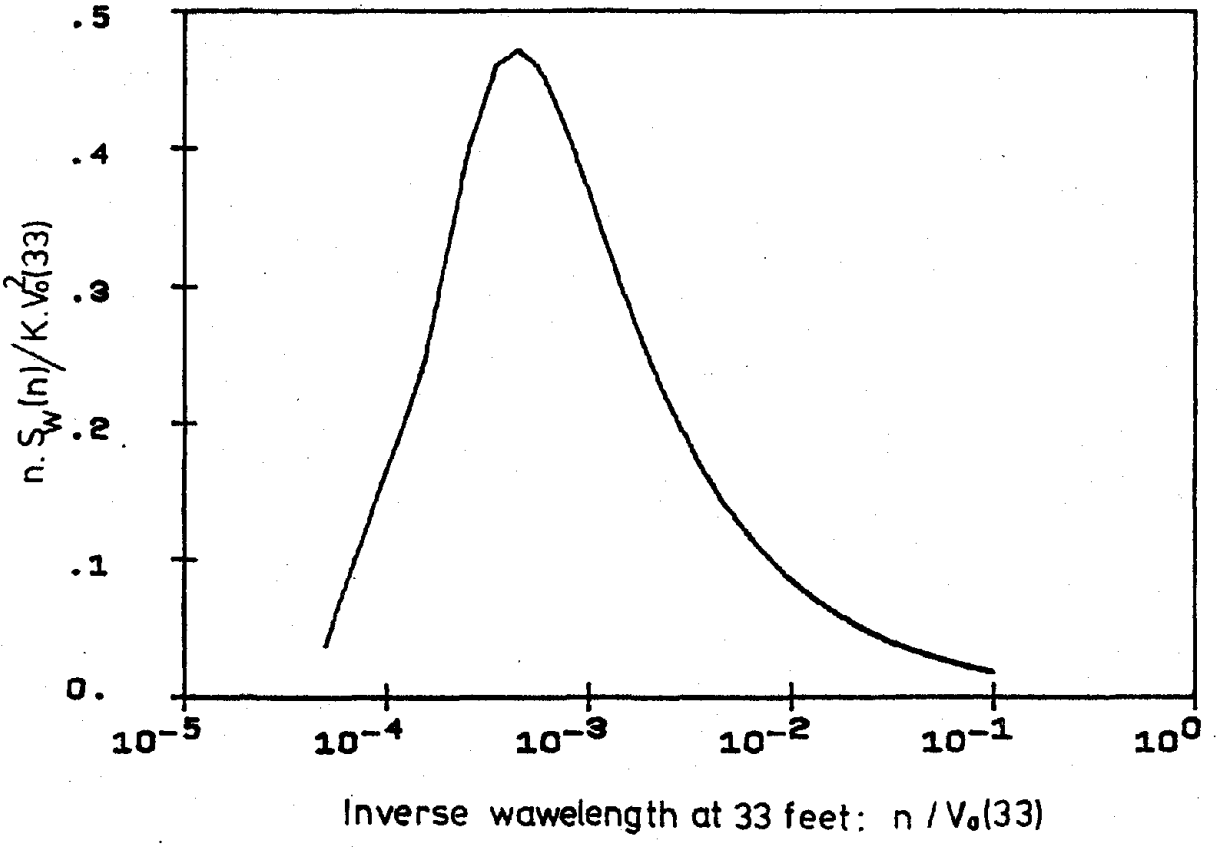

Figure 2.3 Spectrum of horizontal gustiness suggested by Davenport [2]

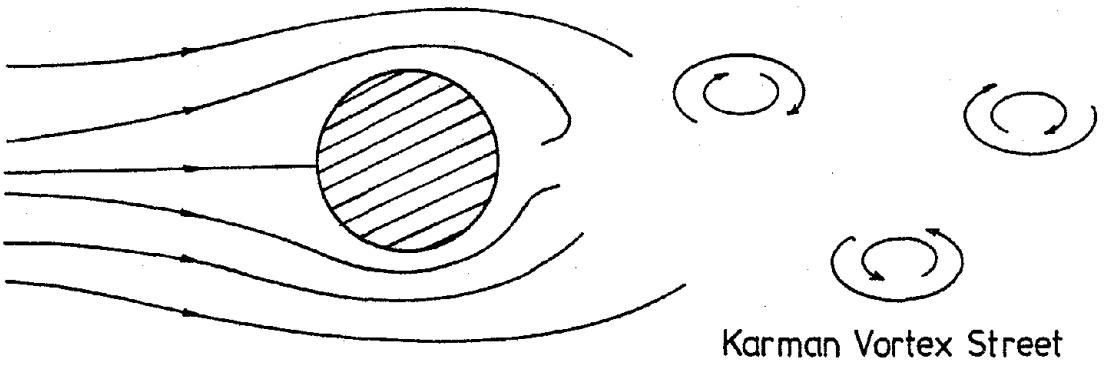

Figure 3.1 Mechanism of vortex shedding

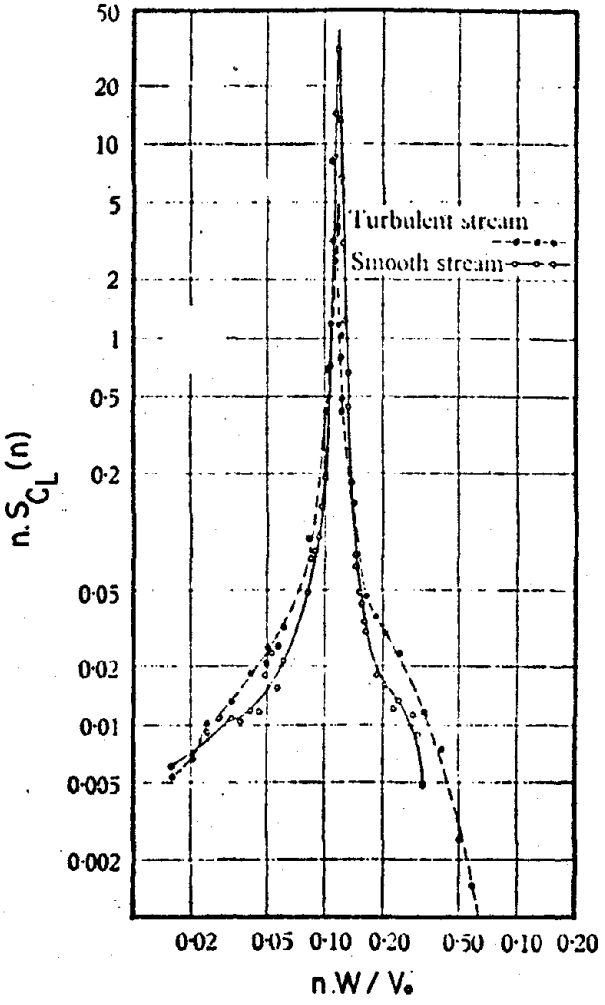

Figure 3.2 Spectrum of lift fluctuations on a square section cylinder for flow normal to a face (after Vickery [35]

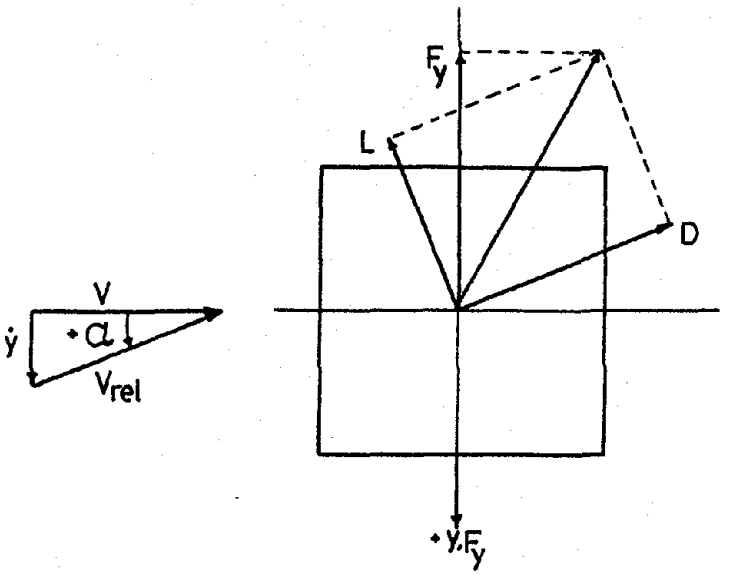

Figure 3.3 Rectangular cross-section in arbitrary wind flow

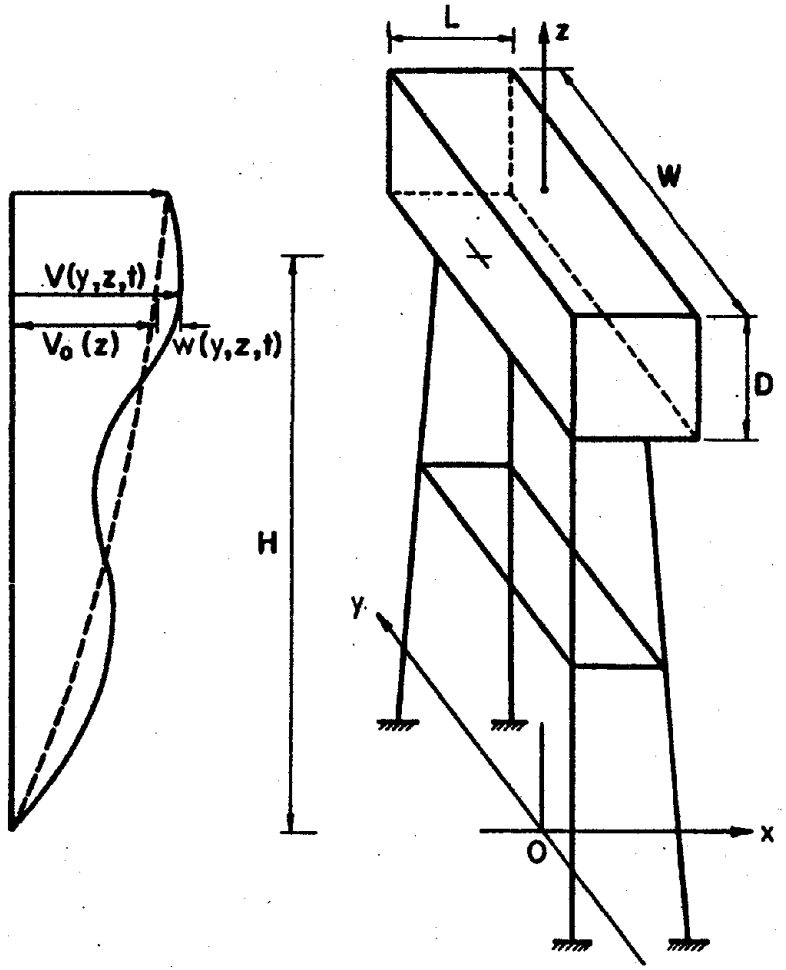

Figure 4.1 Schematic view of a single-mass structure and approaching wind

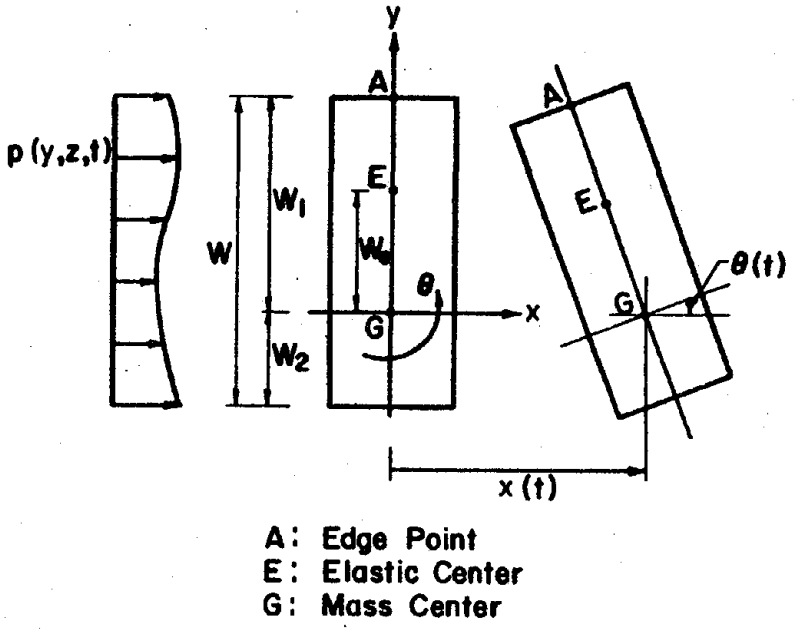

Figure 4.2 Plan view of a single-mass structure and wind pressures

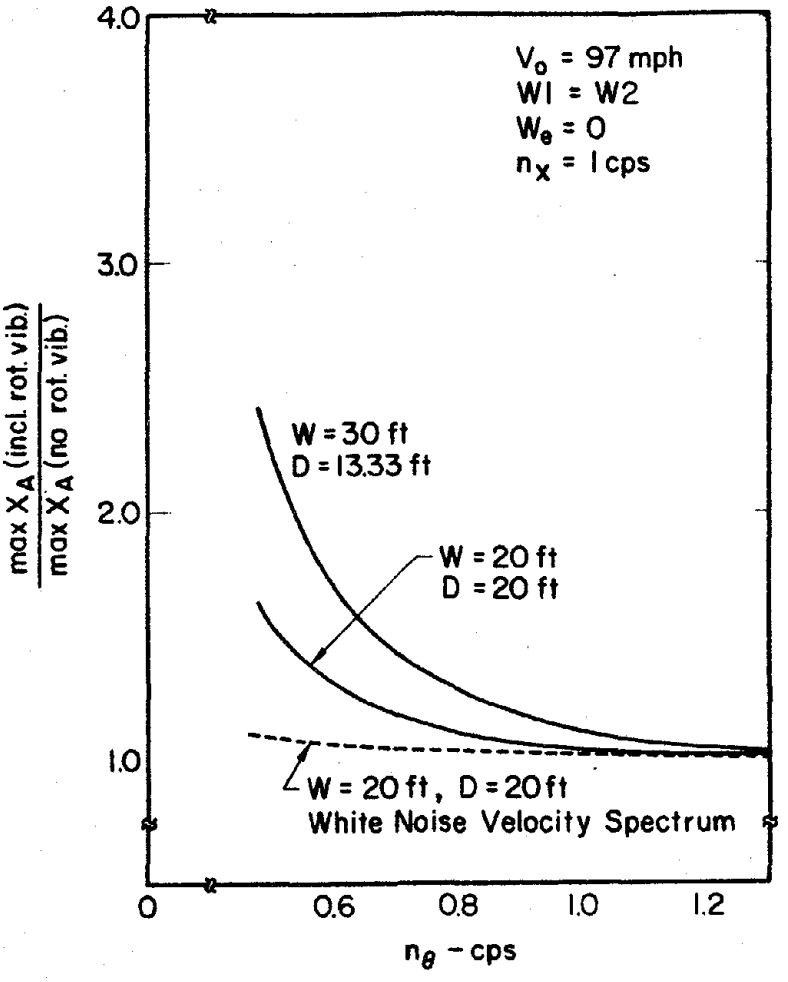

Figure 4.3 Torsional vibration of single-mass symmetric structures

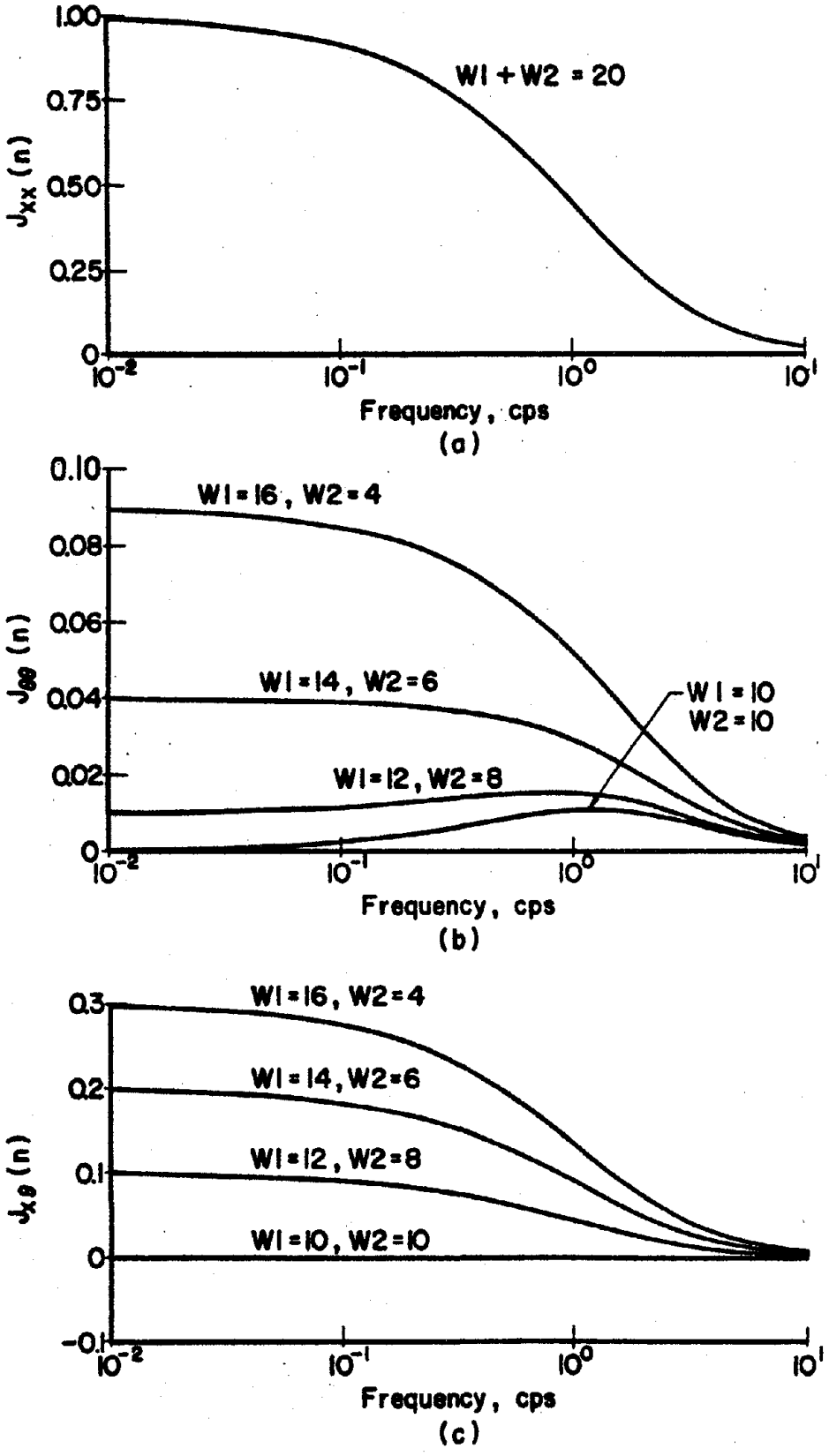

Figure 4.4 Aerodynamic admittance functions

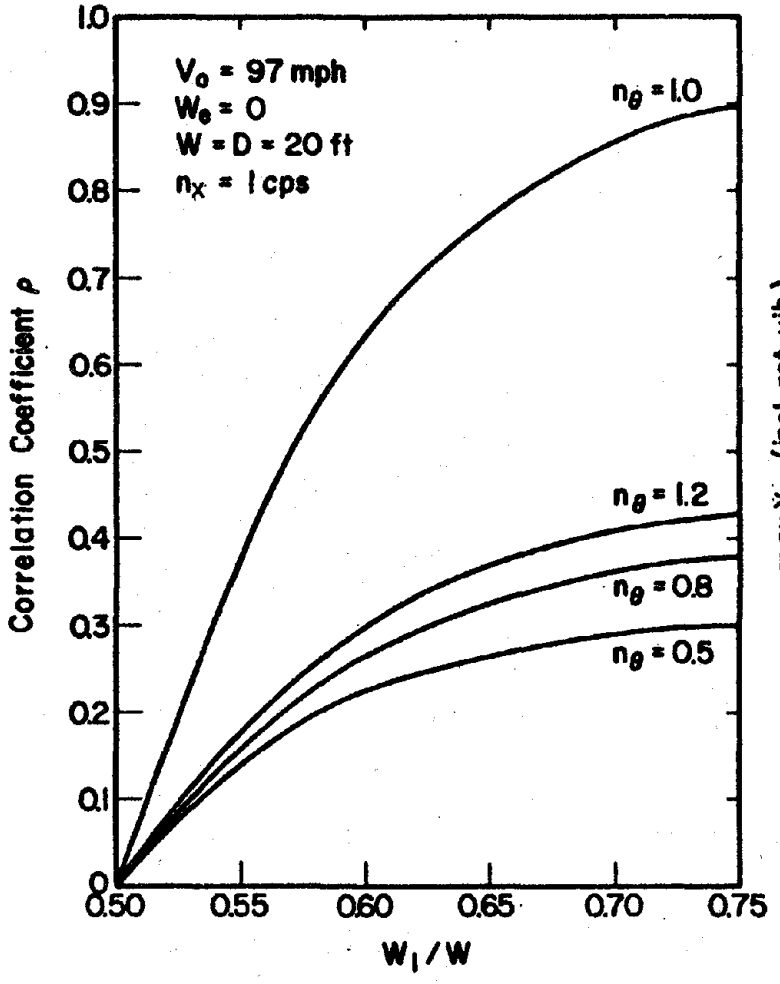

Figure 4.5 Correlation coefficient of responses of single-mass structures with only geometric asymmetry

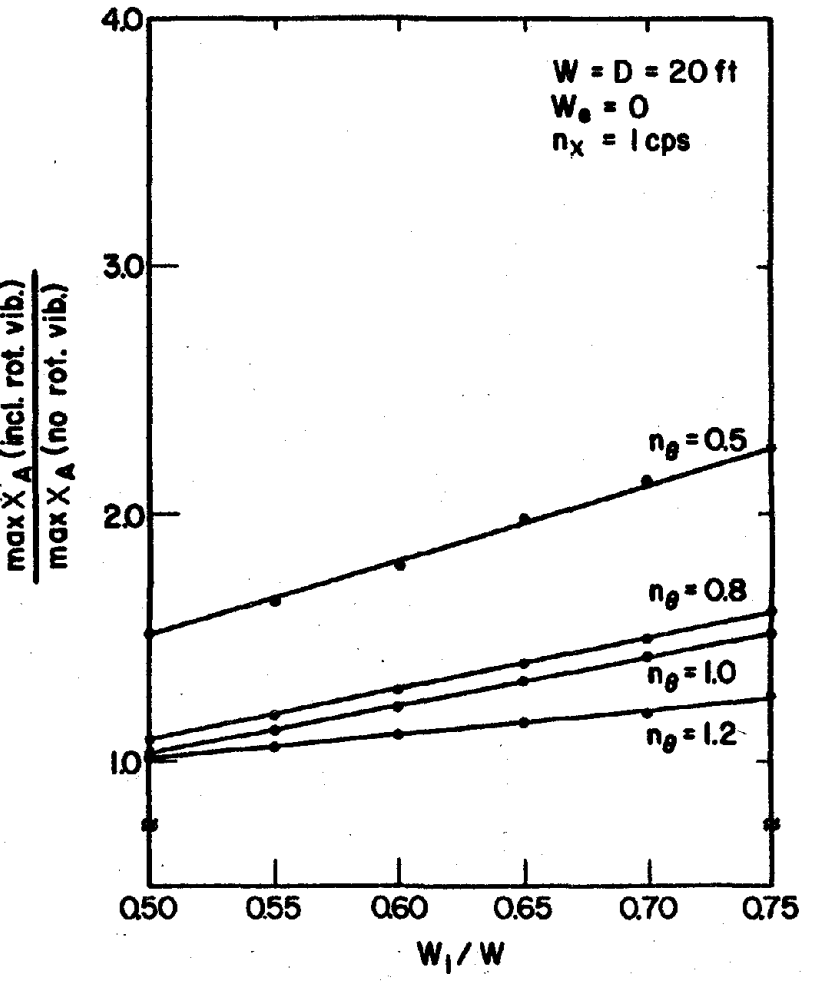

Figure 4.6 Torsional vibration of single-mass structures with only geometric asymmetry

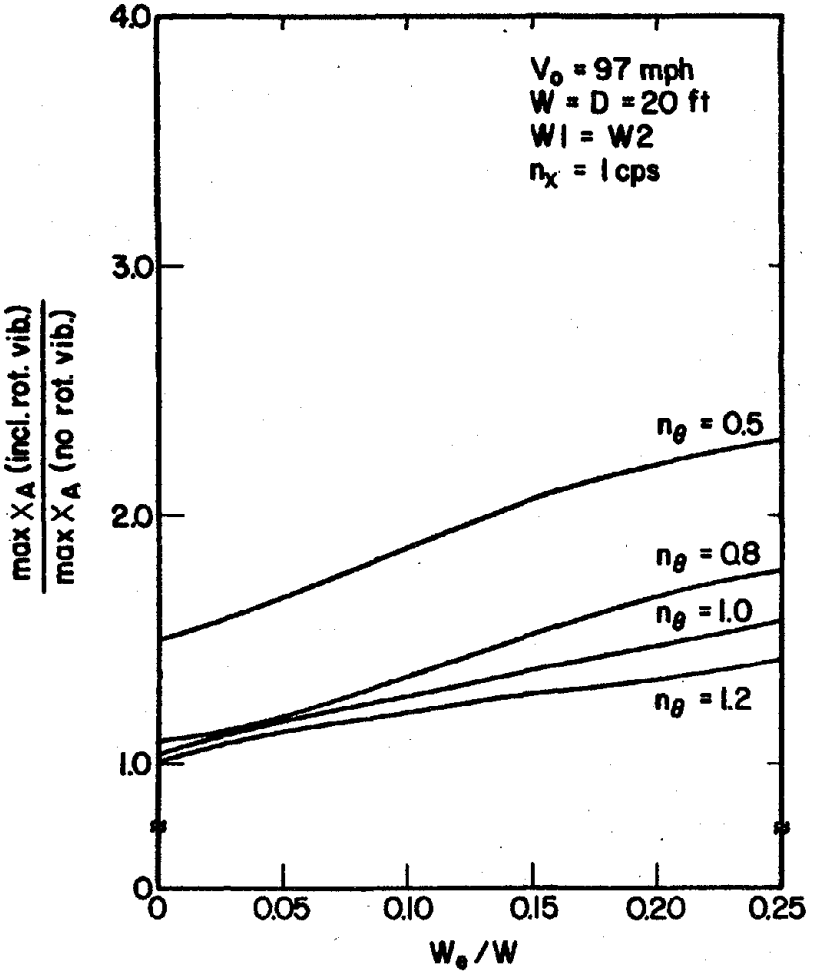

Figure 4.7 Torsional vibration of single-mass structures with only structural asymmetry

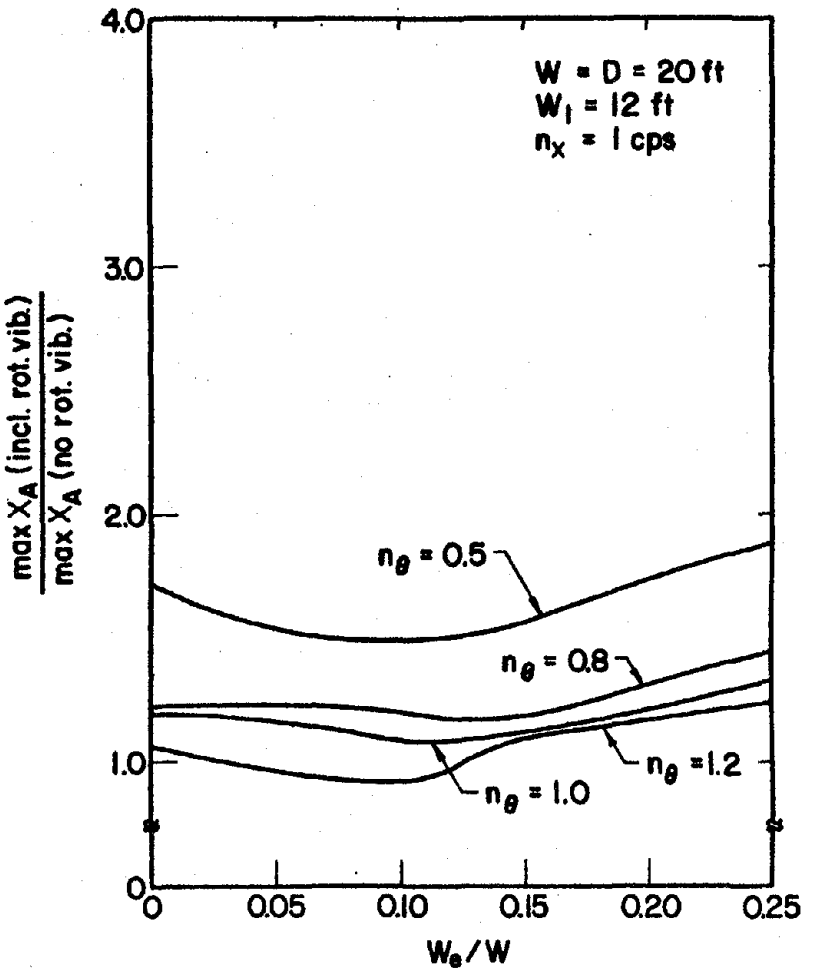

Figure 4.8 Torsional vibration of single-mass structures with both structural and geometric asymmetry

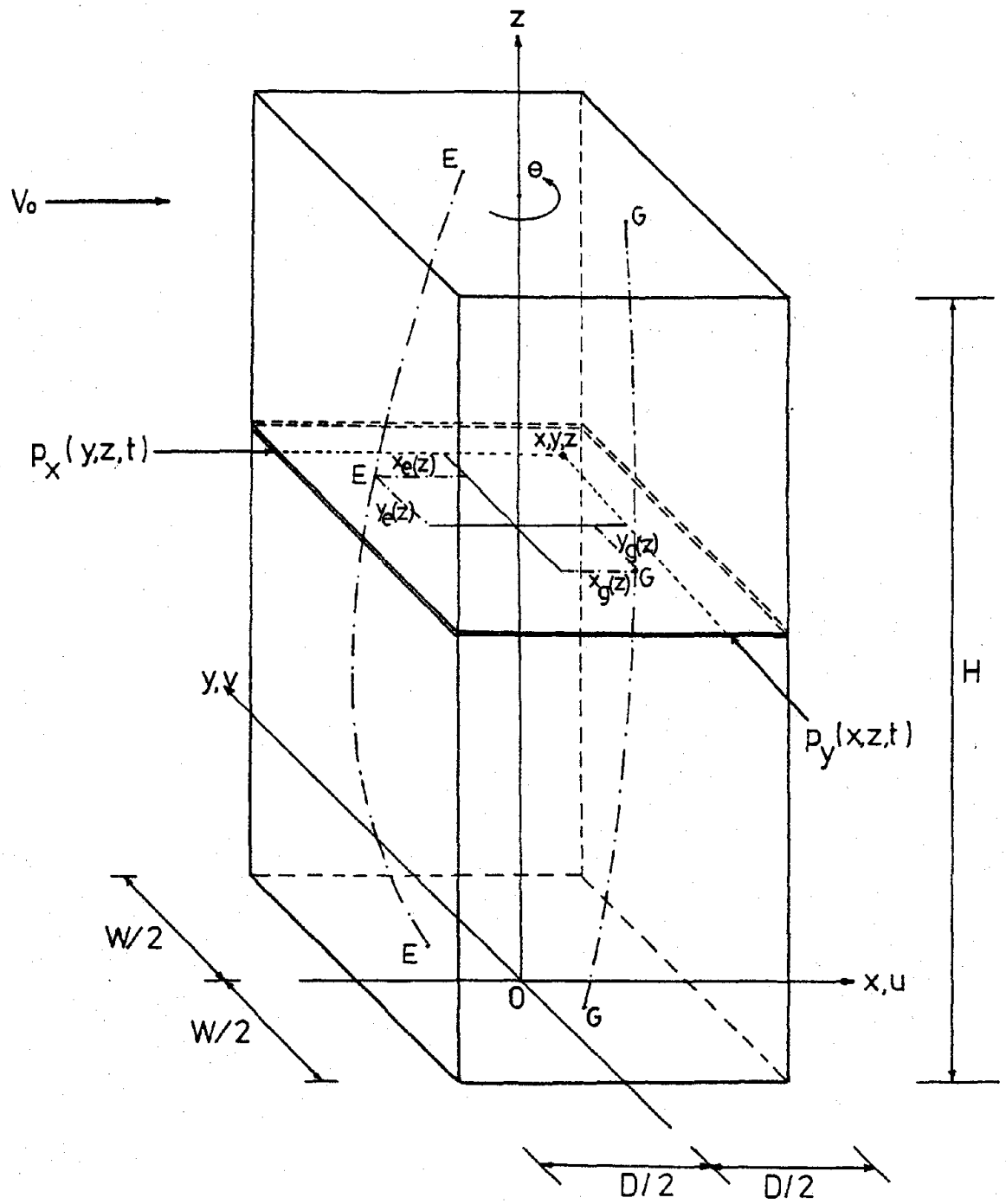

Figure 5.1 Schematic of a building with rectangular cross-section

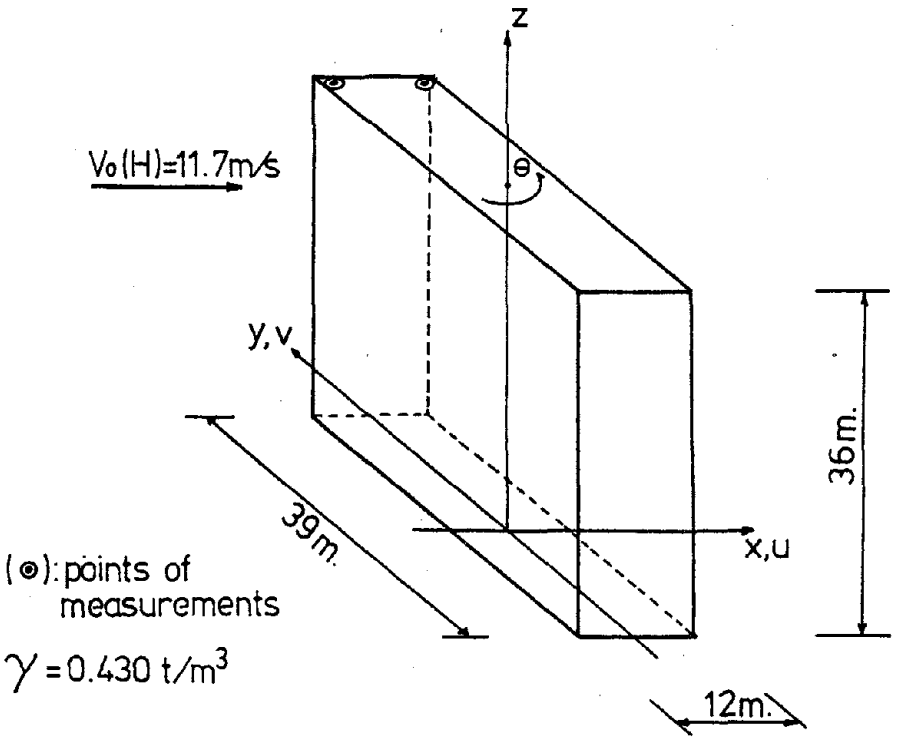

n_x = 1.48 cps $\quad \xi_x$ = 0.015
n_y = 1.23 cps $\quad \xi_y$ = 0.016
n_θ = 2.12 cps $\quad \xi_\theta$ = 0.015

	Measured	Calculated
$\left[\frac{\sigma_v}{\sigma_u}\right]_{corner}$ =	0.719	0.814

Figure 5.4 Schematic of the rectangular building studied by van Koten [17] with a comparison of measured and calculated responses

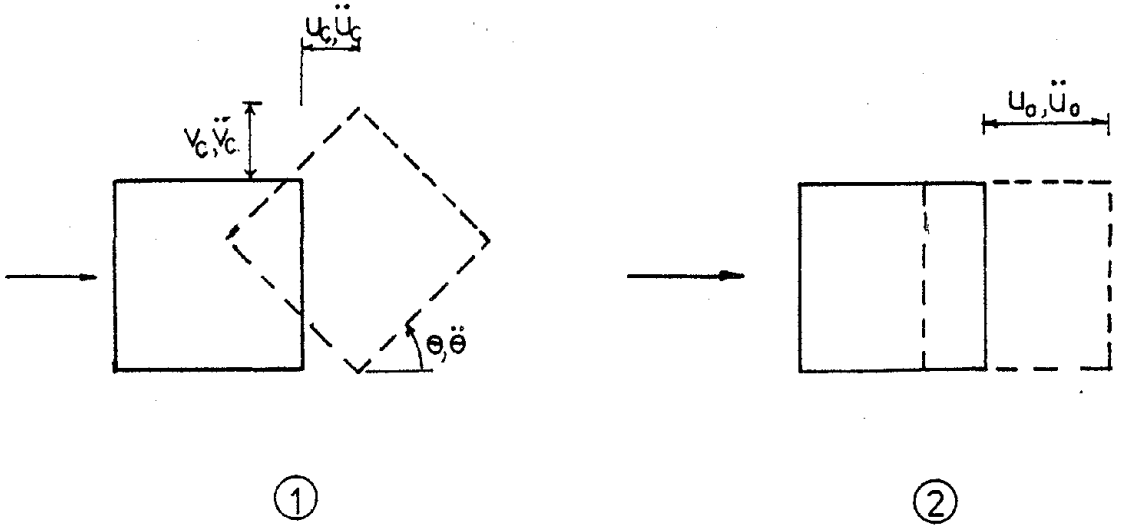

$$r_u = \frac{u_c}{u_o} \qquad r_v = \frac{v_c}{u_o}$$

$$r_{\ddot{u}} = \frac{\ddot{u}_c}{\ddot{u}_o} \qquad r_{\ddot{v}} = \frac{\ddot{v}_c}{\ddot{u}_o}$$

Figure 5.5 Schematic demonstrating response ratios

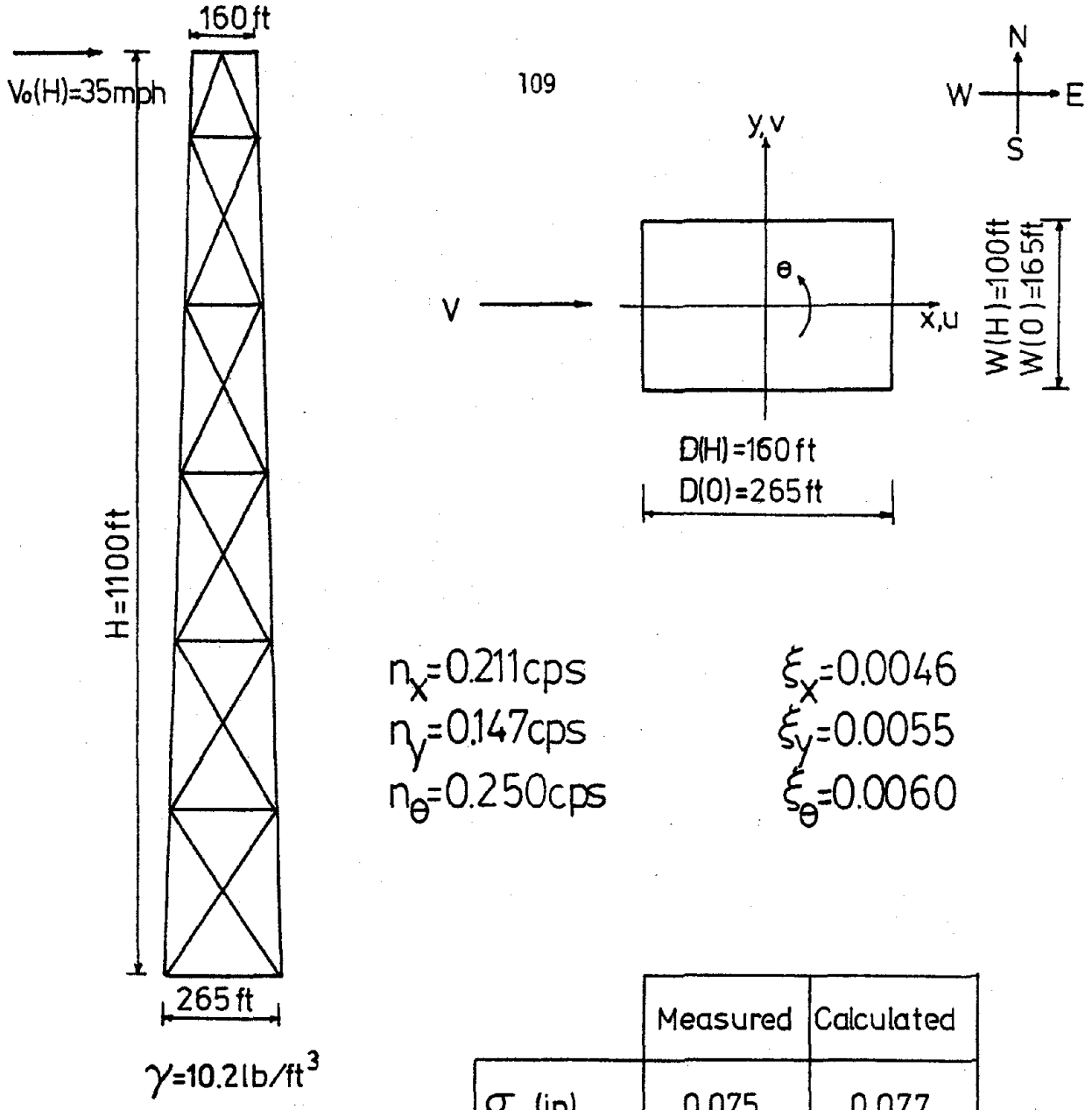

	Measured	Calculated
σ_u (in)	0.075	0.077
σ_v (in)	0.700	0.767
$\sigma_\theta \cdot \frac{D(H)}{2}$ (in)	—	0.007

Figure 5.2 Schematic of the John Hancock Building in Chicago with a comparison of measured and calculated responses

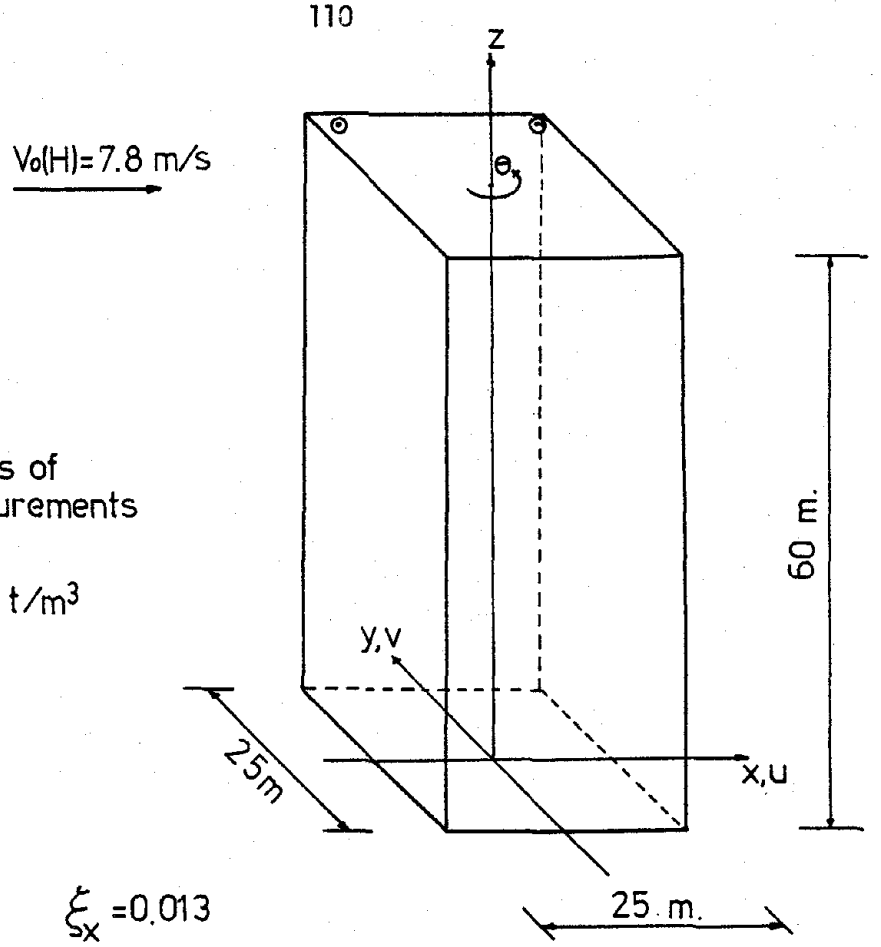

n_x = 0.80 cps $\quad \xi_x$ = 0.013

n_y = 1.04 cps $\quad \xi_y$ = 0.021

n_θ = 1.80 cps $\quad \xi_\theta$ = 0.020

	Measured	Calculated
$\left[\frac{\sigma_v}{\sigma_u}\right]_{corner}$	1.583	1.666

Figure 5.3 Schematic of the square building studied by van Koten [17] with a comparison of measured and calculated responses

$$- y_g m\ddot{u} + x_g m\ddot{v} + I\ddot{\theta} + c_\theta.\dot{\theta} - \phi_x.y_e'' + 2(\phi_x y_e')' - (\phi_x.y_e)''$$

$$+ \phi_y x_e'' - 2(\phi_y x_e')' + (\phi_y x_e)'' - (k_\theta.\theta')' = f_\theta(z,t) \quad (B.15)$$

where

$$\phi_x = k_x [u'' - (y_g.\theta)''] \quad (B.16)$$

$$\phi_y = k_y [v'' + (x_g.\theta)''] \quad (B.17)$$

If $x_e = y_e = 0$ the equations are greatly simplified as given below

$$m\ddot{u} - y_g m\ddot{\theta} + c_x\dot{u} + (k_x u'')'' = f_x(z,t) \quad (B.18)$$

$$m\ddot{v} + x_g m\ddot{\theta} + c_y\dot{v} + (k_y v'')'' = f_y(z,t) \quad (B.19)$$

$$- y_g m\ddot{u} + x_g m\ddot{v} + I.\ddot{\theta} + c_\theta.\dot{\theta} - (k_\theta.\theta')' = f_\theta(z,t) \quad (B.20)$$

This simplified form of equations can also be obtained if the coordinate axis is chosen in such a way that $x_e(z) = y_e(z) = 0$ along the z axis. In this case, the boundaries of the integrals over x and y in section (5.5) should be changed accordingly.

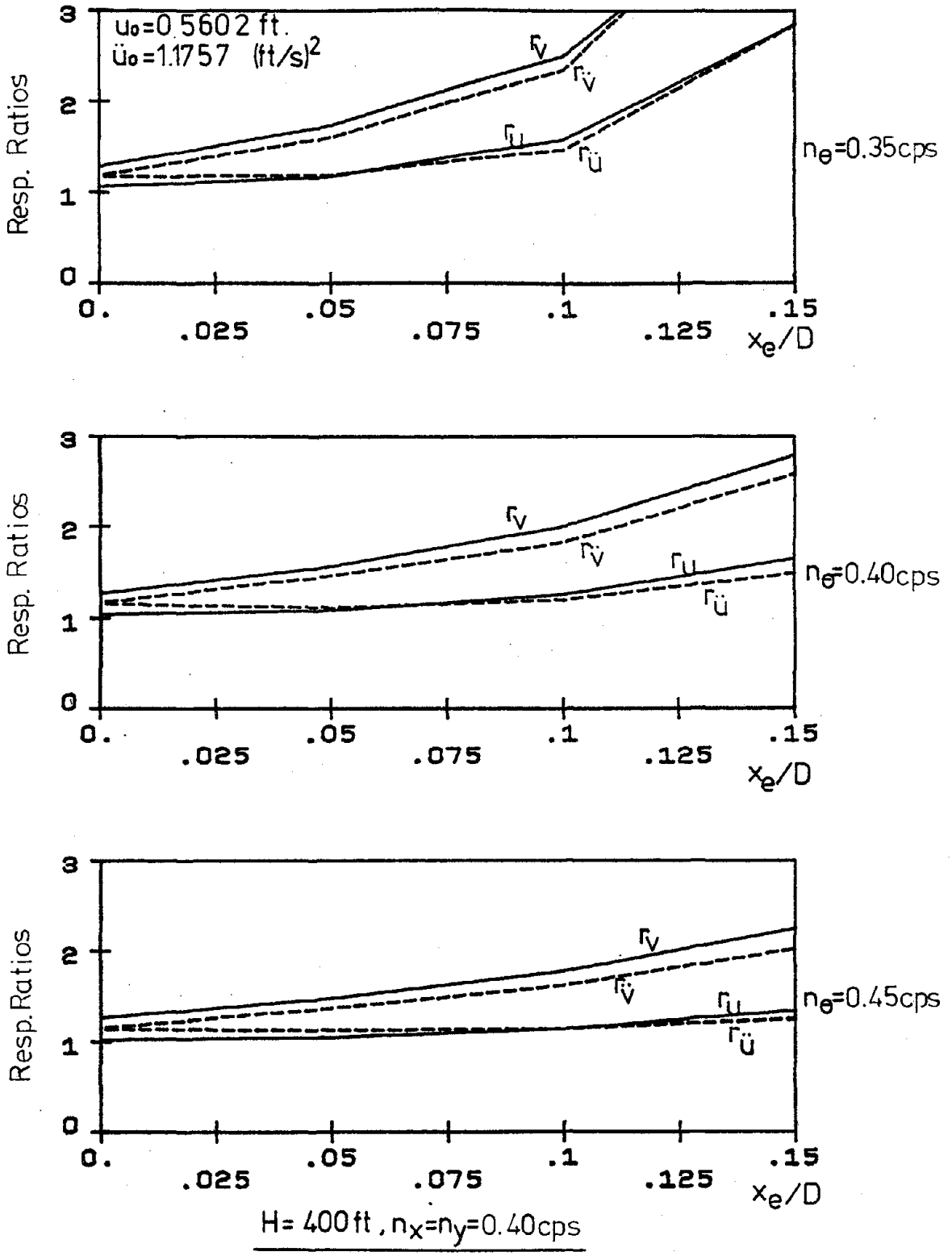

Figure 5.6 Normalized top-story corner responses of Building-I with structural asymmetry in across-wind direction

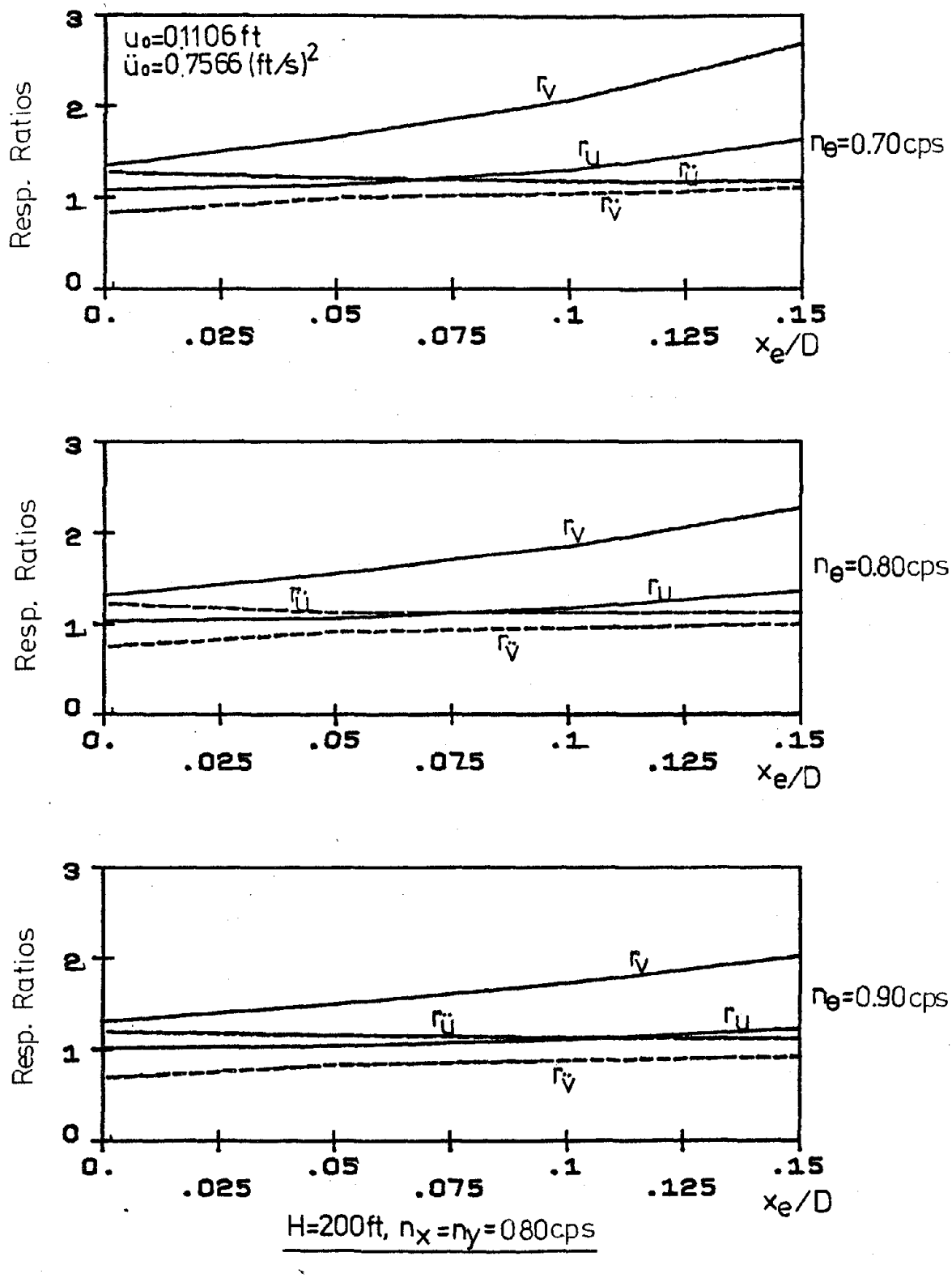

Figure 5.7 Normalized top-corner responses of Building-II with structural asymmetry in across-wind direction

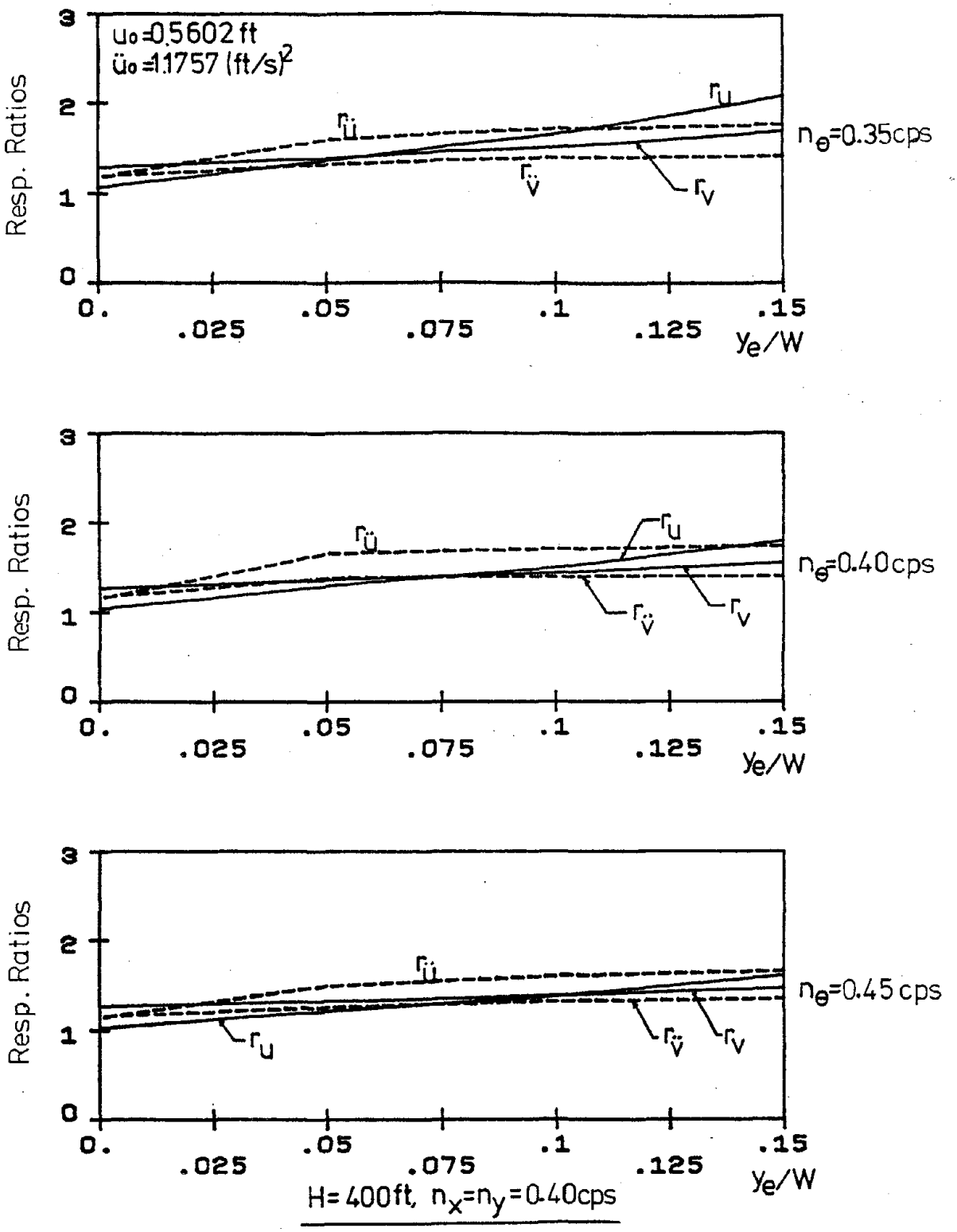

Figure 5.8 Normalized top-story corner responses of Building-I with structural asymmetry in along-wind direction

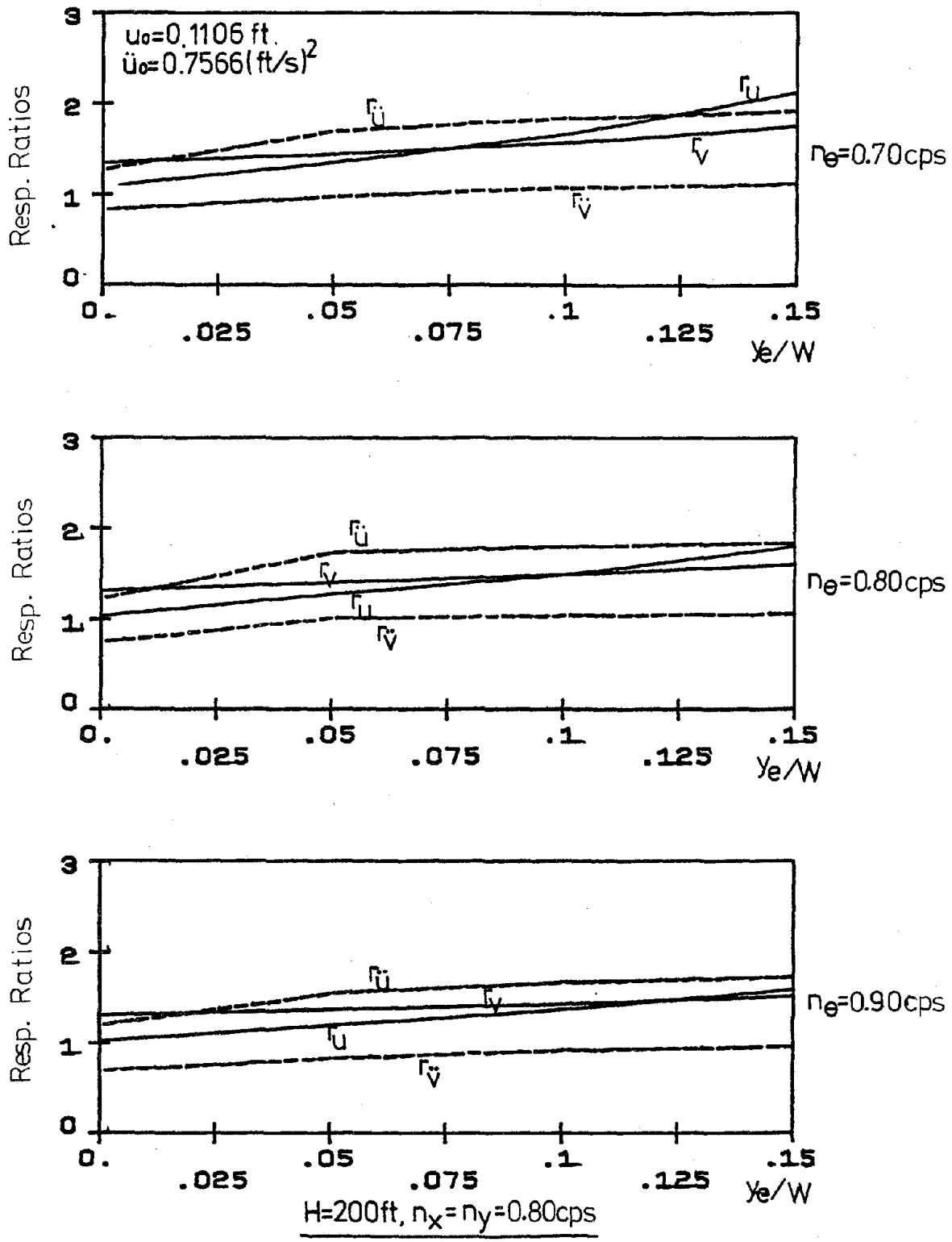

Figure 5.9 Normalized top-story corner responses of Building-II with structural asymmetry in along-wind direction

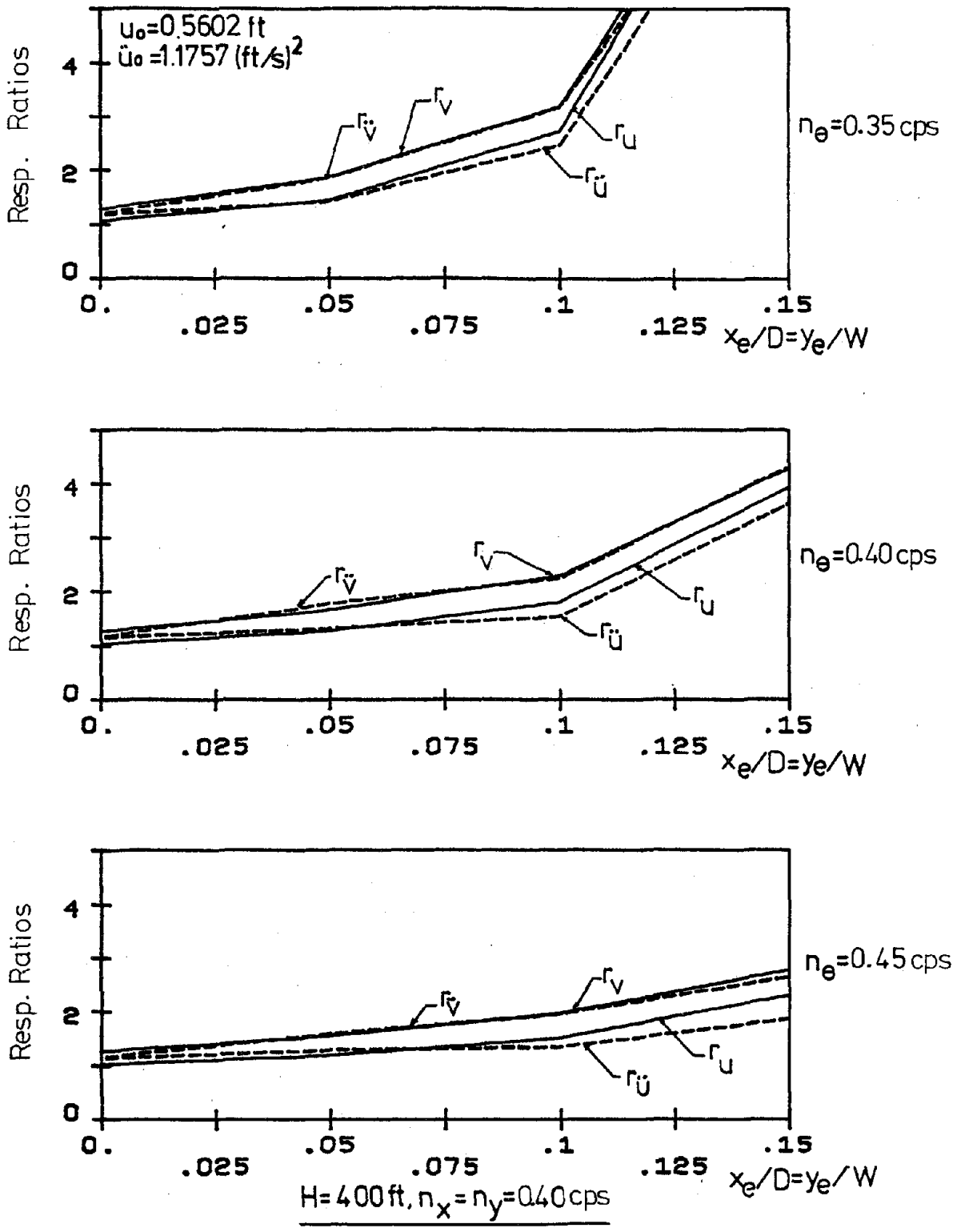

Figure 5.10 Normalized top-story corner responses of Building-I with structural asymmetry both in along-wind direction and across-wind direction

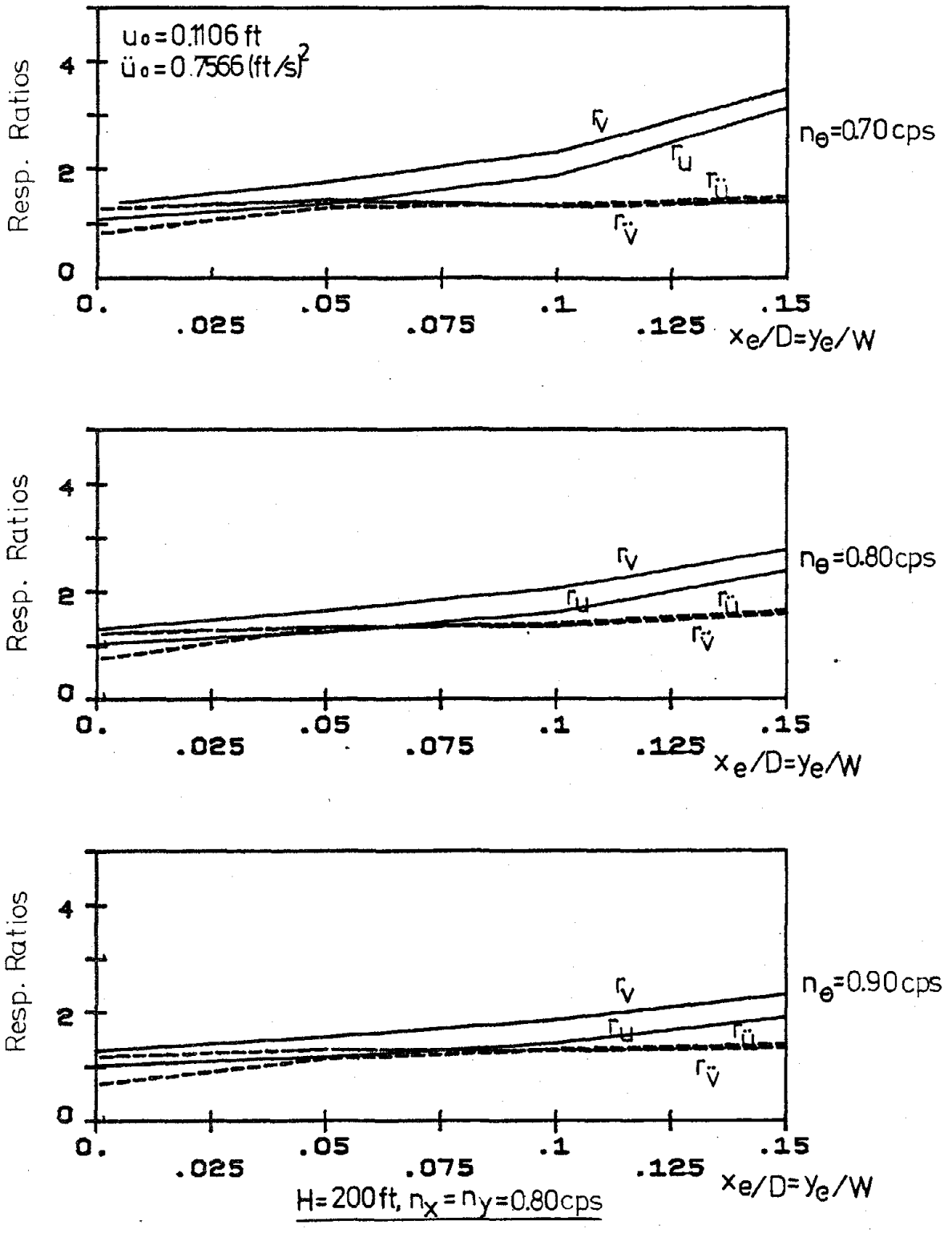

Figure 5.11 Normalized top-story corner responses of Building-II with structural asymmetry both in along-wind direction and across-wind direction

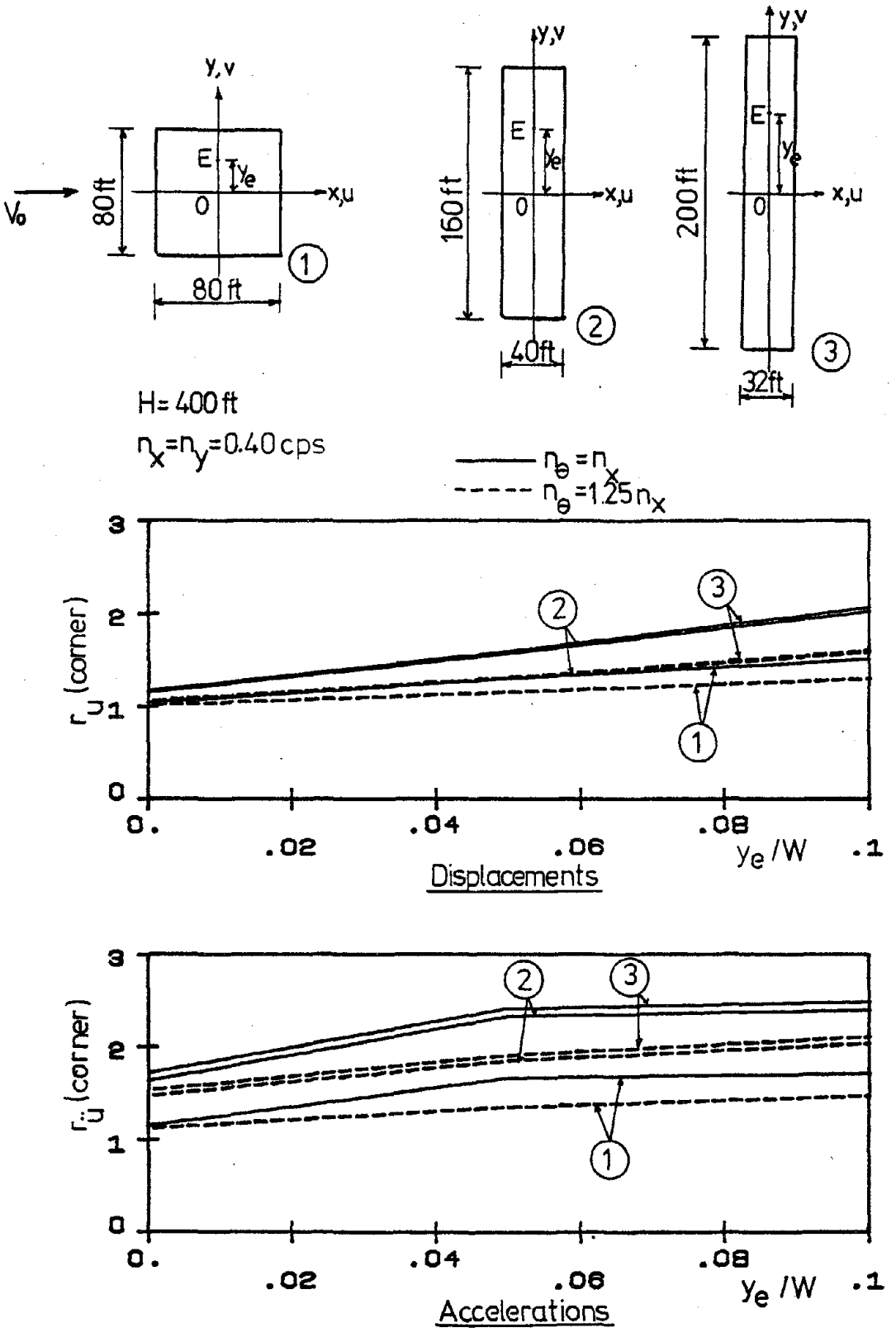

Figure 5.12 Normalized top-story corner responses of Building-I for various frontal widths with structural asymmetry in along-wind direction

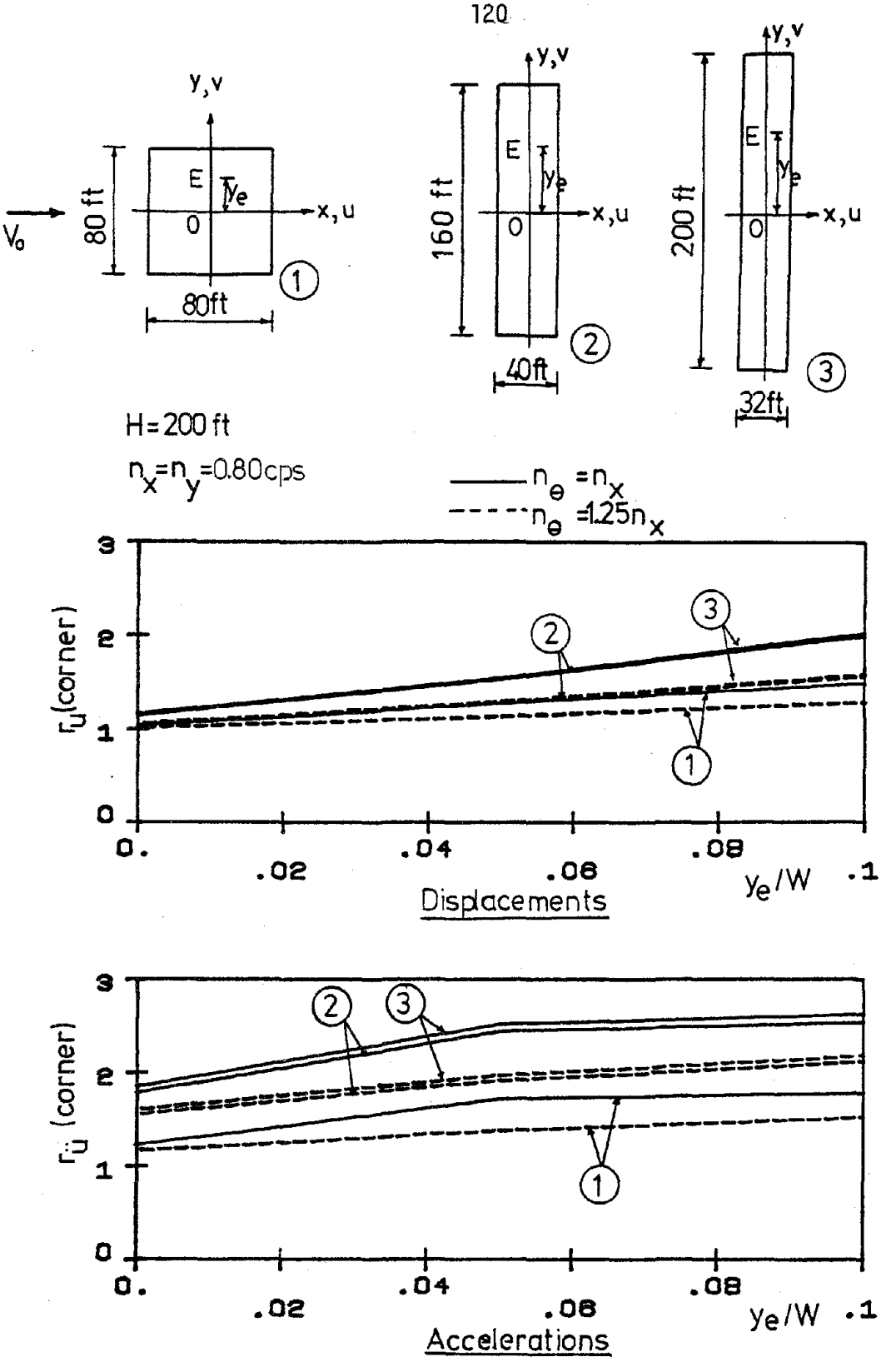

Figure 5.13 Normalized top-story corner responses of Building-II for various frontal widths with structural asymmetry in along-wind direction

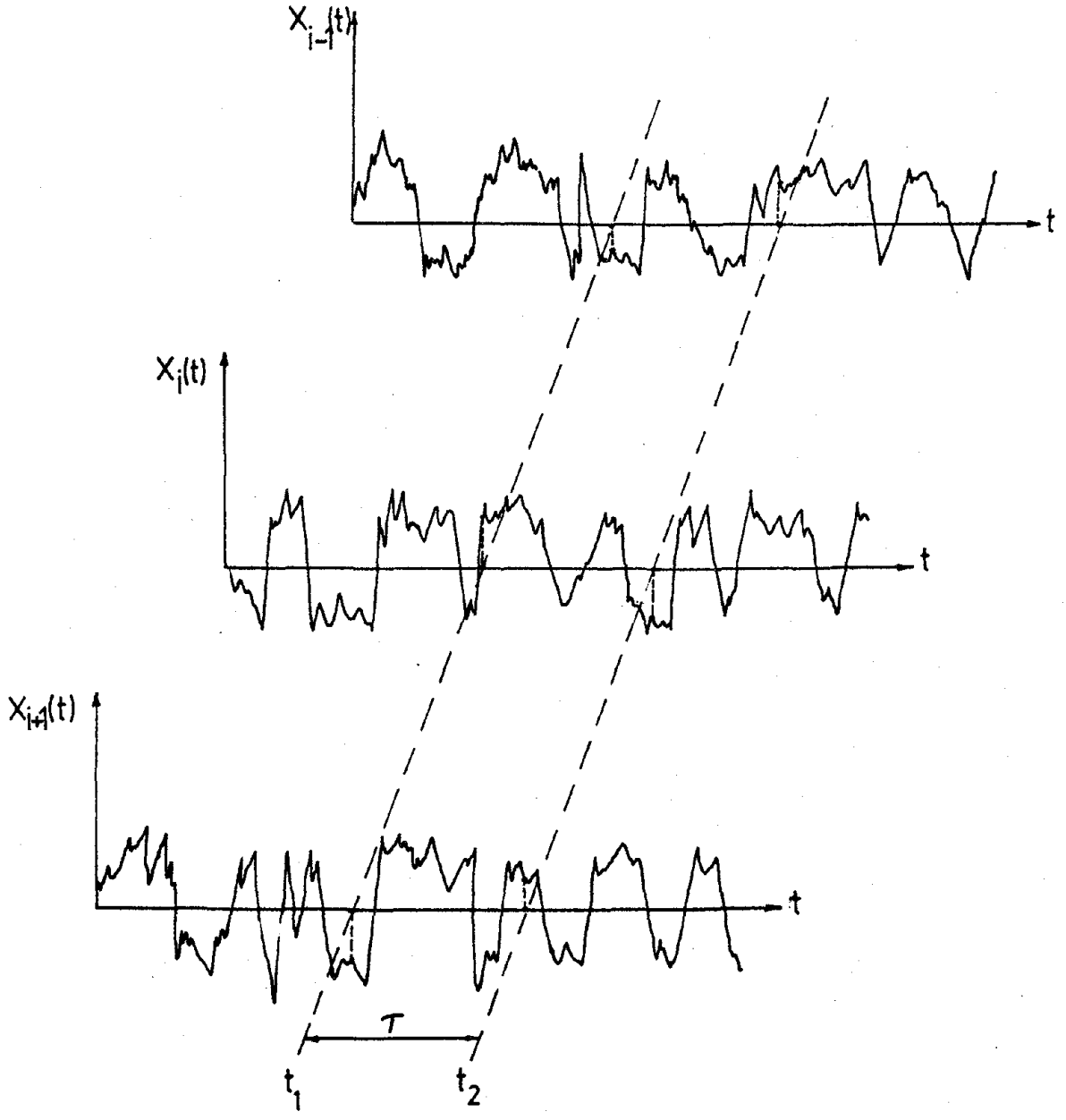

Figure A.1 Schematic of a random process

APPENDIX-A

RANDOM PROCESSES

In this section, a definition of a stationary random process will be given and the mathematical expressions which characterize the process will be introduced. The characterization of functions of random variables will also be presented.

A schematic representation of a random process X(t) is given in Figure (A.1). Each $X_i(t)$ is called a sample function of the ensemble. The mean function of the process, $\overline{X}(t)$, is given by the following formula

$$\overline{X}(t) = E\,[X(t)] \tag{A.1}$$

Where E [ ] denotes the ensemble average. The mean function describes the first-order statistical properties of a random process. The second-order statistical property is defined by the autocorrelation function, R_{xx}, which is given by

$$R_{xx}(t_1,t_2) = E\,[X(t_1).X(t_2)] \tag{A.2}$$

A random process is called stationary if

$$R_{xx}(t_1,t_2) = R_{xx}(t_2-t_1) \tag{A.3}$$

With this definition it may be concluded that the mean function of a stationary random process is constant. By denoting $t_2 - t_1 = \tau$ Eq. (A.2) becomes

$$R_{xx}(\tau) = E\,[X(t).X(t+\tau)] \tag{A.4}$$

A stationary random process is called ergodic if its time averages are equal to its ensemble averages. Thus, only one sample function would be enough to describe the properties of an ergodic process. If X(t) is ergodic, $R_{xx}(\ )$ can be calculated as

$$R_{xx}(\tau) = \lim_{T\to\infty} \frac{1}{T} \int_{-T/2}^{T/2} X(t).X(t+\tau)\, dt \tag{A.5}$$

The correlation function between two stationary random processes, X(t) and Y(t), is called the crosscorrelation function, and given by

$$R_{xy}(\tau) = E\,[X(t).Y(t+\tau)] \tag{A.6}$$

If they are also ergodic

$$R_{xy}(\tau) = \lim_{T\to\infty} \frac{1}{T} \int_{-T/2}^{T/2} X(t).Y(t+\tau)\, dt \tag{A.7}$$

Two important properties of the correlation functions are given below

$$R_{xx}(\tau) = R_{xx}(-\tau) \tag{A.8}$$

$$R_{xy}(\tau) = R_{xy}(-\tau) \tag{A.9}$$

and

$$|R_{xx}(\tau)| \leq R_{xx}(0) \tag{A.10}$$

$$|R_{xy}(\tau)| \leq [R_{xx}(0).R_{yy}(0)]^{1/2} \tag{A.11}$$

If the mean value of the process is zero, it can be written from Eq. (A.4) that

$$R_{xx}(0) = E\,[X^2(t)] = \sigma_{xx}^2 \tag{A.12}$$

where σ_{xx}^2 is the mean square value of the process.

Another important function to describe a stationary random process is the spectral density function. The spectral density functions are defined as the Fourier transform of the correlator functions and are given by the following equations

$$S_{xx}(n) = \int_{-\infty}^{\infty} R_{xx}(\tau)\, e^{-i2\pi n\tau}\, d\tau \tag{A.13}$$

$$S_{xy}(n) = \int_{-\infty}^{\infty} R_{xy}(\tau)\, e^{-i2\pi n\tau}\, d\tau \tag{A.14}$$

where n is the continuously varying cyclic frequency. $S_{xy}(n)$ is called the cross-spectral density function since it involves two different random variables. The product $S_{xx}(n).dn$ represents the contribution

to the mean square value from the values of the random variable lying in the frequency range (n, n+dn). The inverse relations to Figs. (A.13) and (A.14) are

$$R_{xx}(\tau) = \int_{-\infty}^{\infty} S_{xx}(n)\, e^{i2\pi n\tau}\, dn \tag{A.15}$$

$$R_{xy}(\tau) = \int_{-\infty}^{\infty} S_{xy}(n)\, e^{i2\pi n\tau}\, dn \tag{A.16}$$

From the properties of the correlation functions following properties for the spectral density functions can be written

$$S_{xx}(n) = S_{xx}(-n) \tag{A.17}$$

$$S_{xy}(n) = S^{*}_{yx}(n) = S_{yx}(-n) \tag{A.18}$$

The physical significance of the spectral density function can be seen by letting $\tau = 0$ in Eqs. (A.15) and (A.16)

$$R_{xx}(0) = \int_{-\infty}^{\infty} S_{xx}(n)\, dn = \sigma^2_{xx} \tag{A.19}$$

$$R_{xy}(0) = \int_{-\infty}^{\infty} S_{xy}(n)\, dn = \sigma^2_{xy} \tag{A.20}$$

where σ^2_{xx} is the mean square value of the random variable, X(t), and σ^2_{xy} gives a measure of the linear correlation between the random

variables X(t) and Y(t). The correlation coefficient, ρ_{xy}, is defined by

$$\rho_{xy} = \frac{\sigma^2_{xy}}{\sigma_{xx}.\sigma_{yy}} \tag{A.21}$$

For real valued random processes $S_{xx}(n)$ must be real and even in view of Eq. (A.17). For this reason Eq. (A.13) can be written

$$S_{xx}(n) = 2 \int_0^{\infty} R_{xx}(\tau).\cos 2\pi\tau d\tau \tag{A.22}$$

The inverse relation, Eq. (A.15), then becomes

$$R_{xx}(\tau) = 2 \int_0^{\infty} S_{xx}(n).\cos 2\pi\tau dn \tag{A.23}$$

Spectral density functions, with above definitions, are called the two-sided spectral density functions since the frequency n ranges over $(-\infty,\infty)$. The physically realizable spectral density functions, the so-called one-sided spectral density functions are the ones where n varies only over $(0, \infty)$. They are defined by

$$S'_{xx}(n) = 2S_{xx}(n) \tag{A.24}$$

$$S'_{xy}(n) = 2S_{xy}(n) \tag{A.25}$$

These are the quantities measured in practice. With this new definitions Eqs. (A.22) and (A.23) become

$$U_t = \frac{1}{2}\int_0^H k_\theta(z)\,\theta'^2\,dz \tag{B.5}$$

where $k(z)$ is given by

$$k(z) = G.J(z) \tag{B.6}$$

$J(z)$ is the polar moment of inertia of the cross-section of height z and G is the shear modulus. The potential energy of the external forces, as given by Eq. (5.28), is

$$\Omega = -\int_0^H [f_x(z,t)u + f_y(z,t)v + f_\theta(z,t)\theta]\,dz \tag{B.7}$$

The total potential energy of the structure, then, becomes

$$V_{PE} = U_b + U_t + \Omega \tag{B.8}$$

For simplicity lets assume, for now, that the system is conservative (i.e. no damping forces). By applying Hamilton's principle the action integral, A_c, can be written as the definite time intergral of T_{KE}-V_{PE}. Thus,

$$A_c = \frac{1}{2}\int_{t_o}^{t_1}\int_0^H \{m.\dot{u}^2 + m.\dot{v}^2 + I.\dot{\theta}^2 + 2x_g.m.\dot{v}\dot{\theta} - 2y_g.m.\dot{u}\dot{\theta}$$

$$- k_x(u-y_e.\theta)''^2 - k_y(v+x_e\theta)''^2 - k_\theta.\theta'^2$$

$$+ 2f_x.u + 2f_y.v + 2f_\theta.\theta\}\,dzdt \tag{B.9}$$

The dependence of the cross-sectional properties and the forces on z is not written explicitly for clarity. By Hamilton's principle the action integral is stationary, such that

$$\delta A_c = 0 \tag{B.10}$$

This condition yields the Euler differential equations for the integrand of Eq. (B.9). For direction, for instance, the Euler differential equation is given by [19]

$$\frac{\partial F}{\partial u} - \frac{\partial}{\partial t}\left(\frac{\partial F}{\partial \dot{u}}\right) - \frac{\partial}{\partial z}\left(\frac{\partial F}{\partial u'}\right) + \frac{\partial^2}{\partial t^2}\left(\frac{\partial F}{\partial \ddot{u}}\right)$$

$$+ \frac{\partial^2}{\partial t \partial z}\left(\frac{\partial F}{\partial \dot{u}'}\right) + \frac{\partial^2}{\partial z^2}\left(\frac{\partial F}{\partial u''}\right) = 0 \tag{B.11}$$

where

$$F = F\ (t,z,u,v,\theta,\dot{u},\dot{v},\dot{\theta},u',v',\theta',\ddot{u},\ddot{v},\ddot{\theta},u'',v'',\theta'',\dot{u}',\dot{v}',\dot{\theta}') \tag{B.12}$$

is the integrand of the double integral in Eq. (B.9)

Application of the Euler equation for u, v and θ directions and also including the viscous type symmetric damping the equations of motion can be obtained as following:

$$m\ddot{u} - y_g m\ddot{\theta} + c_x\dot{u} + \phi_x'' = f_x(z,t) \tag{B.13}$$

$$m\ddot{v} + x_g m\ddot{\theta} + c_y\dot{v} + \phi_y'' = f_y(z,t) \tag{B.14}$$

3. If

$$\{Z(t)\} = \{g\}.X(t) \tag{A.37}$$

where {g} is n dimensional deterministic vector

$$[R_{zz}(\tau)] = E\{[Z(t)].[Z(t+\tau)]^T\} = \{g\}.R_{xx}(\tau)\{g\}^T \tag{A.38}$$

$$[S_{zz}(n)] = \{g\}.S_{xx}(n).\{g\}^T \tag{A.39}$$

where $[R_{zz}(\tau)]$ and $[S_{zz}(n)]$ are nxn matrices in this case.

4. If

$$\{Z(t)\} = \int [g(z)].\{X(z,t)\}\, dz \tag{A.40}$$

where [g(z)] is a matrix of deterministics functions of z

$$[R_{zz}(\tau)] = \iint [g(z)][R_{xx}(z_1,z_2,\tau)][g(z)]^T dz_1 dz_2 \tag{A.41}$$

$$[S_{zz}(n)] = \iint [g(z)][S_{xx}(z_1,z_2,n)][g(z)]^T dz_1 dz_2 \tag{A.42}$$

More on random processes can be found in references [15], [20] and [31].

APPENDIX-B

EQUATIONS OF MOTION FOR FLEXURAL BEAM MODEL

The kinetic energy of the structure, from Eq. (5.14), is

$$T_{KE} = \frac{1}{2}\int_0^H [m(z)\dot{u}^2 + m(z)\dot{v}^2 + I(z)\dot{\theta}^2 + 2x_g(z)m(z)\dot{v}\dot{\theta} - 2y_g(z)m(z)\dot{u}\dot{\theta}]\, dz \qquad (B.1)$$

The strain energy of bending can be written as the sum of the strain energy of bendings about x axis and about y axis. From elementary beam theory [19]

$$U_b = \frac{1}{2}\int_0^H \{k_x(z).[u-y_e(z)\theta]''^2 + k_y(z).[v+x_e(z)\theta]''^2\}dz \qquad (B.2)$$

where $k_x(z)$ and $k_y(z)$ are the stiffnesses for x and y directions and are given by

$$k_x(z) = E_m.I_y(z) \qquad (B.3)$$

$$k_y(z) = E_m.I_x(z) \qquad (B.4)$$

$I_x(z)$ and $I_y(z)$ are the moment of inertias of the cross-section at height z with respect to x and y axis repsectively, E_m is the modulus of elasticity in bending, and $x_e(z)$ and $y_e(z)$ are the coordinates of the elastic center at height z. The strain energy due to twisting is

$$S'_{xx}(n) = 4 \int_0^\infty R_{xx}(\tau).\cos 2\pi n.d\tau \qquad (A.26)$$

$$R_{xx}(\tau) = \int_0^\infty S'_{xx}(n).\cos 2\pi n.dn \qquad (A.27)$$

The mean square value of X(t) is now calculated by

$$R_{xx}(0) = \int_0^\infty S'_{xx}(n)\, dn = \sigma^2_{xx} \qquad (A.28)$$

The cross spectral density function given by Eq. (A.14) then becomes

$$S'_{xy}(n) = 2 \int_{-\infty}^\infty R_{xy}(\tau).e^{-i2\pi n\tau}\, d\tau \qquad (A.29)$$

where n varies only over $(0, \infty)$. The real part of $S'_{xy}(n)$ is called the co-spectrum, $C_{xy}(n)$, and the complex part is called the quad-spectrum $Q_{xy}(n)$. $C_{xy}(n)$ is a real-valued even function of n where $Q_{xy}(n)$ is a real-valued add function of n. The cross-correlation function, (A.16), now can be calculated as

$$R_{xy}(\tau) = \int_0^\infty C_{xy}(n).\cos 2\pi n\tau dn + \int_0^\infty Q_{xy}(n).\sin 2\pi n\tau.dn \qquad (A.30)$$

For $\tau = 0$

$$R_{xy}(0) = \int_0^\infty C_{xy}(n)dn = \sigma_{xy}^2 \qquad (A.30)$$

Using the definitions given above the following can be written for the correlation and spectral density functions of the functions of stationary random variables X(t) and Y(t).

1. If

$$Z(t) = g_1.X(t) + g_2.Y(t) \qquad (A.31)$$

where g_1 and g_2 are deterministic constants or variables

$$R_{zz}(\tau) = g_1^2R_{xx}(\tau) + g_2^2R_{yy}(\tau) + g_1g_2[R_{xy}(\tau) + R_{yx}(\tau)] \qquad (A.32)$$

$$S_{zz}(n) = g_1^2S_{xx}(n) + g_2^2S_{yy}(n) + g_1g_2[S_{xy}(n) + S_{yx}(n)] \qquad (A.33)$$

2. If

$$Z(t) = \int g(z).X(z,t)dz \qquad (A.34)$$

where g(z) is a deterministic function of z

$$R_{zz}(\tau) = \iint g(z_1)g(z_2)R_{xx}(z_1,z_2,\tau)dz_1dz_2 \qquad (A.35)$$

$$S_{zz}(n) = \iint g(z_1)g(z_2)S_{xx}(z_1,z_2,n)dz_1dz_2 \qquad (A.36)$$